Along-ridge petrological segmentation of the mantle in the Oman ophiolite

Christophe Monnier, Jacques Girardeau, Laurent Le Mée, Mireille Polvé

Geochemistry Geophysics Geosystems G3
AN ELECTRONIC JOURNAL OF THE EARTH SCIENCES
Published by AGU and the Geochemical Society

Article
Volume 7, Number 11
10 November 2006
Q11008, doi:10.1029/2006GC001320
ISSN: 1525-2027

Along-ridge petrological segmentation of the mantle in the Oman ophiolite

Christophe Monnier, Jacques Girardeau, and Laurent Le Mée
Université de Nantes, Nantes Atlantique Universités, CNRS, UMR-6112, Laboratoire de Planétologie et Géodynamique, 2 Rue de la Houssinière, BP 92208, Nantes, F-44000, France (christophe.monnier@univ-nantes.fr)

Mireille Polvé
UMR-CNRS 5562, Laboratoire d'Etude des Mécanismes de Transfert en Géologie, Observatoire Midi-Pyrénées, 14 Avenue Edouard Belin, Toulouse, F-31400, France

[1] Oman ophiolite mantle has been sampled over a distance of about 400 km, all along the paleo-ridge axis. Primary phases have been analyzed in 174 peridotites (mainly harzburgites) and major and trace element contents measured in 90 and 156 samples, respectively. Most samples display depleted characteristics with very low incompatible element bulk rocks and very low HREE contents. On the basis of the spinel Cr# and in agreement with Yb concentrations in the bulk rocks, an average of 16.5% (F_{max}) of melt extraction is estimated. These rocks show light REE enrichments marked by high LREE/MREE ratios that well correlate with the extent of melting. The light REE were possibly gained during the latest stage of melting in an open-system melting model, or through interaction with influxed fluid after melting. Chemical data have been processed Fourier Transforms to study the along-ridge variations, which gives results similar to those obtained using the seven point running average (Le Mée et al., 2004). When plotted along ridge, spinel Cr# display variations with two types of wavelengths, defining four 50–100 km long segments (70 km in average) and numerous 10–20 km shorter ones making undulations within the longer ones. All segments have a center marked by high values of spinel Cr# ($\approx F_{max}$) and edges with the lowest values. The large, 50–100 km segments (70 km in average) may correspond to large asthenospheric mantle upwellings between major deep mantle discontinuities, while the smaller ones possibly relate more superficial mantle instabilities similar to the structural diapirs of Nicolas et al. (1988a). We consider that the variation in degree of melting in the short-scale instabilities relates fluid/melt flux melting variations. By comparison with mid-oceanic ridge models, the long Oman segments can correspond to second-order segments and the smallest to third- to fourth-order ones. Our data on the geometry of the melting zones will constrain models of the dynamics of the mantle beneath ridges. They provide a new perspective for further characterization of the segments in the Oman ophiolite.

Components: 36,779 words, 19 figures, 7 tables.

Keywords: ophiolite; segmentation; geochemistry; mantle.

Index Terms: 1065 Geochemistry: Major and trace element geochemistry; 3042 Marine Geology and Geophysics: Ophiolites (8140); 3621 Mineralogy and Petrology: Mantle processes (1038).

Received 30 March 2006; **Revised** 25 July 2006; **Accepted** 18 September 2006; **Published** 10 November 2006.

Monnier, C., J. Girardeau, L. Le Mée, and M. Polvé (2006), Along-ridge petrological segmentation of the mantle in the Oman ophiolite, *Geochem. Geophys. Geosyst.*, *7*, Q11008, doi:10.1029/2006GC001320.

1. Introduction

1.1. Axial Segmentation of Present Mid-oceanic Ridges

[2] Different types of superficial morphologic axial discontinuities have been recognized and mapped at present mid-oceanic ridges, as for instance major transform faults, overlapping spreading centers and nontransform offsets [e.g., *Cannat*, 1996; *Langmuir et al.*, 1986, 1992; *MacDonald et al.*, 1984, 1987, 1988a; *Schouten et al.*, 1985; *Sempéré et al.*, 1993; *Sempéré and MacDonald*, 1987; *Shaw*, 1992; *Sinton et al.*, 1991]. The along-strike distances between these axial discontinuities were used to distinguish four orders of segmentation, from 200–900 km long (first order) and 30–300 km long (second order) to <10 km short segments (third to fourth order) [*MacDonald et al.*, 1988a, 1988b].

[3] To date, most authors agree that this tectonic segmentation is related to the mantle dynamics [e.g., *Batiza*, 1996; *Cannat*, 1996; *Langmuir et al.*, 1986, 1992; *Sempéré and MacDonald*, 1987]. But presently, there is little petrological information about oceanic rocks to constrain the ridge segmentation model. The data available concern basalts (East Pacific Rise and Mid-Atlantic Ridge [*Batiza*, 1996; *Langmuir et al.*, 1986, 1992; *Reynolds and Langmuir*, 1997; *Reynolds et al.*, 1992; *Schilling et al.*, 1983; *White et al.*, 2000]) and peridotites (South West Indian Ridge [*Seyler et al.*, 2003]) which chemical compositions locally display large-scale variations and discontinuities at transform fault boundaries. However, in all these cases, the density and interval of sampling is not sufficient to characterize precisely the segmentation variability as defined using the ridge morphology.

1.2. Oman Ophiolite: A Good Analogue to Constrain Present Ridges' Deep Segmentation

[4] Ophiolites offer a unique geological setting to sample simultaneously basalts and mantle residues. This is particularly true in the Oman ophiolite (Figure 1), whose lithology and structures have been relatively well preserved during the obduction process [e.g., *Alabaster et al.*, 1982; *Boudier and Coleman*, 1981; *Hopson et al.*, 1981; *Pallister*, 1981; *Pearce et al.*, 1981; *Smewing*, 1980]. This ophiolite has a spectacular size, nearly 20 000 km^2, and has an NW-SE extension of nearly 500 km by about 50 km in the EW direction, and has excellent exposure (Figure 1). Its crustal units, with sheeted dykes dominantly trending NW-SE, outcrop on the eastern part of the ophiolite whereas the mantle ones, 6 km on average under the paleo-Moho, border the west. NW-SE paleo-ridges segments have been recognized along the ophiolite [*Dilek et al.*, 2000] and previous references, allowing us to test the segmentation model defined for present-day oceanic ridges over a distance equivalent to a first-order segment [*Ceuleneer*, 1986; *Nicolas*, 1989; *Reuber et al.*, 1991]. This work describes the chemical variations in the mantle part of the ophiolite, sampled at distance intervals of about 1.5 km, ever done along a paleo-ridge axis [*Le Mée*, 2004; *Le Mée et al.*, 2004].

2. Geological Background

2.1. Paleo-Ridge-Axis Location, Accretion Period, and Geodynamic Setting

[5] The Oman ophiolite (Figure 1) is a portion of a neo-tethysian oceanic lithosphere, formed at 94–95 Ma [*Coleman*, 1984]. It was obducted during Late Cretaceous (during Campanian-Maastrichtian times, at about 78 Ma) on the Arabian margin, as a result of convergence between the Arabian and Eurasian plates [*Coleman*, 1981].

[6] This ophiolite has recorded a paleo-oceanic ridge activity that has been well preserved during its obduction [*Nicolas and Boudier*, 2000; *Nicolas et al.*, 2000a, 2000b]. These records are related to the presence of (1) magma chamber tips in the crust [*Juteau et al.*, 1988a, 1988b; *MacLeod and Rothery*, 1992], (2) frozen diapirs in the mantle [*Ceuleneer*, 1986, 1991; *Ceuleneer et al.*, 1988; *Nicolas et al.*, 1988a, 1988b, 2000a, 1994] and (3) areas of abundant sheeted dykes [*MacLeod and Rothery*, 1992; *Python and Ceuleneer*, 2003]. The fact that these magmatic features, all considered as acquired at an accreting ridge, were preserved in the Oman ophiolite, was a major argument to stress that a paleo-ridge was indeed obducted [*Nicolas et al.*, 2000a].

[7] The characteristics of Oman ophiolite suggest that it formed at a fast- to intermediate-spreading ridge [*Boudier et al.*, 1997; *MacLeod and Rothery*, 1992; *Nicolas*, 1989; *Nicolas et al.*, 1994; *Pallister and Hopson*, 1981; *Tilton et al.*, 1981], with estimated spreading rates between 5 and 12 $cm.an^{-1}$ [*Hacker and Mosenfelder*, 1996]; 6 $cm.an^{-1}$ [*Nicolas et al.*, 2000a]; 12 $cm.an^{-1}$

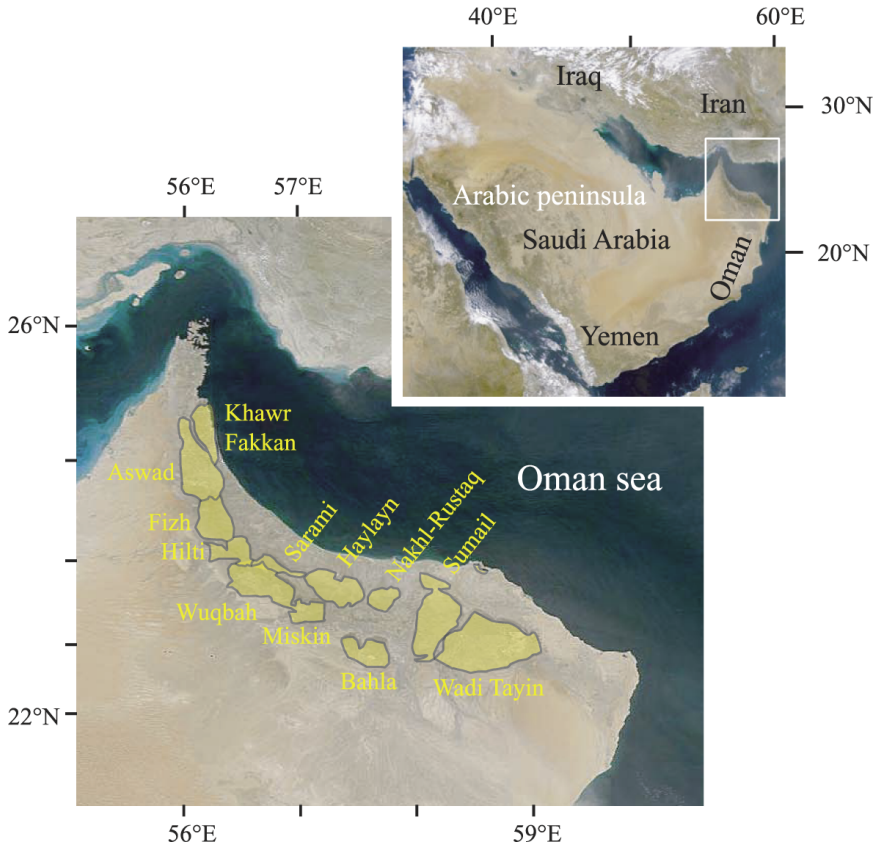

Figure 1. Simplified map of the Arabian peninsula and of the Oman ophiolite showing the different massifs with their respective names. The background photos were done by OrbView-2 satellite (SeaWiFS Project, NASA Goddard Space Flight Center, and ORBIMAGE).

[*Nicolas and Boudier*, 2000]. This point is very important as spreading rate has a strong effect on segmentation features which are different for fast (East Pacific Rise (EPR)) and slow to ultra-slow (Mid-Atlantic Ridge (MAR) and South West Indian Ridge (SWIR)) spreading ridges [e.g., *Grindlay et al.*, 1992; *MacDonald et al.*, 1988a]. To this day, it is still debated whether the Oman ophiolite formed in a true oceanic setting [*Boudier et al.*, 1988; *Boudier and Coleman*, 1981] or in a supra-subduction setting [*Beurrier*, 1987; *Lippard et al.*, 1986; *Miyashiro*, 1973; *Pearce*, 1980, 1982; *Pearce et al.*, 1981]. But this point is not crucial for our study, as ridge segmentation characteristics are quite similar for all geodynamic setting [*MacLeod and Rothery*, 1992; *Parson et al.*, 1990]. This point will be further discussed in the last section of this paper (see section 8.5).

2.2. Attitude of the Moho

[8] The obduction of the neo-tethysian oceanic lithosphere had some effects on the spatial organization of the Oman ophiolite, producing its partial fragmentation [*Nicolas et al.*, 2000a] and the local tilting of the ophiolitic sequence [*Reuber*, 1988]. Tilt of the ophiolite sequence is more pronounced in the central and northern parts of the ophiolite [*Reuber*, 1988]. In these areas, all primary magmatic contacts, including the paleo-Moho, dip between 30 and 60° toward the southeast (Figure 2). In the mantle section, the high-temperature foliation is generally parallel to that of the paleo-Moho, except in zones where mantle diapirs have been recognized and mapped [e.g., *Ceuleneer et al.*, 1988; *Nicolas and Boudier*, 2000; *Nicolas et al.*, 1988a, 1988b]. Using these spatial references, the crustal part of the Oman ophiolite has been tilted back to its preobducted position. This has allowed us to make estimates of the paleo-depth at which the studied rocks were taken.

2.3. Structural Segmentation Features

[9] On the basis of structural data, some first- to third-order segmentation features have previously been described in the Oman ophiolite. Arguments used included (1) thickness variations of both the

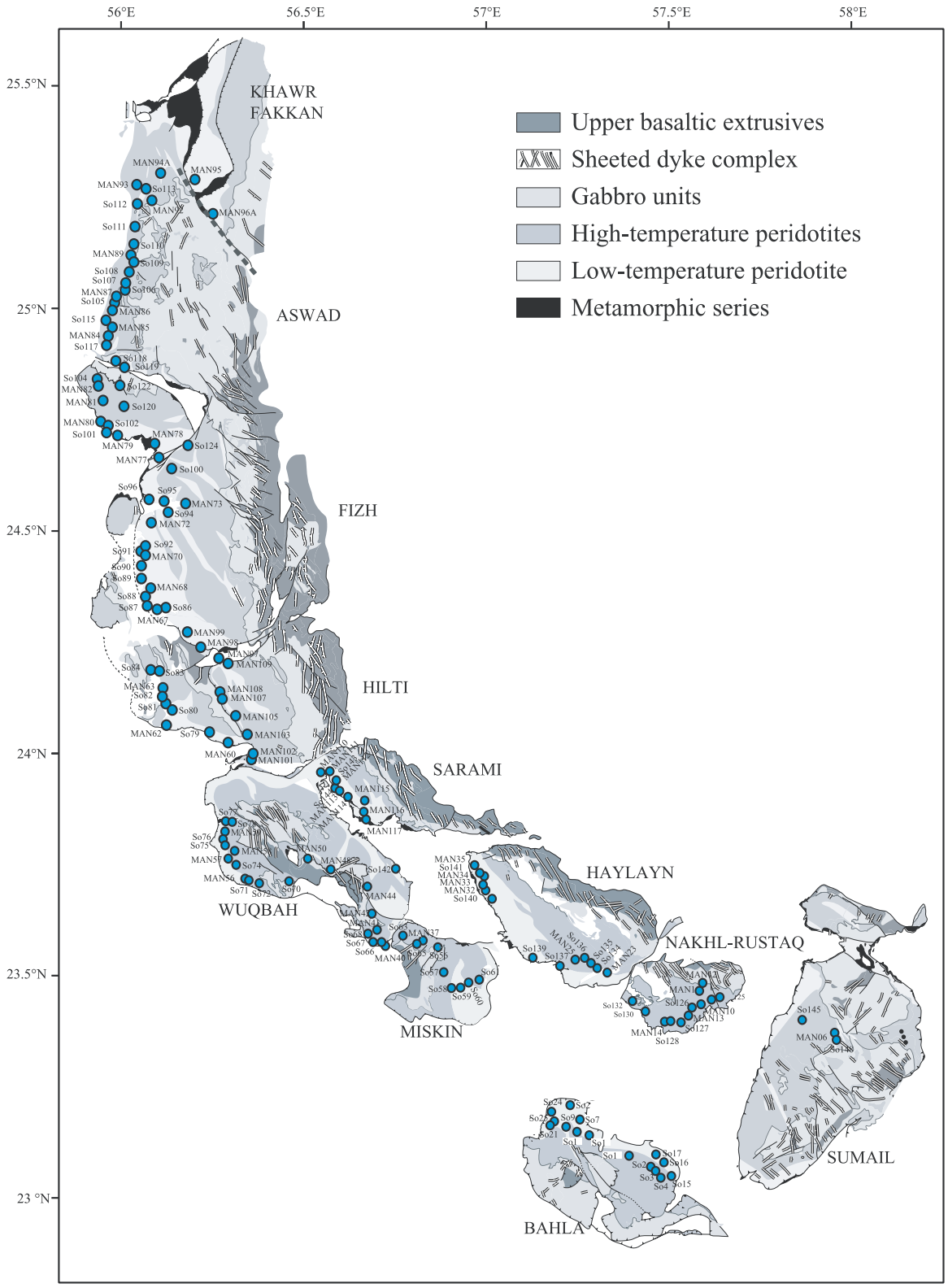

Figure 2. Sampling map of the Oman ophiolite. Lithological definitions of units: 1, upper basaltic extrusives; 2, sheeted dyke complex; 3, gabbro units; 4, high-temperature peridotites; 5, low-temperature peridotites; 6, metamorphic series.

Table 1. GPS Positions of Samples and Results of Modal Analyses[a]

Sample	Rock	Massif	Longitude, ° East	Latitude, ° North	Olivine + Serpentine		Orthopyroxene		Spinelle		Cpx	Total
					Average	SD	Average	SD	Average	SD	Average	
MAN 01	Hz	Sumail	58.616	22.798	78.82	6.97	17.43	7.55	0.95	0.89	2.80	100
MAN 03	Hz	Sumail	58.527	22.980	85.64	5.20	11.97	4.93	0.59	0.71	1.80	100
MAN 06	Du	Sumail	58.076	23.220	92.97	4.32	5.63	3.04	1.39	1.31	<0.1	100
MAN 07	Du	Nakhl-Rustaq	57.773	23.406	93.47	3.24	6.10	3.18	0.42	0.28	<0.1	100
MAN 08	Du	Nakhl-Rustaq	57.740	23.378	93.02	2.41	6.57	2.56	0.42	0.21	<0.1	100
MAN 09	Hz	Nakhl-Rustaq	57.702	23.382	88.40	4.62	11.17	4.68	0.43	0.08	<0.1	100
MAN 10	Hz	Nakhl-Rustaq	57.669	23.368	87.77	6.79	11.46	6.72	0.76	0.35	<0.1	100
MAN 11	Hz	Nakhl-Rustaq	57.664	23.400	84.88	6.52	14.74	6.64	0.38	0.13	<0.1	100
MAN 13	Hz	Nakhl-Rustaq	57.629	23.334	84.00	2.87	15.70	2.56	0.30	0.32	<0.1	100
MAN 14	Hz	Nakhl-Rustaq	57.561	23.321	87.99	2.51	11.74	2.47	0.28	0.12	<0.1	100
MAN 20	Hz	Haylayn	57.365	23.427	79.55	5.08	18.82	6.07	1.13	1.00	0.50	100
MAN 21	Hz	Haylayn	57.383	23.453	88.44	4.07	10.99	4.09	0.46	0.35	0.10	100
MAN 23	Hz	Haylayn	57.301	23.416	80.76	8.89	17.14	8.88	0.20	0.03	1.90	100
MAN 24	Hz	Haylayn	57.258	23.432	72.24	3.45	26.39	3.68	1.37	0.28	<0.1	100
MAN 25	Hz	Haylayn	57.208	23.452	87.29	2.95	12.18	3.50	0.53	0.75	<0.1	100
MAN 26	Du	Haylayn	57.204	23.395	93.63	3.90	5.54	3.45	0.84	0.70	<0.1	100
MAN 27	Hz	Haylayn	57.166	23.424	89.89	4.53	9.88	4.56	0.23	0.11	<0.1	100
MAN 28	Hz	Haylayn	57.114	23.478	89.83	6.63	9.50	6.48	0.57	0.23	0.10	100
MAN 29	Du	Haylayn	57.043	23.474	95.84	0.35	3.80	0.30	0.36	0.23	<0.1	100
MAN 30	Hz	Haylayn	57.023	23.485	89.27	2.24	9.39	2.15	0.84	0.12	0.50	100
MAN 32	Hz	Haylayn	56.943	23.641	85.72	1.78	13.27	1.68	1.00	0.60	<0.1	100
MAN 33	Du	Haylayn	56.931	23.657	90.08	3.02	9.28	2.93	0.44	0.15	0.20	100
MAN 34	Hz	Haylayn	56.935	23.679	75.79	7.57	23.60	7.60	0.61	0.23	<0.1	100
MAN 35	Hz	Haylayn	56.909	23.710	87.52	2.48	11.33	2.61	0.25	0.13	0.90	100
MAN 37	Hz	Wuqbah	56.829	23.505	82.59	9.55	17.11	9.47	0.31	0.11	<0.1	100
MAN 39	Hz	Wuqbah	56.737	23.544	76.28	6.25	23.36	6.12	0.36	0.20	<0.1	100
MAN 40	Hz	Wuqbah	56.716	23.494	85.40	10.34	14.02	10.06	0.58	0.34	<0.1	100
MAN 41	Du	Wuqbah	56.693	23.538	90.53	3.48	5.88	3.60	0.59	0.37	3.00	100
MAN 42	Hz	Wuqbah	56.672	23.578	87.33	7.17	12.30	7.23	0.37	0.10	<0.1	100
MAN 44	Hz	Wuqbah	56.661	23.651	83.00	6.30	16.06	6.28	0.94	0.10	<0.1	100
MAN 48	Hz	Wuqbah	56.550	23.702	89.74	1.39	9.54	1.78	0.72	0.71	<0.1	100
MAN 50	Hz	Wuqbah	56.481	23.732	80.92	7.16	18.58	7.31	0.50	0.20	<0.1	100
MAN 55	Du	Wuqbah	56.366	23.720	90.43	7.31	8.83	7.37	0.24	0.09	0.50	100
MAN 56	Hz	Wuqbah	56.300	23.670	84.27	10.50	15.08	11.31	0.65	0.82	<0.1	100
MAN 57	Du	Wuqbah	56.241	23.726	90.34	6.84	9.44	6.81	0.22	0.16	<0.1	100
MAN 58	Hz	Wuqbah	56.259	23.749	88.67	3.53	11.19	3.45	0.14	0.16	<0.1	100
MAN 59	Hz	Wuqbah	56.231	23.800	87.90	5.47	11.83	5.51	0.28	0.07	<0.1	100
MAN 60	Du	Hilti	56.257	24.019	94.35	2.02	3.45	2.75	0.80	1.25	1.40	100
MAN 62	Hz	Hilti	56.109	24.055	85.32	6.63	14.17	6.67	0.50	0.40	<0.1	100
MAN 63	Du	Hilti	56.098	24.140	91.44	1.62	8.25	1.74	0.32	0.13	<0.1	100
MAN 67	Hz	Fizh	56.085	24.317	81.58	7.59	17.94	7.56	0.47	0.07	<0.1	100
MAN 68	Du	Fizh	56.072	24.365	90.64	6.68	8.42	6.08	0.94	0.97	<0.1	100
MAN 70	Hz	Fizh	56.055	24.436	87.49	6.25	12.18	6.34	0.33	0.18	<0.1	100
MAN 72	Du	Fizh	56.069	24.513	93.80	2.06	5.80	2.15	0.40	0.10	<0.1	100
MAN 73	Hz	Fizh	56.154	24.553	82.73	5.91	16.76	5.98	0.50	0.12	<0.1	100
MAN 77	Hz	Fizh	56.088	24.658	86.15	2.30	12.73	2.01	0.42	0.38	0.70	100
MAN 78	Du	Fizh	56.077	24.690	92.49	2.49	7.02	2.21	0.49	0.45	<0.1	100
MAN 79	Du	Fizh	55.988	24.708	93.90	4.26	5.53	4.24	0.56	0.15	<0.1	100
MAN 80	Hz	Fizh	55.949	24.737	80.33	10.25	18.05	10.26	0.62	0.18	1.00	100
MAN 81	Hz	Fizh	55.951	24.783	80.12	5.45	18.78	5.35	0.79	0.24	0.30	100
MAN 82	Hz	Fizh	55.943	24.818	78.42	4.05	21.26	3.94	0.32	0.11	<0.1	100
MAN 83	Hz	Aswad	55.973	24.897	-	-	-	-	-	-	-	-
MAN 84	Du	Aswad	55.964	24.927	91.46	7.50	7.99	7.67	0.54	0.38	<0.1	100
MAN 85	Du	Aswad	55.977	24.948	93.59	6.06	5.73	6.20	0.67	0.56	<0.1	100
MAN 86	Hz	Aswad	55.977	24.988	81.25	7.03	18.36	7.25	0.38	0.35	<0.1	100
MAN 87	Du	Aswad	55.985	25.018	91.66	11.56	7.89	11.21	0.45	0.35	<0.1	100
MAN 89	Du	Aswad	56.025	25.109	91.37	2.31	7.34	2.64	1.28	0.33	<0.1	100
MAN 92	Hz	Aswad	56.069	25.236	85.28	5.16	14.26	4.98	0.46	0.26	<0.1	100
MAN 93	Hz	Aswad	56.036	25.270	87.61	1.44	11.66	1.60	0.73	0.19	<0.1	100
MAN 94	Hz	Aswad	56.094	25.298	89.92	6.31	9.07	6.44	1.01	0.39	<0.1	100

Table 1. (continued)

Sample	Rock	Massif	Longitude, ° East	Latitude, ° North	Olivine + Serpentine		Orthopyroxene		Spinelle		Cpx	Total
					Average	SD	Average	SD	Average	SD	Average	
MAN 95	Hz	Khawr Fakkan	56.176	25.283	80.87	1.64	15.60	1.87	0.73	0.23	2.80	100
MAN 96	Du	Khawr Fakkan	56.222	25.207	96.09	2.34	3.18	2.69	0.73	0.35	<0.1	100
MAN 98	Du	Fizh	56.192	24.228	91.68	1.23	7.47	0.68	0.85	0.61	<0.1	100
MAN 99	Hz	Fizh	56.161	24.262	84.96	3.56	13.89	4.03	0.65	0.49	0.50	100
MAN 101	Hz	Hilti	56.315	23.977	85.34	4.53	13.80	4.11	0.86	0.45	<0.1	100
MAN 103	Hz	Hilti	56.305	24.035	85.06	0.98	14.49	0.51	0.45	0.48	<0.1	100
MAN 105	Hz	Hilti	56.278	24.077	85.76	3.87	13.64	4.47	0.59	0.68	<0.1	100
MAN 107	Hz	Hilti	56.245	24.116	86.62	4.38	12.30	4.30	0.28	0.14	0.80	100
MAN 109	Hz	Hilti	56.260	24.194	88.33	2.93	11.06	2.47	0.60	0.62	<0.1	100
MAN 110	Hz	Sarami	56.515	23.964	73.24	1.55	26.31	1.72	0.45	0.17	<0.1	100
MAN 111	Hz	Sarami	56.545	23.964	87.01	6.32	12.72	6.17	0.27	0.17	<0.1	100
MAN 112	Hz	Sarami	56.563	23.932	85.37	1.50	14.24	1.53	0.39	0.07	<0.1	100
MAN 113	Hz	Sarami	56.573	23.912	83.21	1.91	14.81	2.17	1.98	0.28	<0.1	100
MAN 114	Du	Sarami	56.603	23.897	90.87	7.07	8.12	7.13	1.01	0.07	<0.1	100
MAN 115	Hz	Sarami	56.655	23.887	79.11	1.24	20.32	1.31	0.47	0.08	0.10	100
MAN 116	Hz	Sarami	56.650	23.859	86.34	3.97	13.21	4.30	0.46	0.33	<0.1	100
MAN 117	Hz	Sarami	56.661	23.833	85.66	3.77	13.12	3.30	0.42	0.47	0.80	100
MAN 149	Hz	Haylayn	57.316	23.499	86.19	10.11	10.78	10.44	0.83	0.52	2.20	100
MAN 150	Hz	Haylayn	57.308	23.501	77.64	8.85	21.57	9.00	0.79	0.59	<0.1	100
MAN 151	Du	Haylayn	57.315	23.511	93.10	6.23	6.70	6.19	0.20	0.06	<0.1	100
MAN 153	Hz	Haylayn	57.332	23.510	80.92	7.54	18.42	7.62	0.67	0.37	<0.1	100
MAN 155	Hz	Haylayn	57.327	23.522	88.23	3.91	11.42	3.73	0.35	0.19	<0.1	100
MAN 157	Du	Haylayn	57.329	23.534	90.53	3.64	8.74	3.18	0.73	0.47	<0.1	100
So_2	Hz	Bahla	57.460	22.994	74.32	4.36	24.99	4.39	0.19	0.11	0.50	100
So_3	Hz	Bahla	57.480	22.986	74.18	7.01	24.35	7.70	0.87	0.82	0.60	100
So_4	Lz	Bahla	57.498	22.968	67.76	5.70	21.59	5.05	1.35	0.71	9.30	100
So_7	Hz	Bahla	57.220	23.070	78.06	4.75	21.54	4.59	0.40	0.19	<0.1	100
So_9	Hz	Bahla	57.185	23.036	77.59	4.48	21.94	4.41	0.48	0.09	<0.1	100
So_10	Du	Bahla	57.226	23.028	91.23	3.69	8.35	3.51	0.43	0.19	<0.1	100
So_11	Hz	Bahla	57.262	23.027	80.81	6.72	17.89	7.08	1.01	0.38	0.30	100
So_15	Hz	Bahla	57.525	22.987	85.99	4.23	13.52	4.33	0.49	0.10	<0.1	100
So_16	Hz	Bahla	57.494	23.012	80.27	6.82	13.65	6.92	1.28	0.15	4.80	100
So_17	Hz	Bahla	57.463	23.027	76.21	0.94	22.59	0.78	0.30	0.17	0.90	100
So_19	Du	Bahla	57.390	23.008	90.47	5.48	8.91	5.38	0.62	0.31	<0.1	100
So_21	Hz	Bahla	57.144	23.028	84.02	5.67	15.55	5.40	0.43	0.28	<0.1	100
So_24	Hz	Bahla	57.134	23.067	86.81	5.21	12.63	5.26	0.56	0.40	<0.1	100
So_25	Hz	Bahla	57.147	23.044	72.39	6.21	27.18	6.21	0.43	0.04	<0.1	100
So_56	Hz	Miskin	56.872	23.489	80.05	8.89	18.89	9.11	0.76	0.22	0.30	100
So_57	Hz	Miskin	56.892	23.422	88.58	7.79	10.68	8.09	0.74	0.53	<0.1	100
So_58	Hz	Miskin	56.915	23.381	76.33	5.27	22.87	5.14	0.80	0.16	<0.1	100
So_59	Hz	Miskin	56.943	23.378	87.45	2.31	11.94	2.06	0.61	0.29	<0.1	100
So_60	Du	Miskin	56.967	23.394	90.02	3.94	8.34	4.34	0.94	0.60	0.70	100
So_61	Hz	Miskin	56.997	23.401	79.50	0.74	20.32	0.80	0.18	0.10	<0.1	100
So_62	Hz	Miskin	57.023	23.360	81.43	9.60	17.24	9.82	0.73	0.24	0.60	100
So_63	Hz	Miskin/Wuqbah	56.768	23.521	79.62	3.51	19.50	3.66	0.38	0.23	0.50	100
So_65	Hz	Miskin/Wuqbah	56.810	23.496	82.12	3.79	17.41	3.53	0.47	0.33	<0.1	100
So_66	Hz	Miskin/Wuqbah	56.704	23.500	86.93	4.71	12.27	5.02	0.79	0.41	<0.1	100
So_67	Hz	Miskin/Wuqbah	56.678	23.508	89.14	4.78	9.50	3.66	1.36	1.29	<0.1	100
So_68	Hz	Miskin/Wuqbah	56.666	23.529	70.51	10.21	23.90	10.43	0.69	0.32	4.90	100
So_70	Lz	Wuqbah	56.422	23.664	81.87	9.80	9.80	9.68	0.43	0.15	7.90	100
So_71	Hz	Wuqbah	56.332	23.661	79.85	6.22	19.42	6.11	0.73	0.30	<0.1	100
So_72	Hz	Wuqbah	56.291	23.673	88.29	7.75	11.18	7.60	0.53	0.28	<0.1	100
So_74	Hz	Wuqbah	56.265	23.711	84.97	3.06	13.29	3.24	0.54	0.20	1.20	100
So_75	Hz	Wuqbah	56.228	23.768	81.84	5.89	17.48	6.38	0.68	0.49	<0.1	100
So_76	Hz	Wuqbah	56.224	23.784	87.13	5.00	11.84	4.47	1.03	0.55	<0.1	100
So_77	Hz	Wuqbah	56.235	23.830	88.89	3.02	10.15	2.70	0.96	0.50	<0.1	100
So_78	Hz	Wuqbah	56.252	23.827	76.35	15.26	21.39	15.43	0.46	0.19	1.80	100
So_79	Hz	Wuqbah	56.217	24.033	77.36	6.00	22.00	5.90	0.64	0.49	<0.1	100
So_80	Du	Hilti	56.121	24.091	91.14	5.44	8.50	5.13	0.36	0.31	<0.1	100
So_81	Hz	Hilti	56.109	24.105	80.45	6.27	19.25	6.42	0.30	0.16	<0.1	100

Table 1. (continued)

Sample	Rock	Massif	Longitude, ° East	Latitude, ° North	Olivine + Serpentine		Orthopyroxene		Spinelle		Cpx	Total
					Average	SD	Average	SD	Average	SD	Average	
So_82	Hz	Hilti	56.097	24.122	87.61	7.24	11.95	7.10	0.44	0.14	<0.1	100
So_83	Hz	Hilti	56.088	24.176	82.84	9.38	16.02	9.15	0.44	0.27	0.70	100
So_84	Hz	Hilti	56.068	24.180	82.45	2.78	16.41	2.68	0.44	0.15	0.70	100
So_85	Hz	Fizh	56.126	24.284	86.42	2.68	13.22	2.67	0.36	0.14	<0.1	100
So_87	Du	Fizh	56.061	24.326	92.75	3.08	6.72	3.25	0.53	0.21	<0.1	100
So_88	Hz	Fizh	56.057	24.347	85.28	2.59	11.11	2.55	0.91	0.24	2.70	100
So_89	Du	Fizh	56.045	24.385	90.37	4.33	8.78	4.26	0.85	0.47	<0.1	100
So_90	Hz	Fizh	56.047	24.416	88.37	3.59	10.89	3.70	0.73	0.14	<0.1	100
So_91	Hz	Fizh	56.045	24.445	78.38	4.16	17.97	3.65	0.75	0.68	2.90	100
So_92	Hz	Fizh	56.053	24.457	79.48	3.16	20.18	3.12	0.34	0.06	<0.1	100
So_94	Hz	Fizh	56.114	24.534	83.47	4.54	16.04	4.17	0.49	0.37	<0.1	100
So_95	Du	Fizh	56.104	24.560	90.27	3.21	8.60	2.77	1.03	0.46	0.10	100
So_96	Lz	Fizh	56.063	24.564	76.69	5.23	17.34	5.19	0.87	0.05	5.10	100
So_100	Du	Fizh	56.124	24.633	90.94	5.83	8.42	5.62	0.64	0.26	<0.1	100
So_101	Hz	Fizh	55.961	24.717	84.12	5.75	14.54	6.14	0.94	0.45	0.40	100
So_102	Hz	Fizh	55.964	24.729	77.08	8.17	21.50	8.35	0.72	0.22	0.70	100
So_104	Hz	Aswad	55.936	24.833	84.54	9.38	15.14	9.57	0.33	0.24	<0.1	100
So_105	Hz	Aswad	55.978	25.004	82.67	5.27	17.03	5.30	0.30	0.19	<0.1	100
So_106	Hz	Aswad	56.008	25.034	85.73	5.06	13.86	5.20	0.41	0.15	<0.1	100
So_107	Hz	Aswad	56.010	25.049	88.83	4.18	9.67	4.58	0.90	0.89	0.60	100
So_108	Hz	Aswad	56.017	25.075	85.37	5.42	12.76	6.39	0.77	0.99	1.10	100
So_109	Hz	Aswad	56.027	25.095	82.71	2.49	16.75	2.08	0.55	0.40	<0.1	100
So_110	Hz	Aswad	56.026	25.135	86.47	4.76	12.62	5.16	0.91	0.54	<0.1	100
So_111	Hz	Aswad	56.031	25.172	86.14	1.61	13.38	1.57	0.49	0.16	<0.1	100
So_112	Du	Aswad	56.038	25.226	93.53	0.89	6.09	0.89	0.38	0.30	<0.1	100
So_113	Du	Aswad	56.057	25.262	92.39	0.69	6.66	0.33	0.95	0.56	<0.1	100
So_114	Hz	Aswad	55.958	24.982	82.14	8.59	17.58	8.69	0.29	0.33	<0.1	100
So_115	Du	Aswad	55.963	24.965	90.90	4.27	8.49	4.44	0.61	0.57	<0.1	100
So_116	Hz	Aswad	55.959	24.938	83.07	8.44	16.38	7.91	0.55	0.53	<0.1	100
So_117	Du	Aswad	55.961	24.909	90.99	3.69	8.29	4.07	0.72	0.76	<0.1	100
So_118	Hz	Aswad	55.985	24.875	85.12	5.18	14.45	5.14	0.43	0.11	<0.1	100
So_119	Hz	Aswad	56.002	24.859	82.94	7.61	16.72	7.41	0.34	0.21	<0.1	100
So_120	Du	Fizh	56.006	24.773	93.30	3.41	4.72	3.97	1.99	2.18	<0.1	100
So_122	Hz	Fizh	55.994	24.821	82.39	1.69	17.15	1.48	0.46	0.21	<0.1	100
So_124	Hz	Fizh	56.158	24.687	85.21	5.84	10.15	5.97	0.54	0.18	4.10	100
So_125	Hz	Nakhl Rustaq	57.722	23.386	88.86	4.30	10.45	4.00	0.69	0.31	<0.1	100
So_126	Hz	Nakhl Rustaq	57.642	23.359	83.66	2.94	13.74	2.86	0.70	0.17	1.90	100
So_127	Hz	Nakhl Rustaq	57.608	23.321	88.19	6.75	10.61	6.34	1.20	0.49	<0.1	100
So_128	Hz	Nakhl Rustaq	57.578	23.320	82.62	9.20	14.90	9.40	1.18	0.31	1.30	100
So_130	Hz	Nakhl Rustaq	57.500	23.347	88.34	4.71	8.77	4.84	0.99	0.52	1.90	100
So_132	Hz	Nakhl Rustaq	57.461	23.378	87.56	5.43	10.48	5.38	0.66	0.14	1.30	100
So_134	Hz	Haylayn	57.271	23.434	84.92	7.55	13.59	7.45	0.49	0.24	1.00	100
So_135	Hz	Haylayn	57.251	23.442	77.08	11.97	22.24	12.09	0.68	0.34	<0.1	100
So_136	Hz	Haylayn	57.233	23.457	83.06	4.24	15.68	4.00	0.56	0.52	0.70	100
So_137	Du	Haylayn	57.164	23.435	90.36	3.30	9.12	3.47	0.52	0.19	<0.1	100
So_139	Hz	Haylayn	57.079	23.460	77.26	2.08	21.05	2.02	0.59	0.34	1.10	100
So_140	Hz	Haylayn	56.962	23.617	88.11	2.40	6.96	2.33	0.43	0.15	4.50	100
So_141	Hz	Haylayn	56.924	23.688	81.90	5.79	16.79	5.77	0.61	0.07	0.70	100
So_142	Lz	Wuqbah	56.750	23.701	88.70	3.44	4.97	3.06	1.04	0.42	5.30	100
So_143	Du	Sarami	56.565	23.939	90.88	2.20	8.60	2.53	0.52	0.39	<0.1	100
So_144	Hz	Sarami	56.566	23.922	85.25	1.38	12.87	1.45	0.48	0.08	1.40	100
So_145	Hz	Samail	57.993	23.260	88.55	4.38	10.16	4.48	0.49	0.26	0.80	100
So_148	Hz	Samail	58.085	23.198	78.76	7.30	20.89	7.13	0.35	0.17	<0.1	100
94-46	Hz	Haylayn	57.169	23.572	77.43	4.67	21.40	3.81	0.87	0.86	0.30	100

[a] GPS positions are in longitude and latitude, and results of modal analyses are in %. To determine the modal characteristics in volumetric proportions, 6 numerical images were done on each of the 174 samples using a video microscope covering 80% of the thin section (i.e., about 8 cm^2, excluding the edges of thin sections): 3 in natural light and 3 of the same zones in polarized light. For each sample, 3 modal analyses have been done using traditional image processor software. All serpentine minerals have been considered to replace olivine (no correction has been realized for volumetric expansion). Analytical uncertainty, calculated after 5 modal analyses of the same sample, is lower than ±0.5%. Intrasample variation: average and standard deviation (SD, indicating the variability of the volume proportions of a phase in a sample) calculated on the 3 modal analysis obtained for each sample. Only 51 samples have a Cpx mode ranging from 0.1% to 3%, and 9 have more than 3%.

crustal unit and the mantle transition zone [*Dahl*, 1984; *Juteau et al.*, 1988a; *Nicolas and Boudier*, 2000; *Nicolas et al.*, 1996], (2) presence of mantle diapirs marked by variations in the attitude of foliations and lineations [e.g., *Ceuleneer et al.*, 1988; *Ceuleneer and Rabinowicz*, 1992; *Girardeau et al.*, 2002a; *Nicolas*, 1989; *Nicolas and Boudier*, 2000; *Nicolas et al.*, 1988a, 1988b; *Reuber et al.*, 1991], (3) relationships between the sheeted dykes and the cumulative gabbros and peridotites [*MacLeod and Rothery*, 1992], and (4) existence of shear zones linked with ridge propagation [*Nicolas et al.*, 2000a]. Evidence for smaller-scale, third- to fourth-order OSC-type discontinuities was also described in the Haylayn [*Juteau et al.*, 1988a] and Wuqbah [*Girardeau et al.*, 2002a] massifs. All these criteria supported the existence, in the Oman ophiolite, of four segments, 50 to 100 km long (70 km in average), separated by second-order discontinuities including at least two OSCs [*MacLeod and Rothery*, 1992; *Nicolas et al.*, 2000a].

[10] Nevertheless, presently, no chemical data on the basaltic part of the ophiolite or on its mantle part are available which could support this structural segmentation pattern. There are data on the petrology and geochemistry of the Oman lavas, sheeted dykes and mantle rocks [e.g., *Gerbert-Gaillard*, 2002; *Godard et al.*, 2000; *Juteau et al.*, 1988a; *Kelemen et al.*, 1997a, 1997b; *Korenaga and Kelemen*, 1997; *Pearce et al.*, 1981; *Quatrevaux*, 1995; *Rochette et al.*, 1991] but they concern only isolated massifs and not the entire ophiolite. Moreover, as the exact sample location is often not precisely known, the data cannot be used to define the ophiolite segmentation pattern as we aim to do in this study.

3. Sampling Strategy

3.1. Main Characteristics of the Mantle Section

[11] The mantle section of the Oman ophiolite (5–10 km in thickness) is composed of harzburgites, commonly interpreted as residual rocks after partial melting of a lherzolitic mantle during the mantle rise under the active mid-oceanic ridge [e.g., *Nicolas*, 1989]. The mantle section also includes dunites that form discordant patches or layers parallel to the main foliation. In the transition zone, Cpx-rich dunites and wehrlites are abundant [*Jousselin and Nicolas*, 2000; *Juteau et al.*, 1988a, 1988b; *Nicolas*, 1986a, 1986b; *Reuber*, 1988]. Locally, discordant dykes of pyroxenites are cutting through the peridotites [e.g., *Benoit et al.*, 1996; *Braun and Kelemen*, 2002; *Kelemen et al.*, 1995; *Python and Ceuleneer*, 2003].

[12] The base of the mantle sequence locally consists of Cpx-harzburgites and lherzolites [*Braun and Kelemen*, 2002; *Godard et al.*, 2000; *Takazawa et al.*, 2003]. Generally, they are strongly serpentinized, a process generally linked to the ophiolite emplacement tectonics [*Rothery*, 1982]. This is not the case in the central and top parts of the sequence that are generally fresher, poorer than 40% serpentine. Peridotites from the base of the sequence are generally brecciated and display emplacement-related textures, acquired at intermediate to low temperatures. Most other peridotites have granoblastic to coarse-grained porphyroclastic textures thought to relate to asthenospheric deformation in a ridge setting [*Nicolas*, 1986a].

3.2. Sampling

[13] The mantle rocks have been sampled all along the ophiolite from the Khawr Fakkan massif in the North to the Sumail massif in the South (Figure 2). The samples, labeled "MAN#" and "So#," were respectively sampled during the 2000 and 2001 campaigns. There are 280 hand-specimens, picked with an average interval of 1.5 kilometers and located precisely with a portable Global Positioning Satellite System (see Table 1 for longitudes and latitudes). Some of the massifs like the Haylayn massif have been more densely sampled than others to test the representativeness of the sampling.

[14] At any given locale, the samples were taken from the least serpentinized and most representative rocks (Figure 3). Hence we sampled the most homogeneous peridotites, away from any layering or dykes (Figure 3a). At the thin section scale, some samples include less than 1 mm thick orthopyroxene clusters or micro-layers (Figures 3d and 3e) interpreted as stretched and transposed former Opx concentrations [*Le Mée et al.*, 2004].

[15] As far as possible, rocks were also sampled at the maximum possible distance from the paleo-Moho and the base of the ophiolite. For logistical reasons, many samples were collected on the western edge of the ophiolite (Figure 2) previously thought to correspond to the most serpentinized and tectonized rocks, and locally to primary lherzolites. But in fact, our data show (see section 4.2) that we never sampled the lherzolites described by

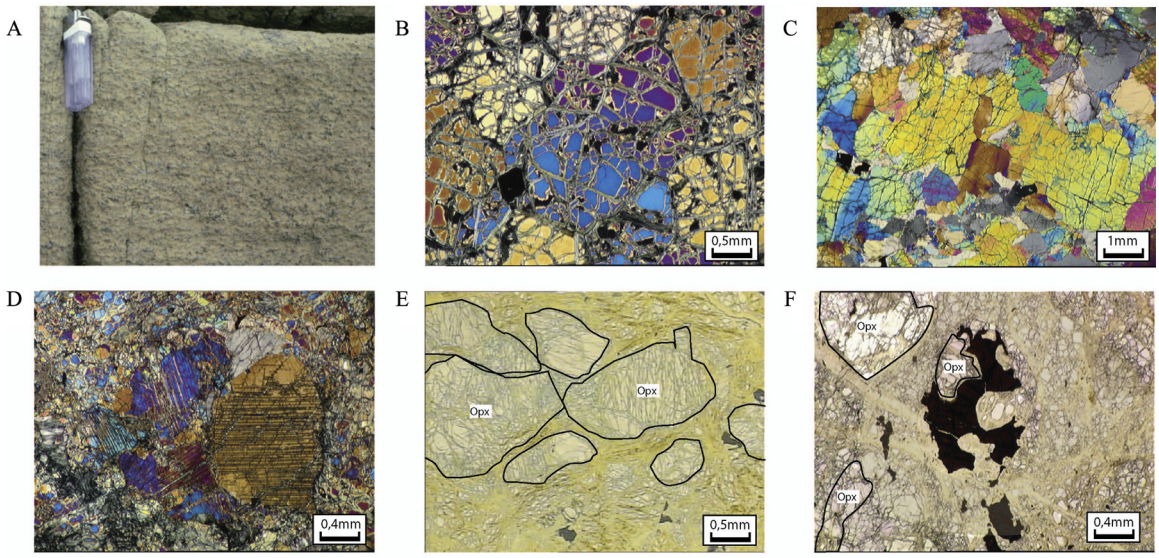

Figure 3. Petrographic photos of peridotites. (a) Typical harzburgite sampled in the field; (b) granoblastic and (c) porphyroclastic harzburgites with subidiomorphic spinels (crossed polarizers); (d and e) pyroxene clusters and micro-layer; (f) holly leaf spinel in association with Opx.

Takazawa et al. [2003], that the base samples are often not more serpentinized than the others, and that only 10% of our samples display emplacement-related structures.

4. Petrological and Geochemical Results

4.1. Analytical Methods

[16] For textural analyses and modal determination, thin sections were cut both perpendicular to the foliation and parallel to the lineation. Textures were described using the classification commonly used for mantle peridotites from massifs and xenoliths [*Harte*, 1977; *Mercier*, 1985; *Mercier and Nicolas*, 1975; *Nicolas*, 1986a]. The modal composition of peridotites has been obtained by image analysis following the procedure developed by *Launeau and Robin* [1996] (see Table 1). The standard deviation (SD) and the relative standard deviation (RDS) have been calculated after three successive image analyses on each one thin section.

[17] Major element compositions of minerals were analyzed using a Camebax SX50 electron microprobe (University of Brest, France). Major element compositions in whole rocks (WR) were analyzed, using an ICP-AES (JOBIN YVON 70 PLUS: University of Brest, France). The trace element compositions were analyzed by ICP-MS (Perkin-Elmer-Sciex Elan 6000: University of Toulouse, France). The data, limit of quantification and the standard deviations are presented in Table 7.

4.2. Peridotite Petrography and Textures

[18] The average Oman peridotites mode corresponds to a harzburgite with 85.2% olivine ($SD_{Olivine}$ = 5%), 13.6% orthopyroxene (SD_{Opx} = 5%), 0.6% clinopyroxene and 0.6% of spinel (SD_{Spinel} = 0.3%). In detail, 131 samples are harzburgites, 4 are lherzolites and 39 are dunites (pyroxenes <10%). Whereas the Opx average content in the harzburgite is nearly 15%, a few samples contain 20 to 27% modal Opx. This large Opx amount may result from the tectonic transposition of former orthopyroxenitic concentrations during plastic deformation. The 4 lherzolites contain 5 to 9.3% Cpx and less than 22% Opx, suggesting that these rocks are basal lherzolites probably restricted to small areas, as in the North of the Fizh massif [*Takazawa et al.*, 2003]. The dunites contain more than 90% olivine, 7.20% Opx and traces of Cpx (95% of the samples below 0.1%).

[19] The peridotites display three types of textures irrespective of their mineralogy: 30% have granoblastic textures (Figure 3b), 60% coarse-porphyroclastic textures (Figure 3c) and 10% fine-porphyroclastic to mylonitic textures in the sense defined by [*Harte*, 1977; *Mercier*, 1985; *Mercier and Nicolas*, 1975; *Nicolas*, 1986a]. In the granoblastic rocks, olivine is up to 4 to 5 mm in diameter, has subisotropic shapes with curvilinear

Table 2. Olivine Average Major Element Compositions From 739 Analyses[a]

Sample	Rock	N	SiO_2	TiO_2	Al_2O_3	FeO	MnO	MgO	CaO	Cr_2O_3	NiO	Na_2O	K_2O	P_2O_5	SO_2	Total	Mg#
MAN 01	Hz	3	41.13	-	0.01	9.53	0.16	49.93	0.01	0.04	0.38	0.02	0.01	0.02	-	101.24	0.904
MAN 03	Hz	3	41.17	0.02	0.02	9.61	0.17	49.35	0.03	0.05	0.27	0.01	-	0.04	-	100.73	0.902
MAN 06	Du	3	41.55	0.05	0.02	9.25	0.15	50.51	0.01	0.01	0.36	0.00	-	0.05	-	101.96	0.908
MAN 07	Du	7	41.19	0.03	0.02	9.09	0.13	50.25	0.02	0.03	0.37	0.01	0.02	0.01	0.01	101.18	0.909
MAN 08	Du	5	41.29	-	0.03	8.91	0.14	50.29	0.02	0.04	0.32	0.01	0.02	0.02	0.01	101.09	0.910
MAN 09	Hz	5	41.28	0.01	0.02	9.35	0.13	50.12	0.01	0.02	0.34	0.01	-	0.01	0.03	101.32	0.906
MAN 10	Hz	4	41.20	0.02	0.02	9.14	0.12	49.69	0.01	0.04	0.33	0.01	0.01	-	0.02	100.60	0.907
MAN 11	Hz	4	41.32	0.01	0.02	8.45	0.12	50.63	0.01	-	0.33	0.01	0.01	0.01	0.05	100.96	0.915
MAN 13	Hz	5	41.22	0.03	0.02	9.00	0.11	50.22	0.01	0.04	0.35	0.01	-	-	0.02	101.02	0.909
MAN 14	Hz	5	41.54	0.02	0.02	9.06	0.09	50.02	0.02	0.02	0.40	0.01	0.02	0.02	0.02	101.25	0.908
MAN 20	Hz	5	41.28	0.06	0.02	9.30	0.11	49.66	0.03	0.08	0.30	-	-	-	-	100.86	0.906
MAN 21	Hz	6	41.60	0.03	0.01	9.05	0.10	50.16	0.03	0.08	0.39	-	-	-	-	101.44	0.909
MAN 23	Hz	7	41.16	0.01	0.02	9.74	0.16	49.86	0.02	0.02	0.39	0.01	0.01	0.02	0.03	101.46	0.902
MAN 24	Hz	3	41.41	0.06	0.01	8.31	0.11	50.53	-	0.09	0.18	-	-	-	-	100.70	0.916
MAN 25	Hz	4	41.50	0.01	0.01	8.88	0.15	50.59	0.03	0.02	0.39	-	-	-	-	101.58	0.911
MAN 26	Du	3	41.71	0.04	0.02	9.00	0.14	50.48	0.02	0.03	0.44	-	-	-	-	101.88	0.910
MAN 27	Hz	4	41.91	0.07	0.06	8.89	0.13	50.42	0.03	0.06	0.42	-	-	-	-	101.98	0.911
MAN 28	Hz	4	41.61	0.01	0.01	9.34	0.13	50.08	0.01	0.01	0.26	-	-	-	-	101.46	0.906
MAN 29	Du	-	-	-	-	-	-	-	-	-	-	-	-	-	-	-	-
MAN 30	Hz	-	-	-	-	-	-	-	-	-	-	-	-	-	-	-	-
MAN 32	Hz	3	41.01	0.03	0.02	9.60	0.11	49.95	0.02	0.03	0.28	0.01	0.00	-	0.05	101.11	0.903
MAN 33	Du	4	41.52	0.02	0.01	9.40	0.12	49.87	0.01	0.05	0.35	-	-	-	-	101.35	0.905
MAN 34	Hz	4	41.23	0.01	0.01	9.06	0.13	50.25	0.02	0.04	0.29	0.01	0.01	-	0.06	101.12	0.909
MAN 35	Hz	5	41.06	0.03	0.03	9.83	0.10	49.98	0.01	0.04	0.41	0.01	0.01	0.01	0.04	101.56	0.901
MAN 37	Hz	3	41.30	0.02	0.01	9.53	0.16	49.93	0.01	0.04	0.31	0.01	-	0.02	0.05	101.38	0.904
MAN 39	Hz	3	41.47	0.00	0.01	9.11	0.10	50.29	0.02	0.08	0.42	0.00	0.01	0.01	0.01	101.54	0.908
MAN 40	Hz	3	40.88	0.02	0.02	9.44	0.13	49.90	0.01	0.00	0.39	0.01	-	-	0.01	100.82	0.905
MAN 41	Du	3	41.05	0.01	0.01	9.69	0.16	50.00	0.03	-	0.37	0.01	0.01	0.03	0.02	101.39	0.903
MAN 42	Hz	3	41.17	0.00	0.03	9.08	0.12	49.98	0.07	0.02	0.32	0.01	-	0.02	0.04	100.88	0.908
MAN 44	Hz	5	41.44	0.01	0.01	8.99	0.14	50.49	0.02	0.02	0.40	0.01	0.01	0.02	0.03	101.58	0.910
MAN 48	Hz	3	41.35	0.01	0.01	8.86	0.11	50.09	0.02	0.01	0.38	0.01	0.01	-	0.05	100.92	0.910
MAN 50	Hz	4	40.99	0.01	0.02	9.37	0.21	49.84	0.02	0.03	0.36	0.00	0.02	0.03	0.03	100.92	0.905
MAN 55	Du	3	41.09	0.02	0.04	8.77	0.15	49.93	0.04	0.04	0.39	0.02	-	0.07	-	100.56	0.911
MAN 56	Hz	4	41.11	0.03	0.04	8.91	0.16	50.96	0.01	0.07	0.40	0.01	-	0.05	-	101.75	0.911
MAN 57	Du	4	41.07	0.03	0.00	9.05	0.19	50.19	0.01	0.02	0.51	0.01	0.01	0.02	-	101.13	0.909
MAN 58	Hz	6	41.34	0.04	0.02	8.92	0.14	50.19	0.01	-	0.41	0.00	0.02	0.02	0.02	101.14	0.910
MAN 59	Hz	3	40.95	0.02	0.02	9.15	0.17	49.71	-	0.01	0.43	-	-	0.04	-	100.50	0.907
MAN 60	Du	5	41.29	0.01	0.03	9.34	0.12	49.74	0.02	0.07	0.40	0.04	0.02	0.04	-	101.12	0.905
MAN 62	Hz	4	41.33	0.01	0.01	9.16	0.14	50.15	0.03	0.06	0.44	0.01		0.06	-	101.39	0.908
MAN 63	Du	4	41.41	0.02	0.04	8.82	0.18	49.78	0.01	-	0.36	0.01	0.01	0.07	-	100.72	0.910
MAN 67	Hz	5	41.65	-	0.04	9.12	0.11	50.19	0.01	0.05	0.34	0.01	0.01	0.02	-	101.53	0.908
MAN 68	Du	8	41.32	0.02	0.04	8.79	0.11	50.55	0.03	0.04	0.38	0.01	0.01	0.04	-	101.33	0.912
MAN 70	Hz	4	41.15	0.02	0.02	9.00	0.15	50.57	0.01	0.00	0.41	0.01	0.03	0.03	-	101.39	0.910
MAN 72	Du	6	41.44	0.03	0.03	9.13	0.11	50.44	0.03	0.04	0.46	0.01	0.03	0.04	-	101.78	0.908
MAN 73	Hz	10	41.43	0.03	0.05	8.76	0.12	50.28	0.03	0.07	0.45	0.02	0.03	0.03	-	101.28	0.912
MAN 77	Hz	5	41.17	0.04	0.03	9.53	0.14	49.57	0.02	0.06	0.35	0.02	0.00	0.05	-	100.97	0.903
MAN 78	Du	4	41.14	0.00	0.04	9.41	0.14	49.75	0.03	0.02	0.37	0.02	0.01	0.07	-	101.00	0.905
MAN 79	Du	3	41.39	0.06	0.02	8.53	0.18	50.40	0.03	0.07	0.44	-	0.03	0.05	-	101.18	0.914
MAN 80	Hz	3	41.25	0.02	0.03	9.56	0.12	49.38	-	0.07	0.38	-	0.00	0.03	-	100.86	0.903
MAN 81	Hz	3	41.04	0.03	0.01	9.25	0.19	49.75	0.02	-	0.46	0.02	0.01	-	-	100.76	0.906
MAN 82	Hz	3	41.41	0.00	0.02	9.35	0.18	50.62	-	0.03	0.44	0.01	0.01	0.01	-	102.09	0.907
MAN 83	Hz	-	-	-	-	-	-	-	-	-	-	-	-	-	-	-	-
MAN 84	Du	4	41.59	0.03	-	9.10	0.15	50.70	0.02	0.06	0.53	0.01	0.01	0.02	-	102.22	0.909
MAN 85	Du	4	41.12	0.02	0.03	9.05	0.11	50.45	0.03	0.03	0.47	0.03	0.00	0.04	-	101.37	0.909
MAN 86	Hz	4	41.57	0.04	0.02	8.48	0.09	50.86	0.03	0.12	0.39	0.00	0.00	-	-	101.61	0.915
MAN 87	Du	9	40.88	0.04	0.04	8.67	0.15	50.49	0.02	0.04	0.39	0.01	0.02	0.05	-	100.79	0.913
MAN 89	Du	4	41.05	0.01	0.03	8.83	0.14	50.56	0.02	0.06	0.47	0.01	-	0.03	-	101.21	0.911
MAN 92	Hz	4	41.50	0.02	0.03	8.94	0.15	50.63	0.03	0.09	0.25	0.02	0.01	0.02	-	101.70	0.910
MAN 93	Hz	3	41.42	0.00	0.01	8.37	0.20	50.43	0.02	0.11	0.36	0.01	0.00	0.02	-	100.95	0.915
MAN 94	Hz	4	41.50	0.04	0.04	9.31	0.13	50.53	0.02	0.04	0.40	0.03	0.01	0.02	-	102.06	0.907
MAN 95	Hz	4	40.74	0.01	0.18	9.28	0.11	49.66	0.04	0.05	0.33	0.02	-	0.08	-	100.50	0.906
MAN 96	Du	5	41.14	0.02	0.02	9.15	0.12	50.41	0.04	0.07	0.38	0.02	0.01	0.02	-	101.41	0.908

Table 2. (continued)

Sample	Rock	N	SiO_2	TiO_2	Al_2O_3	FeO	MnO	MgO	CaO	Cr_2O_3	NiO	Na_2O	K_2O	P_2O_5	SO_2	Total	Mg#
MAN 98	Du	4	41.28	0.03	0.02	9.41	0.13	50.19	0.03	0.04	0.46	0.01	0.01	0.04	-	101.65	0.906
MAN 99	Hz	5	41.49	0.02	0.04	9.18	0.13	49.95	0.05	0.08	0.43	0.01	0.02	0.06	-	101.44	0.907
MAN 101	Hz	6	41.08	0.04	0.02	9.48	0.12	50.37	0.03	0.09	0.42	0.02	0.02	-	-	101.68	0.905
MAN 103	Hz	4	41.24	0.03	0.03	9.27	0.10	50.03	0.02	0.11	0.32	0.02	-	0.05	-	101.21	0.907
MAN 105	Hz	3	40.34	0.05	0.02	9.28	0.08	49.92	0.02	0.01	0.36	0.01	-	0.01	-	100.10	0.906
MAN 107	Hz	3	40.52	0.01	0.02	8.69	0.18	50.12	0.06	0.04	0.41	0.02	0.01	0.02	-	100.10	0.912
MAN 109	Hz	3	40.47	-	0.02	9.12	0.15	49.87	0.07	0.07	0.37	0.02	0.04	0.04	-	100.23	0.908
MAN 110	Hz	4	41.27	-	0.02	9.30	0.17	50.08	0.01	0.09	0.40	0.04	-	-	-	101.36	0.906
MAN 111	Hz	4	40.85	0.02	0.03	8.93	0.15	50.55	0.01	0.02	0.38	0.02	0.02	0.01	-	101.00	0.910
MAN 112	Hz	4	41.02	0.03	0.01	9.68	0.18	49.82	0.01	0.08	0.40	0.02	0.01	0.01	-	101.28	0.902
MAN 113	Hz	4	41.20	0.01	0.02	9.32	0.09	50.07	0.01	0.06	0.40	0.01	0.02	0.02	-	101.23	0.906
MAN 114	Du	8	41.44	0.02	0.02	9.09	0.12	50.63	0.01	0.03	0.37	0.01	0.01	0.03	-	101.79	0.909
MAN 115	Hz	3	40.93	0.05	0.02	9.51	0.09	50.19	0.01	0.02	0.30	0.01	0.03	0.03	-	101.19	0.905
MAN 116	Hz	4	40.96	0.05	0.02	9.35	0.11	50.14	0.01	0.05	0.39	0.01	0.01	0.02	-	101.12	0.906
MAN 117	Hz	5	41.44	0.01	0.02	9.38	0.15	50.27	0.03	0.02	0.45	0.03	0.01	0.03	-	101.83	0.906
MAN 149	Hz	3	41.86	-	0.02	8.62	0.12	50.24	0.04	0.00	0.38	-	-	-	-	101.28	0.913
MAN 150	Hz	3	41.47	-	0.02	8.29	0.13	50.31	0.02	0.06	0.41	-	-	-	-	100.69	0.916
MAN 151	Du	4	41.55	0.05	0.03	8.92	0.13	49.87	0.04	0.01	0.29	-	-	-	-	100.89	0.909
MAN 153	Hz	5	41.70	0.03	0.02	9.19	0.11	50.11	0.03	0.02	0.29	-	-	-	-	101.50	0.907
MAN 155	Hz	7	41.48	0.04	0.01	9.43	0.13	50.29	0.02	0.05	0.38	-	-	-	-	101.83	0.905
MAN 157	Du	6	41.40	0.02	0.02	9.00	0.11	49.99	0.03	0.09	0.35	-	-	-	-	101.00	0.909
So_2	Hz	3	41.08	0.04	0.01	8.51	0.09	50.85	0.01	0.03	0.39	0.01	0.01	0.04	-	101.07	0.915
So_3	Hz	8	41.17	0.08	0.00	9.04	0.10	50.17	0.01	0.04	0.38	0.01		0.03	-	101.02	0.909
So_4	Lz	4	41.01	0.01	0.02	9.41	0.13	50.05	0.01	0.02	0.42	0.00	0.01	0.04	-	101.13	0.905
So_7	Hz	5	41.19	0.02	0.01	9.16	0.10	50.54	0.00	0.01	0.47	0.02	0.01	0.04	-	101.57	0.908
So_9	Hz	2	41.29	0.03	0.02	9.37	0.12	50.12	0.01	0.04	0.41	0.00	0.01	0.03	-	101.45	0.906
So_10	Du	5	41.19	0.00	0.03	9.45	0.15	49.76	0.01	0.04	0.49	0.03	0.02	-	-	101.19	0.904
So_11	Hz	5	40.98	0.03	0.02	9.36	0.10	50.35	0.00	0.03	0.38	0.01	0.01	0.02	-	101.30	0.906
So_15	Hz	3	41.18	-	0.05	9.53	0.10	49.66	-	0.10	0.37	0.00	0.03	0.08	-	101.11	0.903
So_16	Hz	4	41.12	0.02	0.03	9.27	0.12	50.07	0.00	0.03	0.40	0.01	0.01	0.02	-	101.09	0.907
So_17	Hz	4	41.17	0.02	0.01	9.50	0.15	49.94	0.01	0.04	0.39	0.01	-	-	-	101.25	0.904
So_19	Du	3	41.11	0.02	0.02	8.92	0.13	50.10	0.02	0.01	0.45	0.00	0.02	0.03	-	100.84	0.910
So_21	Hz	6	41.32	0.03	0.04	9.08	0.13	50.31	0.01	0.03	0.41	0.00	-	0.01	-	101.38	0.909
So_24	Hz	4	41.26	-	0.04	8.60	0.12	51.00	0.02	0.08	0.38	0.01	0.01	0.01	-	101.53	0.914
So_25	Hz	7	41.19	0.02	0.01	9.03	0.15	50.24	0.00	0.02	0.43	0.02	-	0.03	-	101.15	0.909
So_56	Hz	4	41.13	0.02	0.01	9.43	0.09	49.61	0.02	0.06	0.37	0.01	-	0.04	-	100.79	0.904
So_57	Hz	3	41.01	0.02	0.03	9.34	0.12	49.53	0.03	0.03	0.34	0.01	-	0.03	-	100.47	0.905
So_58	Hz	5	41.43	0.01	0.04	8.71	0.16	50.48	0.01	0.04	0.44	0.02	0.01	0.00	-	101.35	0.912
So_59	Hz	4	41.36	-	0.03	9.13	0.13	50.01	0.04	0.02	0.39	0.01	0.03	0.06	-	101.21	0.908
So_60	Du	3	41.54	0.07	0.04	9.23	0.17	49.61	0.04	0.08	0.42	0.02	0.01	0.04	-	101.26	0.906
So_61	Hz	4	41.40	0.03	0.03	9.34	0.14	49.99	0.04	0.01	0.36	0.02	0.04	0.06	-	101.48	0.906
So_62	Hz	3	41.47	0.03	0.02	9.08	0.09	49.71	0.04	0.08	0.53	-	0.02	0.02	-	101.09	0.908
So_63	Hz	4	41.34	0.02	0.04	9.50	0.17	49.60	0.04	0.04	0.28	0.01	-	0.04	-	101.08	0.904
So_65	Hz	4	41.47	0.03	0.01	9.22	0.12	50.34	0.01	0.09	0.42	0.01	-	-	-	101.72	0.907
So_66	Hz	4	41.44	0.06	-	8.97	0.09	49.82	0.03	0.03	0.52	0.01	0.02	0.01	-	101.01	0.909
So_67	Hz	4	41.16	0.03	0.04	9.20	0.11	49.48	0.01	0.06	0.38	0.01	0.02	0.01	-	100.52	0.906
So_68	Hz	4	41.39	0.02	0.01	9.08	0.11	49.89	0.00	0.04	0.46	0.01	-	-	-	101.00	0.908
So_70	Lz	5	41.53	-	0.03	9.48	0.14	49.44	0.03	0.04	0.38	0.01	0.01	0.03	-	101.13	0.904
So_71	Hz	4	41.45	0.03	0.01	9.02	0.16	50.00	-	0.01	0.47	-	0.00	0.06	-	101.20	0.909
So_72	Hz	6	41.25	0.03	0.04	9.45	0.13	49.72	0.04	0.05	0.44	0.03	0.01	0.02	-	101.20	0.904
So_74	Hz	4	41.32	0.00	0.03	9.36	0.09	49.70	0.02	0.08	0.52	0.01	0.01	0.02	-	101.16	0.905
So_75	Hz	4	41.01	-	0.03	9.32	0.19	49.92	0.01	0.10	0.37	0.02	0.01	-	-	100.99	0.906
So_76	Hz	3	40.96	-	0.01	8.72	0.19	49.69	0.02	0.04	0.42	0.01	-	0.01	-	100.07	0.911
So_77	Hz	4	41.34	0.02	0.04	8.85	0.14	49.74	0.02	0.03	0.34	0.01	0.02	0.04	-	100.59	0.910
So_78	Hz	4	41.22	0.03	0.03	8.91	0.16	49.88	0.01	0.01	0.38	0.01	0.00	-	-	100.64	0.910
So_79	Hz	4	41.37	-	0.03	8.71	0.15	50.21	0.03	0.08	0.36	0.03	-	0.07	-	101.04	0.912
So_80	Du	4	41.24	0.02	0.01	8.47	0.13	50.60	0.01	0.02	0.40	0.01	0.00	0.02	-	100.93	0.915
So_81	Hz	4	41.32	0.03	0.02	8.54	0.14	50.49	0.05	0.03	0.37	0.02		0.03	-	101.06	0.914
So_82	Hz	4	41.48	0.05	0.01	9.28	0.11	49.72	0.02	0.05	0.38	0.02	0.03	0.04	-	101.18	0.906
So_83	Hz	7	41.37	-	0.01	9.37	0.10	50.30	0.03	0.06	0.38	0.01	-	0.03	-	101.65	0.906
So_84	Hz	4	41.19	0.00	0.02	9.10	0.15	49.66	0.03	0.08	0.35	0.01	0.04	-	-	100.63	0.907
So_85	Hz	5	41.50	0.02	0.03	8.78	0.15	50.24	0.03	0.05	0.48	0.03	-	0.01	-	101.32	0.911

Table 2. (continued)

Sample	Rock	N	SiO_2	TiO_2	Al_2O_3	FeO	MnO	MgO	CaO	Cr_2O_3	NiO	Na_2O	K_2O	P_2O_5	SO_2	Total	Mg#
So_87	Du	3	41.03	0.02	0.02	8.99	0.15	49.99	0.02	0.01	0.42	0.03	0.02	0.01	-	100.71	0.909
So_88	Hz	5	41.26	0.01	0.03	9.65	0.14	50.01	0.05	0.05	0.35	0.04	0.00	0.03	-	101.62	0.903
So_89	Du	8	41.16	0.02	0.03	9.16	0.17	50.15	0.05	0.09	0.34	0.01	0.02	0.03	-	101.21	0.908
So_90	Hz	4	41.28	0.00	0.01	9.32	0.10	49.63	0.03	0.03	0.48	0.02	0.01	0.03	-	100.94	0.905
So_91	Hz	6	41.14	0.03	0.02	9.75	0.14	49.64	0.04	0.09	0.42	0.01	-	0.04	-	101.33	0.901
So_92	Hz	5	41.13	0.04	0.00	9.89	0.14	49.71	0.04	0.09	0.39	0.02	0.02	-	-	101.47	0.900
So_94	Hz	5	41.38	0.03	0.03	9.34	0.17	50.22	0.04	0.03	0.39	0.02	0.03	0.01	-	101.70	0.906
So_95	Du	5	41.37	0.04	0.02	9.11	0.13	49.95	0.03	0.04	0.35	0.02	0.02	0.02	-	101.09	0.908
So_96	Lz	3	41.00	0.05	0.03	9.45	0.12	49.03	0.03	0.14	0.40	0.03	0.02	-	-	100.30	0.903
So_100	Du	3	41.31	0.00	0.02	9.55	0.11	49.38	0.04	0.01	0.35	0.03	0.01	0.02	-	100.83	0.903
So_101	Hz	4	41.46	0.05	0.02	8.75	0.10	50.57	0.03	0.02	0.47	0.01	0.01	0.00	-	101.50	0.912
So_102	Hz	6	41.30	-	0.02	9.48	0.13	50.04	0.05	0.04	0.41	0.02	0.01	0.03	-	101.55	0.905
So_104	Hz	5	41.58	0.03	0.03	9.07	0.20	50.49	0.03	0.10	0.39	0.00	0.01	0.01	-	101.95	0.909
So_105	Hz	3	41.33	0.01	0.01	8.45	0.16	50.09	0.01	0.06	0.42	0.01	-	-	-	100.55	0.914
So_106	Hz	4	41.51	0.02	0.02	8.87	0.11	50.06	0.05	0.04	0.46	0.03	0.02	0.02	-	101.22	0.910
So_107	Hz	5	41.07	0.04	0.02	8.91	0.16	49.47	0.03	0.04	0.43	0.01	0.02	0.05	-	100.25	0.909
So_108	Hz	6	41.29	0.02	0.02	9.39	0.11	50.10	0.03	0.02	0.36	0.02	0.01	0.03	-	101.41	0.906
So_109	Hz	5	41.32	0.02	0.01	9.50	0.16	50.03	0.02	0.08	0.35	0.01	0.01	0.04	-	101.54	0.904
So_110	Hz	5	41.39	0.01	0.01	8.93	0.15	50.20	0.03	0.06	0.42	0.01	0.03	0.01	-	101.25	0.910
So_111	Hz	5	41.66	0.04	0.03	9.33	0.11	49.79	0.03	0.11	0.34	0.02	-	0.06	-	101.52	0.906
So_112	Du	4	41.73	0.03	0.00	8.45	0.14	50.90	0.03	0.04	0.33	0.04	0.02	-	-	101.72	0.915
So_113	Du	4	41.67	0.01	-	9.05	0.11	50.73	0.06	0.06	0.43	0.04	0.01	0.03	-	102.19	0.910
So_114	Hz	5	41.11	0.03	0.01	9.32	0.14	49.85	0.03	0.07	0.49	0.01	0.00	0.03	-	101.09	0.906
So_115	Du	4	41.39	0.06	0.02	9.13	0.11	50.06	0.02	0.07	0.43	0.02	0.01	0.04	-	101.36	0.908
So_116	Hz	4	41.21	-	0.02	9.11	0.10	50.03	0.04	0.06	0.41	0.02	0.03	0.08	-	101.10	0.908
So_117	Du	3	41.47	0.03	0.01	8.78	0.13	50.06	0.01	0.07	0.31	0.01	0.03	0.01	-	100.92	0.911
So_118	Hz	5	41.53	0.03	0.02	8.78	0.13	50.23	0.02	-	0.35	0.02	0.02	0.01	-	101.14	0.911
So_119	Hz	4	41.14	0.03	0.06	9.27	0.14	49.89	0.04	0.07	0.40	0.02	0.02	-	-	101.07	0.906
So_120	Du	3	41.09	-	0.01	8.42	0.20	50.31	0.02	0.05	0.40	0.03	0.01	0.00	-	100.53	0.915
So_122	Hz	3	41.12	0.01	-	9.54	0.06	49.20	0.07	0.04	0.30	0.01	-	0.10	-	100.44	0.903
So_124	Hz	3	41.24	0.02	0.02	9.39	0.10	49.60	0.02	0.09	0.38	0.02	0.02	0.04	-	100.95	0.905
So_125	Hz	4	41.49	0.03	0.07	8.38	0.07	50.30	0.04	0.06	0.45	0.00	-	0.05	-	100.94	0.915
So_126	Hz	4	41.18	0.01	0.01	9.51	0.13	50.01	0.04	0.07	0.47	0.02	0.01	0.00	-	101.46	0.904
So_127	Hz	5	41.49	0.07	0.02	8.87	0.13	50.44	0.04	0.07	0.40	0.01	0.02	0.03	-	101.59	0.911
So_128	Hz	5	41.40	0.01	0.02	9.25	0.12	49.87	0.02	0.02	0.36	0.02	0.01	0.04	-	101.14	0.906
So_130	Hz	5	41.36	0.04	0.02	9.51	0.16	50.00	0.04	0.04	0.44	0.02	0.00	0.03	-	101.67	0.904
So_132	Hz	5	41.07	0.04	0.00	9.14	0.15	50.45	0.02	0.02	0.43	0.02	0.01	0.01	-	101.35	0.908
So_134	Hz	12	40.09	0.02	0.02	9.30	0.16	49.75	0.03	0.08	0.41	0.02	0.01	0.02	-	99.93	0.906
So_135	Hz	6	41.20	0.03	0.01	8.63	0.10	50.75	0.04	0.05	0.28	0.02	0.02	0.00	-	101.14	0.914
So_136	Hz	3	40.63	-	-	8.83	0.08	50.07	0.01	0.08	0.39	0.01	-	0.02	-	100.11	0.911
So_137	Du	3	40.12	0.02	-	9.20	0.16	50.23	0.03	0.04	0.36	0.00	0.01	0.01	-	100.18	0.907
So_139	Hz	3	40.50	0.06	0.02	9.27	0.12	50.24	0.04	0.07	0.44	0.02	-	0.07	-	100.84	0.907
So_140	Hz	3	40.17	0.02	0.03	8.51	0.11	50.40	0.02	0.03	0.34	0.01	-	0.03	-	99.67	0.914
So_141	Hz	3	40.31	0.02	0.01	9.70	0.17	49.78	0.38	-	0.27	0.01	0.03	0.07	-	100.75	0.902
So_142	Lz	3	40.30	0.06	0.03	9.82	0.20	49.34	0.01	0.01	0.46	-	0.02	0.07	-	100.32	0.900
So_143	Du	5	40.32	0.00	0.02	8.66	0.19	49.94	0.02	0.06	0.35	0.02	0.00	0.03	-	99.60	0.912
So_144	Hz	5	40.29	0.02	0.02	10.16	0.14	49.76	0.01	0.02	0.37	0.02	-	0.06	-	100.88	0.898
So_145	Hz	3	40.61	-	0.03	9.19	0.11	49.98	0.01	0.05	0.37	0.00	0.01	0.02	-	100.38	0.907
So_148	Hz	3	40.26	-	0.00	8.87	0.14	50.00	0.03	0.03	0.39	0.03	-	-	-	99.75	0.910
94-46	Hz	3	41.37	0.00	0.04	8.73	0.13	49.81	-	0.01	0.25	-	-	-	-	100.35	0.911

[a] The "N" value indicates the number of analyses per sample. Mg# is molar $Mg^{2+}/(Mg^{2+} + Fe^{2+})$. Olivines were systematically analyzed in the core zones. Operating conditions of the microprobe: accelerating voltage: 15 kV; beam current: 12 nA; 20 to 30 seconds/cycle counting time; beam diameter: 1 micron. Synthetic oxides and natural minerals were used as standards for calibration. A selection of unaltered and well-polished minerals has been analyzed, and minerals in contact have been preferentially chosen to test the equilibrium of the primary paragenesis. In each sample, variability of mineral compositions was tested by several measurements on 3 minerals at least. The calculated Relative Standard Deviations (RSD) for the most abundant elements are as follows: $RSD_{Si} < 0.45\%$; $RSD_{Al} < 1.91\%$; $RSD_{Fe} < 1.5\%$; $RSD_{Mg} < 0.45\%$; $RSD_{Cr} < 0.37\%$; $RSD_{Ca} < 0.43\%$.

boundaries and rarely displays kink-bands. Orthopyroxenes form equant 1 to 4 mm isolated crystals or more rarely constitute small aggregates. Clinopyroxenes either form small blebs exsolved from Opx or 1 to 3 mm size crystals in contact with Opx. These rocks contain mostly 1 to 3 mm long brown-colored holly leaf-shaped spinels (type 1 spinels, Figure 3f) that are commonly in association with

Table 3. Opx Average Major Element Compositions From 689 Analyses[a]

Sample	Rock	N	SiO_2	TiO_2	Al_2O_3	FeO	MnO	MgO	CaO	Cr_2O_3	NiO	Na_2O	K_2O	P_2O_5	SO_2	Total	Mg#	Cr#
MAN 01	Hz	4	56.03	0.03	2.82	6.58	0.15	33.74	1.04	0.63	0.10	0.01	0.02	0.03	-	101.17	0.902	0.262
MAN 03	Hz	3	56.52	0.07	2.66	6.30	0.18	33.64	0.86	0.68	0.03	0.02	0.02	-	-	100.97	0.906	0.296
MAN 06	Du	3	57.05	0.07	1.96	6.13	0.17	34.43	0.80	0.67	0.15	0.02	-	0.03	-	101.47	0.910	0.379
MAN 07	Du	6	56.62	0.00	1.73	6.07	0.16	34.31	0.95	0.53	0.08	0.01	0.01	-	0.02	100.49	0.910	0.341
MAN 08	Du	5	56.43	0.02	2.02	5.53	0.13	33.70	1.66	0.68	0.05	0.01	0.00	0.03	0.01	100.27	0.916	0.370
MAN 09	Hz	6	56.52	0.02	1.93	5.97	0.16	33.59	1.79	0.68	0.10	0.01	0.01	0.02	0.02	100.81	0.910	0.385
MAN 10	Hz	3	56.70	-	2.13	6.23	0.15	34.38	0.67	0.49	0.06	0.01	0.00	0.01	0.03	100.87	0.908	0.271
MAN 11	Hz	4	56.32	0.02	2.68	5.37	0.16	33.92	1.14	0.80	0.06	0.01	0.01	0.03	-	100.52	0.919	0.335
MAN 13	Hz	5	56.58	-	2.22	5.79	0.17	33.47	2.02	0.79	0.05	0.01	0.00	0.02	0.02	101.14	0.912	0.388
MAN 14	Hz	4	57.29	0.04	1.77	5.91	0.14	34.28	0.79	0.68	0.06	0.01	0.01	0.01	0.02	101.00	0.912	0.410
MAN 20	Hz	7	56.79	0.06	2.30	6.16	0.20	33.72	0.92	0.66	0.08	0.02	-	-	-	100.91	0.908	0.325
MAN 21	Hz	6	57.10	0.03	2.00	6.15	0.15	34.12	0.77	0.65	0.10	0.02	0.01	-	-	101.10	0.909	0.361
MAN 23	Hz	3	55.54	0.02	3.20	6.16	0.09	32.97	1.68	0.89	0.11	0.01	-	0.01	0.01	100.68	0.906	0.315
MAN 24	Hz	11	57.09	0.05	2.39	5.70	0.15	34.43	0.66	0.51	0.07	0.01	0.04	-	-	101.09	0.916	0.251
MAN 25	Hz	4	57.10	0.04	2.11	5.72	0.10	34.34	0.97	0.75	0.12	-	0.01	0.00	-	101.25	0.915	0.384
MAN 26	Du	5	57.45	0.02	2.14	5.63	0.11	33.87	1.81	0.75	0.08	0.02	0.02	-	-	101.91	0.915	0.385
MAN 27	Hz	6	57.30	0.06	2.35	5.71	0.16	34.28	0.98	0.69	0.19	0.02	0.01	-	-	101.76	0.915	0.334
MAN 28	Hz	6	57.48	0.04	2.26	6.05	0.20	33.86	1.38	0.69	0.09	0.02	0.02	-	-	102.08	0.909	0.343
MAN 29	Du	-	-	-	-	-	-	-	-	-	-	-	-	-	-	-	-	-
MAN 30	Hz	-	-	-	-	-	-	-	-	-	-	-	-	-	-	-	-	-
MAN 32	Hz	2	55.93	0.05	3.30	6.25	0.22	33.71	0.90	0.55	-	0.02	0.02	-	0.01	100.94	0.906	0.202
MAN 33	Du	4	56.97	0.04	2.82	6.14	0.20	34.06	0.71	0.57	0.15	0.02	0.02	-	-	101.69	0.909	0.241
MAN 34	Hz	4	56.11	0.05	3.10	5.83	0.13	33.75	0.95	0.68	0.08	0.01	0.01	0.03	0.01	100.74	0.912	0.258
MAN 35	Hz	3	55.65	0.01	3.15	6.36	0.16	33.16	1.35	0.74	0.10	0.01	-	-	0.05	100.73	0.904	0.272
MAN 37	Hz	5	56.00	0.01	2.98	6.14	0.13	33.06	1.86	0.71	0.07	0.01	0.02	-	0.03	101.03	0.906	0.278
MAN 39	Hz	4	56.57	0.02	1.70	5.64	0.13	33.13	2.62	0.60	0.11	0.01	-	0.02	0.04	100.58	0.913	0.385
MAN 40	Hz	4	56.73	0.03	1.86	5.93	0.12	34.21	0.89	0.60	0.10	0.01	-	0.01	-	100.47	0.912	0.359
MAN 41	Du	4	56.37	0.02	2.17	6.05	0.16	33.72	1.30	0.69	0.09	-	0.01	0.01	0.02	100.60	0.909	0.352
MAN 42	Hz	5	56.21	0.02	2.72	6.03	0.12	33.15	2.04	0.80	0.04	0.01	-	0.02	0.02	101.19	0.908	0.331
MAN 44	Hz	4	56.93	0.01	1.63	5.73	0.21	34.13	1.59	0.61	0.13	0.01	0.02	0.01	0.05	101.06	0.915	0.403
MAN 48	Hz	4	56.74	0.01	1.98	5.87	0.13	33.70	1.87	0.77	0.07	0.01	0.01	0.06	0.01	101.24	0.912	0.416
MAN 50	Hz	4	56.68	0.05	1.83	5.86	0.12	33.21	2.22	0.71	0.13	0.01	-	0.02	0.01	100.84	0.911	0.415
MAN 55	Du	4	57.16	0.06	1.49	5.98	0.14	34.34	0.80	0.65	0.16	0.02	0.01	0.04	-	100.87	0.912	0.464
MAN 56	Hz	4	56.35	0.01	2.10	5.22	0.06	31.94	4.69	0.73	0.12	0.04	-	0.03	-	101.30	0.917	0.389
MAN 57	Du	3	56.16	0.01	2.13	5.69	0.09	33.41	1.75	0.81	0.05	0.01	0.04	0.01	-	100.16	0.913	0.409
MAN 58	Hz	6	57.49	0.01	1.35	5.81	0.16	34.44	1.27	0.53	0.11	0.00	-	0.04	0.01	101.24	0.914	0.419
MAN 59	Hz	4	56.98	0.04	1.94	5.51	0.13	34.34	0.91	0.68	0.10	0.01	-	-	-	100.65	0.918	0.385
MAN 60	Du	3	56.53	0.02	1.84	5.83	0.16	33.81	1.11	0.58	0.14	0.02	0.02	0.06	-	100.13	0.912	0.356
MAN 62	Hz	3	56.83	0.02	1.91	5.95	0.19	34.17	1.05	0.61	0.16	0.03	-	0.06	-	100.98	0.912	0.359
MAN 63	Du	9	56.77	0.02	1.86	5.81	0.16	33.91	1.31	0.64	0.08	0.01	0.01	0.03	-	100.62	0.913	0.379
MAN 67	Hz	5	56.12	0.03	3.22	5.57	0.18	33.44	1.74	0.76	0.10	0.01	0.01	0.01	-	101.18	0.915	0.276
MAN 68	Du	3	56.19	0.06	2.77	5.46	0.10	33.73	1.42	0.74	0.03	0.02	0.01	0.03	-	100.56	0.917	0.307
MAN 70	Hz	5	56.90	0.02	1.72	5.69	0.11	33.92	2.02	0.67	0.18	0.02	0.02	0.02	-	101.30	0.915	0.423
MAN 72	Du	5	56.54	0.04	2.34	5.79	0.13	33.81	1.62	0.84	0.09	0.01	0.01	0.01	-	101.22	0.913	0.390
MAN 73	Hz	7	57.13	0.05	1.86	5.76	0.14	34.53	0.77	0.59	0.09	0.01	0.00	0.02	-	100.94	0.915	0.351
MAN 77	Hz	1	55.92	0.05	3.77	6.68	0.10	33.29	0.72	0.66	-	0.01	0.03	0.01	-	101.23	0.900	0.211
MAN 78	Du	3	56.83	0.02	1.79	5.87	0.19	34.25	0.58	0.61	0.06	0.01	0.01	0.02	-	100.24	0.913	0.373
MAN 79	Du	5	56.72	0.05	2.57	5.79	0.17	34.54	0.57	0.59	0.09	0.01	0.02	0.03	-	101.16	0.915	0.269
MAN 80	Hz	4	55.64	0.05	3.51	5.68	0.12	31.37	3.76	0.62	0.10	0.02	-	0.02	-	100.89	0.908	0.215
MAN 81	Hz	4	56.53	0.03	2.18	6.06	0.16	34.08	0.82	0.59	0.18	0.01	-	0.02	-	100.65	0.910	0.308
MAN 82	Hz	3	56.67	0.01	2.27	5.56	0.15	34.08	1.20	0.70	0.15	0.02	0.00	-	-	100.82	0.917	0.347
MAN 83	Hz	-	-	-	-	-	-	-	-	-	-	-	-	-	-	-	-	-
MAN 84	Du	2	57.02	0.03	1.81	5.85	0.20	34.69	0.89	0.61	0.12	0.01	-	-	-	101.21	0.914	0.368
MAN 85	Du	4	56.71	0.01	1.85	5.84	0.22	34.07	1.39	0.71	0.03	0.03	0.02	0.10	-	100.98	0.913	0.418
MAN 86	Hz	3	56.61	-	2.25	5.32	0.08	33.69	2.03	0.68	0.14	0.02	0.01	0.05	-	100.89	0.919	0.341
MAN 87	Du	3	55.83	0.04	2.38	5.28	0.19	33.68	1.55	0.77	0.14	0.01	0.01	-	-	99.88	0.920	0.361
MAN 89	Du	3	56.33	0.10	1.86	5.92	0.26	33.96	1.72	0.70	0.02	0.02	0.01	0.10	-	101.02	0.912	0.412
MAN 92	Hz	3	57.18	0.06	1.93	5.67	0.13	34.47	1.01	0.59	0.06	0.02	0.01	0.02	-	101.14	0.916	0.347
MAN 93	Hz	4	57.45	0.01	1.59	5.70	0.13	34.67	1.13	0.53	0.12	0.02	-	-	-	101.34	0.916	0.372
MAN 94	Hz	3	56.93	0.05	2.34	5.78	0.10	34.06	1.22	0.61	0.17	0.01	-	0.03	-	101.30	0.914	0.300
MAN 95	Hz	6	55.55	0.03	3.00	6.23	0.22	33.98	0.64	0.54	0.09	0.02	0.01	0.02	-	100.33	0.907	0.216
MAN 96	Du	3	56.82	0.02	2.09	5.85	0.10	34.43	1.03	0.74	0.00	0.02	-	0.02	-	101.12	0.914	0.386

Table 3. (continued)

Sample	Rock	N	SiO_2	TiO_2	Al_2O_3	FeO	MnO	MgO	CaO	Cr_2O_3	NiO	Na_2O	K_2O	P_2O_5	SO_2	Total	Mg#	Cr#
MAN 98	Du	3	56.38	0.01	2.62	5.75	0.17	33.62	1.55	0.76	0.13	0.01	0.01	0.00	-	101.01	0.913	0.327
MAN 99	Hz	6	56.68	0.02	2.14	5.91	0.15	33.83	1.54	0.75	0.15	0.01	0.00	0.03	-	101.21	0.911	0.381
MAN 101	Hz	3	56.10	0.03	2.37	5.67	0.25	33.55	1.99	0.82	0.06	0.02	-	-	-	100.86	0.914	0.381
MAN 103	Hz	3	57.14	0.07	1.34	5.70	0.11	34.05	1.72	0.56	0.03	0.03	0.02	0.04	-	100.80	0.915	0.454
MAN 105	Hz	4	55.90	0.05	1.75	5.79	0.14	34.07	1.18	0.61	0.17	0.03	0.02	0.02	-	99.74	0.914	0.389
MAN 107	Hz	4	55.89	0.01	1.64	5.91	0.15	34.06	1.25	0.54	0.08	0.01	0.00	0.01	-	99.57	0.912	0.368
MAN 109	Hz	3	55.76	0.04	1.69	5.94	0.13	34.17	0.92	0.61	0.10	0.02	0.00	0.01	-	99.40	0.912	0.397
MAN 110	Hz	3	55.96	0.05	2.81	6.17	0.15	33.85	0.81	0.69	0.11	0.02	-	0.01	-	100.63	0.908	0.287
MAN 111	Hz	4	56.72	0.01	2.04	5.77	0.14	34.58	1.07	0.70	0.11	0.01	0.02	0.00	-	101.18	0.915	0.376
MAN 112	Hz	4	55.51	0.05	3.81	6.52	0.16	33.53	0.55	0.56	0.10	0.02	0.03	0.04	-	100.89	0.902	0.182
MAN 113	Hz	4	56.01	0.02	2.71	5.89	0.19	33.94	1.04	0.64	0.13	0.01	-	0.04	-	100.63	0.912	0.275
MAN 114	Du	4	56.34	0.03	2.73	5.75	0.15	34.05	1.08	0.75	0.11	0.02	0.02	0.00	-	101.03	0.914	0.312
MAN 115	Hz	3	56.44	0.02	2.83	6.18	0.12	34.02	0.75	0.64	0.12	0.01	0.03	0.01	-	101.18	0.908	0.265
MAN 116	Hz	4	55.98	0.05	2.71	6.68	0.14	34.07	0.90	0.71	0.09	0.02	0.01	-	-	101.38	0.902	0.302
MAN 117	Hz	3	55.75	0.12	3.77	6.01	0.13	33.36	1.41	0.82	0.13	0.01	0.01	0.01	-	101.53	0.909	0.256
MAN 149	Hz	5	57.49	0.02	1.83	5.66	0.12	34.16	1.26	0.59	0.09	0.01	0.02	-	-	101.24	0.916	0.357
MAN 150	Hz	5	56.54	0.04	2.65	5.68	0.14	33.90	1.10	0.75	0.09	0.01	0.01	-	-	100.92	0.915	0.322
MAN 151	Du	5	57.77	0.04	2.00	5.92	0.20	34.10	0.91	0.66	0.10	0.01	0.02	-	-	101.74	0.912	0.368
MAN 153	Hz	9	57.40	0.05	1.98	5.67	0.14	33.61	2.11	0.71	0.07	0.01	0.02	-	-	101.77	0.914	0.391
MAN 155	Hz	7	57.47	0.02	1.82	6.18	0.14	34.40	0.81	0.62	0.07	0.01	0.01	-	-	101.54	0.909	0.373
MAN 157	Du	5	57.19	0.05	2.22	5.78	0.11	33.91	0.91	0.70	0.06	0.02	0.02	-	-	100.98	0.913	0.353
So_2	Hz	3	56.49	0.05	2.50	5.39	0.11	34.48	0.82	0.76	0.16	0.02	0.02	-	-	100.80	0.920	0.342
So_3	Hz	3	56.22	0.06	3.01	6.32	0.09	33.98	0.80	0.71	0.14	0.01	-	0.04	-	101.38	0.906	0.274
So_4	Lz	3	56.09	0.01	2.51	6.28	0.15	34.15	0.74	0.68	0.15	0.02	0.02	0.06	-	100.87	0.907	0.312
So_7	Hz	4	57.11	0.02	1.78	5.95	0.14	34.28	1.25	0.61	0.09	0.01	0.01	0.03	-	101.28	0.912	0.378
So_9	Hz	4	57.16	0.03	1.77	6.06	0.16	34.15	1.32	0.59	0.07	0.01	-	0.07	-	101.40	0.910	0.370
So_10	Du	5	56.87	0.02	1.86	6.16	0.14	34.25	1.13	0.45	0.14	0.02	0.01	0.01	-	101.06	0.909	0.284
So_11	Hz	3	56.93	0.02	1.78	6.22	0.14	34.49	0.75	0.54	0.13	0.01	-	-	-	101.01	0.909	0.344
So_15	Hz	4	56.40	0.01	2.79	6.29	0.17	33.85	0.71	0.65	0.11	0.02	0.02	0.03	-	101.04	0.906	0.271
So_16	Hz	4	55.81	0.07	3.46	6.03	0.12	33.58	1.16	0.80	0.18	0.03	0.02	-	-	101.26	0.909	0.270
So_17	Hz	5	55.71	0.05	3.35	6.06	0.12	32.97	1.94	0.75	0.14	0.02	-	0.02	-	101.11	0.907	0.263
So_19	Du	3	56.99	-	2.27	5.84	0.17	34.40	0.92	0.68	0.10	0.00	0.01	0.01	-	101.40	0.914	0.336
So_21	Hz	5	57.01	0.02	1.75	5.97	0.20	34.46	1.21	0.61	0.10	0.02	0.01	0.02	-	101.37	0.912	0.384
So_24	Hz	4	56.96	0.06	2.04	5.72	0.14	34.81	0.67	0.72	0.13	0.02	-	0.01	-	101.27	0.916	0.386
So_25	Hz	3	57.00	0.01	2.25	5.89	0.20	34.40	0.79	0.74	0.13	0.00	-	0.02	-	101.41	0.913	0.360
So_56	Hz	3	56.51	0.04	2.21	6.21	0.10	33.74	0.92	0.48	0.10	0.02	-	0.05	-	100.39	0.907	0.261
So_57	Hz	3	56.84	0.05	1.82	6.02	0.11	33.74	1.43	0.70	0.10	-	0.01	0.07	-	100.89	0.910	0.411
So_58	Hz	4	57.28	0.05	1.76	5.76	0.18	34.80	0.84	0.56	0.11	0.02	0.03	0.04	-	101.44	0.916	0.358
So_59	Hz	4	56.66	0.03	2.14	5.86	0.15	34.05	0.84	0.59	0.18	0.03	0.01	0.02	-	100.57	0.913	0.320
So_60	Du	3	56.92	0.07	1.84	6.02	0.15	33.89	1.19	0.66	0.04	0.01		0.02	-	100.80	0.910	0.391
So_61	Hz	3	57.17	0.00	1.49	5.96	0.13	33.84	1.32	0.50	0.06	0.02	0.01	0.05	-	100.56	0.911	0.375
So_62	Hz	5	56.68	0.09	2.33	5.83	0.15	33.49	1.52	0.67	0.13	0.01	0.01	0.05	-	100.94	0.912	0.325
So_63	Hz	3	56.42	0.04	2.29	6.01	0.13	33.29	1.73	0.69	0.14	0.04	0.02	0.07	-	100.86	0.909	0.344
So_65	Hz	4	56.23	0.04	3.00	5.59	0.23	33.00	1.91	0.89	0.19	0.04	-	0.01	-	101.14	0.914	0.337
So_66	Hz	3	56.99	0.00	1.97	5.87	0.13	34.49	0.52	0.72	0.12	-	-	0.04	-	100.85	0.913	0.397
So_67	Hz	4	56.35	0.04	2.68	6.03	0.12	33.53	1.10	0.68	0.08	0.01	0.01	0.01	-	100.65	0.909	0.293
So_68	Hz	4	56.16	0.02	2.91	6.03	0.16	33.55	1.16	0.64	0.07	0.03	0.02	0.05	-	100.79	0.909	0.260
So_70	Lz	3	56.01	0.02	2.91	6.09	0.18	33.12	1.27	0.62	0.25	0.02	0.02	-	-	100.50	0.907	0.251
So_71	Hz	7	56.87	0.03	2.35	6.10	0.13	34.03	1.11	0.58	0.13	0.02	0.01	0.02	-	101.38	0.909	0.289
So_72	Hz	3	56.48	0.03	2.44	5.84	0.25	33.57	1.16	0.70	0.13	-	-	0.05	-	100.65	0.912	0.323
So_74	Hz	3	56.06	0.00	2.69	5.53	0.08	32.43	2.85	0.75	0.10	-	-	0.02	-	100.52	0.913	0.314
So_75	Hz	4	56.49	0.03	2.50	5.89	0.16	33.60	1.40	0.61	0.10	0.02	0.06	0.03	-	100.90	0.911	0.285
So_76	Hz	4	56.32	0.03	2.40	6.03	0.11	33.37	1.79	0.63	0.17	0.04	0.00	0.08	-	100.96	0.909	0.309
So_77	Hz	3	56.63	0.01	2.11	6.06	0.18	34.00	0.65	0.61	0.06	0.04		0.02	-	100.37	0.910	0.331
So_78	Hz	3	56.43	0.02	2.86	5.70	0.17	32.93	2.03	0.92	0.20	0.01	0.02	-	-	101.28	0.912	0.358
So_79	Hz	3	56.63	0.02	1.96	5.68	0.10	34.21	0.85	0.63	0.07	0.02	-	-	-	100.16	0.915	0.360
So_80	Du	4	56.73	0.03	2.43	5.39	0.17	34.29	0.95	0.74	0.14	0.02	-	0.01	-	100.91	0.920	0.345
So_81	Hz	6	56.45	0.04	2.50	5.80	0.21	33.92	1.13	0.68	0.11	0.01	0.02	-	-	100.88	0.913	0.311
So_82	Hz	4	56.33	0.05	2.42	5.80	0.16	33.73	1.26	0.60	0.09	0.02	0.04	0.03	-	100.53	0.913	0.286
So_83	Hz	5	56.82	0.04	2.11	6.12	0.13	33.92	1.03	0.62	0.14	0.02	-	0.09	-	101.05	0.909	0.335
So_84	Hz	4	57.20	0.01	1.81	5.72	0.14	33.33	2.02	0.64	0.16	0.03	0.03	0.02	-	101.10	0.913	0.392
So_85	Hz	5	57.49	0.05	1.70	5.77	0.13	34.87	0.73	0.56	0.18	0.01	0.01	0.03	-	101.54	0.916	0.364

Table 3. (continued)

Sample	Rock	N	SiO_2	TiO_2	Al_2O_3	FeO	MnO	MgO	CaO	Cr_2O_3	NiO	Na_2O	K_2O	P_2O_5	SO_2	Total	Mg#	Cr#
So_87	Du	5	57.34	0.03	1.55	5.94	0.14	34.70	0.55	0.48	0.07	0.01	0.02	0.03	-	100.85	0.913	0.343
So_88	Hz	4	55.82	0.03	3.52	6.02	0.16	32.72	1.84	0.72	0.18	0.01	-	-	-	101.02	0.907	0.242
So_89	Du	3	56.78	0.02	1.70	5.56	0.17	32.61	2.94	0.69	0.06	0.02	0.01	0.03	-	100.60	0.913	0.433
So_90	Hz	4	57.03	0.04	1.89	5.70	0.16	33.91	1.20	0.56	0.08	0.01	-	0.06	-	100.64	0.914	0.334
So_91	Hz	3	56.37	0.05	2.40	6.01	0.12	33.62	1.05	0.75	0.09	0.01	-	0.03	-	100.50	0.910	0.347
So_92	Hz	5	55.64	0.02	3.36	6.18	0.08	33.17	1.20	0.69	0.14	0.02	0.01	0.06	-	100.57	0.906	0.244
So_94	Hz	5	56.68	0.05	2.38	6.14	0.19	34.36	0.90	0.75	0.12	0.02	0.01	0.02	-	101.62	0.910	0.353
So_95	Du	3	56.23	0.01	2.88	5.71	0.14	33.08	1.62	0.57	0.05	0.01	0.03	0.05	-	100.37	0.912	0.236
So_96	Lz	2	55.71	0.01	3.59	6.47	0.23	33.20	0.63	0.48	0.16	0.01	0.04	-	-	100.53	0.902	0.166
So_100	Du	4	57.43	0.04	1.28	6.17	0.14	34.31	0.73	0.47	0.10	0.02	-	0.05	-	100.74	0.909	0.401
So_101	Hz	3	55.89	0.07	3.87	5.62	0.11	33.63	0.76	0.60	0.09	0.03	0.00	0.05	-	100.73	0.915	0.191
So_102	Hz	4	56.28	0.04	3.04	6.22	0.17	33.38	1.38	0.74	0.10	0.01	0.01	-	-	101.37	0.906	0.283
So_104	Hz	4	57.92	-	1.43	5.63	0.18	34.62	0.99	0.57	0.11	-	-	0.05	-	101.50	0.917	0.421
So_105	Hz	3	56.18	-	2.52	5.46	0.15	32.72	2.27	0.82	0.15	0.04	-	0.02	-	100.33	0.915	0.363
So_106	Hz	4	56.95	0.08	2.03	5.90	0.08	34.09	1.21	0.70	0.12	0.00	-	-	-	101.16	0.912	0.379
So_107	Hz	4	56.84	0.03	1.75	6.05	0.17	34.10	0.84	0.61	0.06	0.02	0.01	0.06	-	100.53	0.910	0.384
So_108	Hz	3	57.05	0.00	1.68	6.34	0.16	34.18	0.84	0.54	0.10	0.01	0.01	0.07	-	100.99	0.906	0.360
So_109	Hz	4	57.31	0.05	1.84	5.89	0.11	34.43	0.90	0.60	0.09	0.02	-	-	-	101.23	0.913	0.364
So_110	Hz	3	56.70	0.01	2.19	5.72	0.13	34.12	0.79	0.70	0.09	0.02	0.00	-	-	100.45	0.915	0.356
So_111	Hz	4	56.77	0.05	1.76	5.92	0.12	33.01	2.85	0.69	0.15	0.02	-	0.05	-	101.39	0.909	0.423
So_112	Du	3	56.96	0.03	2.29	5.22	0.15	33.83	1.44	0.57	0.15	0.03	-	0.02	-	100.70	0.921	0.292
So_113	Du	3	57.18	0.05	1.94	6.03	0.09	34.31	1.01	0.53	0.12	0.04	-	0.03	-	101.31	0.911	0.317
So_114	Hz	8	56.95	0.04	1.73	6.02	0.11	33.07	2.80	0.71	0.17	0.02	-	0.03	-	101.64	0.908	0.438
So_115	Du	4	57.28	-	1.48	5.89	0.14	34.52	1.15	0.60	0.09	0.02	0.00	0.04	-	101.20	0.913	0.438
So_116	Hz	3	56.72	0.05	1.93	5.81	0.19	33.72	1.23	0.70	0.06	0.01	0.00	0.04	-	100.45	0.913	0.395
So_117	Du	4	57.04	0.02	2.04	5.70	0.15	33.93	1.30	0.72	0.10	0.01	-	0.05	-	101.07	0.914	0.387
So_118	Hz	3	56.61	0.03	2.08	5.75	0.16	33.82	1.37	0.63	0.11	-	0.00	0.02	-	100.58	0.914	0.336
So_119	Hz	4	57.18	0.01	1.60	6.15	0.10	34.34	1.08	0.50	0.05	0.03	0.00	0.00	-	101.05	0.909	0.357
So_120	Du	4	56.44	0.01	2.17	5.55	0.12	33.91	1.29	0.79	0.09	0.03	0.02	0.03	-	100.45	0.916	0.400
So_122	Hz	3	56.45	0.07	1.89	5.85	0.17	32.22	2.67	0.80	0.10	0.01	0.03	0.01	-	100.27	0.908	0.448
So_124	Hz	3	56.42	0.05	2.05	6.19	0.19	33.91	0.74	0.59	0.10	0.03	0.01	0.04	-	100.33	0.908	0.330
So_125	Hz	5	56.88	0.07	2.20	5.65	0.14	34.06	1.29	0.57	0.10	0.01	-	0.03	-	100.99	0.915	0.300
So_126	Hz	4	55.49	0.08	2.66	5.06	0.25	29.46	6.97	0.71	0.12	0.03	-	-	-	100.81	0.913	0.308
So_127	Hz	3	56.95	0.01	2.07	5.62	0.15	34.40	1.26	0.46	0.02	-	-	0.01	-	100.94	0.917	0.260
So_128	Hz	3	56.36	0.10	3.02	5.89	0.14	33.71	0.80	0.66	0.08	0.01	0.01	0.06	-	100.84	0.911	0.259
So_130	Hz	4	56.61	0.05	2.74	6.10	0.13	33.96	0.96	0.65	0.11	0.02	0.01	0.02	-	101.36	0.909	0.277
So_132	Hz	3	56.11	0.02	2.45	5.83	0.17	33.90	1.47	0.56	0.13	-	0.02	-	-	100.65	0.913	0.264
So_134	Hz	6	55.68	0.04	1.64	6.02	0.12	34.07	1.06	0.54	0.09	0.02	0.01	0.02	-	99.32	0.910	0.369
So_135	Hz	5	56.71	0.02	2.36	5.47	0.14	34.45	1.05	0.60	0.16	0.02	0.03	0.02	-	101.02	0.919	0.295
So_136	Hz	3	55.28	0.04	2.48	5.91	0.14	33.49	1.33	0.65	0.08	0.03	-	-	-	99.42	0.911	0.304
So_137	Du	5	54.89	0.04	2.47	5.75	0.15	33.69	1.20	0.63	0.06	0.02	0.02	0.04	-	98.95	0.913	0.295
So_139	Hz	3	55.08	0.06	3.10	6.18	0.19	34.05	0.71	0.70	0.16	0.01	0.01	0.06	-	100.31	0.908	0.264
So_140	Hz	3	54.92	0.05	3.54	5.34	0.21	33.42	1.40	0.79	0.12	0.03	0.00	0.04	-	99.85	0.918	0.263
So_141	Hz	3	54.11	0.06	4.25	6.01	0.12	32.05	2.09	0.99	0.15	0.02	0.02	0.02	-	99.88	0.906	0.273
So_142	Lz	4	54.17	0.05	3.61	5.85	0.14	31.23	3.32	0.91	0.09	0.03	-	-	-	99.40	0.906	0.292
So_143	Du	4	55.68	0.01	1.95	5.58	0.11	33.99	1.24	0.63	0.08	0.06	-	0.04	-	99.36	0.916	0.371
So_144	Hz	4	53.62	0.04	4.36	6.21	0.13	32.07	1.76	0.82	0.05	0.02	0.02	0.02	-	99.11	0.903	0.225
So_145	Hz	3	55.91	0.04	2.36	6.29	0.13	34.32	0.94	0.53	0.17	-	0.01	0.03	-	100.74	0.907	0.263
So_148	Hz	4	55.42	0.04	2.27	5.84	0.20	34.01	0.83	0.61	0.10	0.02	0.00	0.01	-	99.36	0.913	0.308
94-46	Hz	3	56.74	0.03	2.09	5.50	0.22	33.28	1.30	0.72	0.10	0.01	0.04	-	-	100.03	0.916	0.379

[a] "N" and Mg# are the same as for Table 2. Cr# is 2Cr/(Cr + Al − Na). The chemical zonations have been investigated by comparing core and rim analyses. Operating conditions and uncertainty: see Table 2 footnote.

the Opx and, more rarely, isolated subidiomorphic small-sized crystals at grain boundaries (type 2 spinels, Figures 3b and 3c). While this later spinels are commonly considered as "secondary" [*Augé*, 1982, 1987], the holly leaf-shaped ones are generally considered to be characteristic of primary spinels that were exsolved from the pyroxenes during decompression melting of the peridotite [e.g., *Augé*, 1982, 1987; *Mercier and Nicolas*, 1975; *Quatrevaux*, 1995]. The elongated shape of the crystals in the porphyroclastic rocks define the foliation, acquired at low temperature [*Nicolas*, 1986a]. It locally grades into mylonitic textures

Table 4. Cpx Average Major Element Compositions From 133 Analyses[a]

Sample	Rock	N	SiO_2	TiO_2	Al_2O_3	FeO	MnO	MgO	CaO	Cr_2O_3	NiO	Na_2O	K_2O	P_2O_5	SO_2	Total	Mg#	Cr#
MAN 01	Hz	2	52.46	0.02	3.06	2.30	0.11	17.05	24.46	0.90	0.09	0.05	-	-	-	100.50	0.930	0.337
MAN 03	Hz	2	52.49	0.10	3.12	2.82	0.20	17.72	22.38	1.34	0.03	0.10	-	0.00	-	100.30	0.919	0.466
MAN 06	Du	1	54.34	-	2.02	2.27	0.10	18.98	21.62	0.93	0.21	0.27	-	-	-	100.74	0.938	0.566
MAN 11	Hz	3	52.74	0.07	2.86	2.29	0.03	17.04	24.02	1.40	0.15	0.04	-	-	-	100.65	0.930	0.503
MAN 20	Hz	2	53.39	0.08	2.18	2.16	0.08	17.57	24.04	0.75	0.09	0.04	-	-	-	100.38	0.936	0.385
MAN 21	Hz	3	53.57	0.03	2.22	2.20	0.17	17.59	23.84	0.69	0.05	-	-	-	-	100.36	0.935	0.343
MAN 23	Hz	1	51.75	-	4.15	3.01	0.14	18.09	21.59	1.22	0.06	0.04	0.00	-	0.01	100.06	0.915	0.334
MAN 28	Hz	4	54.13	0.06	2.64	2.44	0.09	17.96	23.21	1.00	0.06	0.05	0.02	-	-	101.67	0.930	0.418
MAN 30	Hz	6	54.01	0.06	2.10	2.07	0.10	17.78	24.26	0.82	0.03	0.01	0.01	-	-	101.24	0.939	0.418
MAN 32	Hz	1	51.48	0.08	4.71	2.67	0.08	17.39	22.36	1.17	0.02	0.21	-	0.04	-	100.21	0.921	0.304
MAN 33	Du	1	52.20	0.06	4.02	2.28	-	16.96	23.55	1.00	-	0.14	-	-	-	100.20	0.930	0.302
MAN 35	Hz	2	51.91	0.06	3.74	2.35	0.05	16.81	24.06	1.25	0.00	0.06	-	0.03	0.01	100.32	0.928	0.374
MAN 41	Du	5	53.32	0.03	2.47	2.35	0.08	17.77	23.67	0.95	0.03	0.01	-	0.01	-	100.69	0.931	0.412
MAN 48	Hz	1	53.02	0.05	2.68	2.16	0.09	17.15	23.99	1.29	0.02	0.07	-	0.05	-	100.58	0.935	0.505
MAN 55	Du	3	53.58	0.04	1.57	1.93	0.11	17.50	24.21	0.88	0.10	0.05	0.03	0.04	-	100.04	0.942	0.569
MAN 60	Du	1	54.28	0.06	1.52	2.05	0.20	18.36	24.12	0.53	0.04	0.02	-	0.06	-	101.24	0.942	0.387
MAN 77	Hz	2	53.92	0.06	3.42	3.63	0.14	24.17	13.75	0.69	-	0.09	0.01	0.03	-	99.91	0.923	0.248
MAN 80	Hz	3	53.42	0.14	2.58	2.08	0.07	16.85	24.45	0.59	0.02	0.08	0.00	0.05	-	100.33	0.936	0.277
MAN 81	Hz	1	53.55	0.01	1.97	1.93	-	17.71	24.62	0.66	-	0.01	-	0.10	-	100.56	0.943	0.369
MAN 95	Hz	4	52.16	0.11	2.91	1.90	0.13	17.08	24.54	0.71	0.02	0.09	0.02	0.04	-	99.71	0.942	0.294
MAN 99	Hz	3	53.41	0.02	2.25	2.11	0.06	17.55	24.63	0.93	0.11	0.06	0.04	0.02	-	101.21	0.937	0.450
MAN 107	Hz	1	53.02	-	1.91	2.57	0.05	18.06	23.49	0.61	0.10	-	0.01	0.07	-	99.90	0.927	0.351
MAN 114	Du	1	52.70	0.05	2.72	1.96	0.15	17.21	24.14	1.02	0.13	0.11	0.04	0.02	-	100.25	0.940	0.423
MAN 117	Hz	2	52.20	0.10	4.13	2.31	0.20	17.57	23.05	1.22	0.12	0.07	-	0.02	-	101.01	0.932	0.339
MAN 149	Hz	5	53.77	0.07	2.31	2.01	0.10	17.14	24.41	1.20	0.01	0.13	0.02	-	-	101.17	0.939	0.557
MAN 151	Du	1	54.12	0.06	2.21	2.40	0.01	18.76	22.82	0.94	0.03	0.06	0.02	-	-	101.41	0.934	0.456
So_2	Hz	1	53.70	0.06	2.62	1.98	0.07	17.57	24.28	1.20	-	0.04	-	0.01	-	101.51	0.941	0.478
So_3	Hz	1	52.17	0.07	3.84	2.71	0.06	17.78	22.34	1.34	0.09	-	-	-	-	100.41	0.922	0.380
So_4	Lz	3	52.04	0.05	3.50	2.50	0.10	17.11	24.00	1.32	-	0.05	-	0.09	-	100.74	0.925	0.410
So_10	Du	1	53.66	-	2.06	2.62	0.12	18.41	23.14	0.60	-	0.03	-	0.02	-	100.66	0.926	0.334
So_11	Hz	1	53.99	0.05	2.01	2.10	0.11	17.69	24.39	0.90	-	0.00	-	-	-	101.24	0.938	0.461
So_16	Hz	3	52.38	0.12	3.54	2.04	0.06	16.74	24.32	0.91	0.10	0.09	-	-	-	100.30	0.936	0.306
So_17	Hz	3	52.22	0.07	3.61	2.34	0.13	17.14	24.11	0.86	0.09	0.03	0.00	0.01	-	100.61	0.929	0.279
So_56	Hz	1	52.53	-	2.61	2.25	0.01	17.54	23.78	1.08	0.08	0.05	-	-	-	99.92	0.933	0.447
So_60	Du	1	53.41	0.00	2.28	2.37	0.09	17.46	24.25	1.01	0.06	0.01	-	0.00	-	100.94	0.930	0.463
So_62	Hz	1	53.24	0.08	2.94	2.15	0.12	16.97	23.71	0.84	-	0.11	-	-	-	100.16	0.934	0.340
So_63	Hz	1	52.81	0.05	2.90	2.72	0.13	18.06	22.52	0.99	0.10	0.26	-	-	-	100.54	0.923	0.426
So_68	Hz	2	52.34	0.01	3.69	2.28	0.06	16.66	24.24	1.20	0.09	0.06	-	0.06	-	100.67	0.929	0.365
So_70	Lz	1	52.08	0.03	3.59	2.28	0.03	16.56	24.09	1.29	0.11	0.12	0.02	0.02	-	100.20	0.929	0.407
So_74	Hz	3	52.78	0.04	3.19	2.06	0.11	16.83	24.34	1.22	0.03	0.10	0.03	0.02	-	100.75	0.936	0.427
So_78	Hz	2	52.60	0.06	3.39	2.09	0.11	17.73	23.68	1.13	0.02	0.04	0.03		-	100.88	0.938	0.372
So_83	Hz	1	54.22	-	2.51	1.93	0.07	17.70	24.28	1.23	0.05	0.04	-	0.06	-	102.10	0.943	0.503
So_84	Hz	2	53.36	-	2.41	2.18	0.01	17.60	24.64	1.57	0.22	0.03	-	0.05	-	102.07	0.935	0.617
So_88	Hz	1	52.67	0.06	3.88	2.17	0.11	16.55	24.12	1.00	-	0.11	-	0.01	-	100.69	0.932	0.308
So_91	Hz	2	53.31	0.00	2.51	2.03	0.14	17.22	24.39	0.99	0.11	0.01	-	-	-	100.71	0.938	0.420
So_95	Du	2	52.58	0.07	3.67	2.52	0.12	17.14	22.94	1.25	0.11	0.02	-	-	-	100.41	0.924	0.373
So_96	Lz	3	52.02	0.09	4.05	2.21	0.06	16.56	24.08	1.09	0.11	0.25	-	-	-	100.54	0.931	0.336
So_101	Hz	3	52.80	0.09	4.50	2.51	0.17	17.40	21.37	1.28	0.05	0.79	0.01	0.03	-	100.99	0.926	0.423
So_102	Hz	1	53.71	0.04	1.78	2.34	0.07	17.46	24.91	0.48	0.21	0.05		0.05	-	101.09	0.931	0.317
So_107	Hz	1	52.71	0.04	2.28	2.06	0.15	17.12	23.87	0.81	0.20	0.03	0.03	0.02	-	99.32	0.937	0.394
So_108	Hz	1	54.10	0.03	1.77	2.25	0.11	17.80	23.62	0.77	0.00	0.17	-	-	-	100.63	0.934	0.518
So_124	Hz	4	52.95	0.07	2.36	1.98	0.13	17.18	24.36	0.88	0.16	0.04	0.01	0.04	-	100.16	0.940	0.410
So_125	Hz	1	54.46	0.04	4.20	2.77	0.09	22.57	12.53	0.68	0.03	1.02	-	0.06	-	98.45	0.936	0.305
So_126	Hz	3	52.60	0.08	3.05	2.22	0.12	16.94	23.91	1.10	0.10	0.03	-	0.03	-	100.17	0.932	0.393
So_128	Hz	1	53.52	0.05	2.14	2.31	-	17.98	24.12	0.56	0.01	0.09	-	0.05	-	100.83	0.933	0.320
So_130	Hz	1	53.50	0.07	2.91	2.51	0.10	17.87	23.48	1.15	0.19	0.04	-	-	-	101.83	0.927	0.427
So_132	Hz	2	52.77	0.05	2.62	2.14	0.11	17.11	24.87	1.01	-	0.03	0.00	0.01	-	100.72	0.935	0.417
So_134	Hz	1	52.32	0.01	1.84	1.97	0.11	17.61	23.82	0.77	-	0.15	-	0.05	-	98.64	0.941	0.488
So_136	Hz	1	52.67	-	2.21	2.00	-	17.25	24.77	0.74	0.12	0.01	-	-	-	99.76	0.939	0.370
So_139	Hz	2	52.25	0.04	3.03	2.66	0.09	17.92	23.09	0.91	0.17	0.13	0.02	0.00	-	100.31	0.924	0.357
So_140	Hz	2	51.22	0.07	4.07	2.00	0.10	16.23	23.80	1.05	0.00	0.29	-	0.04	-	98.88	0.936	0.329
So_141	Hz	2	51.90	0.06	3.40	3.11	0.11	19.88	19.66	0.70	-	0.16	-	0.01	-	98.99	0.920	0.261

Table 4. (continued)

Sample	Rock	N	SiO_2	TiO_2	Al_2O_3	FeO	MnO	MgO	CaO	Cr_2O_3	NiO	Na_2O	K_2O	P_2O_5	SO_2	Total	Mg#	Cr#
So_142	Lz	2	50.76	0.07	3.52	2.16	0.07	16.55	24.03	1.13	0.02	0.12	-	0.04	-	98.47	0.932	0.372
So_144	Hz	3	51.76	0.10	3.49	2.47	0.05	16.82	23.77	0.72	0.17	0.18	-	0.05	-	99.58	0.924	0.262
So_145	Hz	3	52.59	0.04	2.78	2.49	0.06	17.36	23.60	0.92	0.02	0.19	-	0.05	-	100.10	0.926	0.402
94-46	Hz	2	53.52	0.06	2.55	2.16	0.14	17.24	23.71	1.03	-	0.14	-	-	-	100.55	0.935	0.459

[a] "N," Mg#, and Cr# are the same as for Table 3. As in opx, the chemical zonations have been investigated by comparing core and rim analyses. Operating conditions and uncertainty: see Table 2 footnote.

(only 5 samples) where the Opx are elongated and the olivine strongly recrystallized.

4.3. Mineral Chemistry

[20] Mineral analyses have been done on 174 samples, including 739 olivines, 689 Opx, 133 Cpx and 718 holly leaf-shaped spinels. Their mean compositions are presented in Tables 2, 3, 4, and 5.

[21] Olivines are magnesium-rich, their Mg# (=molar $Mg^{2+}/(Mg^{2+} + Fe^{2+})$) values ranging from 0.898 to 0.916 (Figure 4a), with an average of 0.908 (SD = 0.003). This is comparable to the Fo range obtained for some olivines in abyssal peridotites [e.g., *Bonatti and Michael*, 1989]. Their NiO and CaO contents are very low, respectively ranging from 0.18 to 0.53% (average $NiO_{(olivine)}$ = 0.39%, SD = 0.06%) and from 0 to 0.07% (average $CaO_{(olivine)}$ = 0.03%, SD 0.01%). These elements are not correlated with Mg#.

[22] The Opx porphyroclasts are unzoned. They correspond to enstatites with En: 88.90% (SD = 1.36%); Fs: 8.63% (SD = 0.42%); Wo: 2.47% (SD = 1.45%). These minerals display a rather large chemical variability as recorded by their Mg# which vary between 0.900 and 0.921 (Figure 4a) and by their Cr# (= 2 Cr/(Cr + Al − Na)) which range from 0.166 to 0.464 (Figure 4b).

[23] All Cpx correspond to residual NaO-poor (average $Na_2O_{(cpx)}$ = 0.08%, SD = 0.05%) and TiO_2-poor (average $TiO_{2(cpx)}$ = 0.06%, SD = 0.03%) diopsides, with an average modal composition of En: 49.51% (SD = 3.72%), Fs: 3.62% (SD = 0.53%) and Wo: 46.87% (SD = 4.10%). As the Opx, they display a large Mg# variability (0.915 and 0.943, Figure 4e) and Cr# (= 2 Cr/(Cr + Al − Na)) variability which ranges from 0.248 to 0.617 (Figure 4c).

[24] The holly leaf-shaped spinels correspond to chromites and spinels *s.s.* The Cr-Al-Fe^{3+} triangular plot (in cations) shows that these spinels are particularly poor in Fe^{3+} (average Fe^{3+} = 2.78%; SD = 1.01%) and rich in Cr and Al (average Cr = 47.14%, SD = 10.29%; average Al = 50.08% with SD = 10.64%). They display a large variability of their Cr# content ($Cr\#_{(sp)}$ = molar Cr/(Cr+Al)) that ranges from 0.207 to 0.669 with a mean value of 0.49 and Mg# contents (average $Mg\#_{(sp)}$ = 0.61) (Figure 4d). The higher values, between $Cr\#_{(sp)}$ 0.5 and 0.6, are well illustrated on the $Cr\#_{(sp)}$ versus $Mg\#_{(olivine)}$ diagram (Figure 4f). Their compositions encompass that of the abyssal peridotites from various tectonic settings, slow to fast accretion rates. But the highest values, that are in average those of the smaller-size idiomorphic spinels [*Le Mée et al.*, 2004], better resemble to spinels from back-arc basin [*Monnier et al.*, 1995] and of fore-arc areas as Izu-Bonin/Mariana (IBM) [*Ishii et al.*, 1992]. All these spinels have very low TiO_2 contents (average 0.05%, SD = 0.02%) and MnO (average = 0.22% with SD = 0.05%) compared to spinels in abyssal peridotites [*Barnes and Roeder*, 2001].

[25] As the Cr# of primary spinels is known to reflect the extent of melting of the host peridotites and has been used as such during the last 40 years [*Barnes and Roeder*, 2001; *Bonatti and Michael*, 1989; *Bonatti et al.*, 1992; *Dick*, 1977; *Dick and Bullen*, 1984; *Evans and Frost*, 1975; *Hellebrand et al.*, 2001; *Irvine*, 1965, 1967; *Michael and Bonatti*, 1985; *Sack and Ghiorso*, 1991; *Seyler et al.*, 2003], we will use it in the following discussions as a reference chemical index. Arguments for such an interpretation will be discussed later.

4.4. Primary Phase Equilibria

[26] On the basis of the variation diagrams presented in Figure 4, it can be stressed that most elements show equilibrium between the coexisting phases, plotting on the typical trends already defined for ophiolitic and abyssal peridotites. This is illustrated on the olivine Mg# versus Opx Mg# diagram (Figure 4a) where the equilibrium constant is close to unity ($0.9 < K_d < 1.0$) for all samples, Mg# in peridotite silicates being positively correlated with the extent of melting [e.g., *Arai*, 1994a,

Table 5. Spinel Average Major Element Compositions From 718 Analyses[a]

Sample	Rock	N	SiO_2	TiO_2	Al_2O_3	FeO	Fe_2O_3	MnO	MgO	CaO	Cr_2O_3	NiO	Na_2O	K_2O	P_2O_5	SO_2	Total	Mg#	Cr#	SD
MAN 01	Hz	3	0.02	0.07	34.99	14.47	3.47	0.16	14.90	-	32.00	0.14	0.02	0.02	0.02	-	100.28	0.649	0.380	0.011
MAN 03	Hz	4	0.01	0.04	32.19	15.51	2.71	0.16	13.76	0.02	34.90	0.17	0.02	0.01	-	-	99.49	0.614	0.421	0.025
MAN 06	Du	4	0.02	0.07	24.14	16.46	3.21	0.28	12.53	0.02	43.71	0.08	0.03	0.02	0.01	-	100.57	0.578	0.549	0.005
MAN 07	Du	8	0.03	0.01	24.76	16.77	3.14	0.26	12.14	0.01	42.06	0.08	0.02	0.01	0.04	0.02	99.34	0.565	0.533	0.012
MAN 08	Du	6	0.03	0.03	25.69	16.41	2.26	0.19	12.51	0.51	42.29	0.04	0.02	0.04	0.01	0.02	100.04	0.578	0.525	0.007
MAN 09	Hz	5	0.04	0.03	23.85	17.03	4.12	0.23	12.02	-	42.29	0.07	0.02	0.01	0.01	0.01	99.72	0.559	0.543	0.016
MAN 10	Hz	3	0.03	0.05	30.60	15.80	3.56	0.24	13.59	0.02	36.20	0.15	0.01	-	-	0.03	100.28	0.607	0.443	0.008
MAN 11	Hz	5	0.02	0.07	28.79	15.29	3.40	0.19	13.62	0.02	37.89	0.12	0.01	0.02	0.01	0.04	99.49	0.615	0.494	0.007
MAN 13	Hz	5	0.03	0.09	23.70	20.31	6.41	0.27	9.89	0.02	39.28	0.16	0.02	0.01	0.04	-	100.23	0.467	0.515	0.002
MAN 14	Hz	3	0.01	0.05	21.88	17.01	2.91	0.16	11.89	0.01	45.79	0.09	0.03	-	-	0.01	99.85	0.557	0.584	0.015
MAN 20	Hz	7	0.06	0.09	29.46	15.66	2.51	0.14	13.28	-	37.48	-	-	-	-	-	98.68	0.604	0.461	0.017
MAN 21	Hz	6	0.05	0.05	26.40	16.25	3.84	0.23	12.61	-	39.82	-	-	-	-	-	99.25	0.582	0.503	0.023
MAN 23	Hz	6	0.03	0.03	36.65	14.46	2.27	0.16	15.07	0.01	31.09	0.10	0.01	-	-	0.01	99.88	0.652	0.363	0.001
MAN 24	Hz	8	0.03	0.05	32.77	14.06	2.85	0.18	14.83	-	34.85	-	-	-	-	-	99.61	0.655	0.417	0.032
MAN 25	Hz	3		0.15	25.50	15.74	3.01	0.25	13.08	-	42.29	0.09	0.03	0.02	-	-	100.13	0.599	0.513	0.036
MAN 26	Du	5	0.04	0.04	26.22	15.29	2.61	0.17	13.58	-	42.50	-	-	-	-	-	100.46	0.615	0.521	0.005
MAN 27	Hz	4	-	0.07	31.40	14.77	1.42	0.15	14.46	-	38.05	-	-	-	-	-	100.33	0.638	0.449	0.008
MAN 28	Hz	4	0.01	0.04	27.27	15.74	1.85	0.17	13.47	-	42.28	-	-	-	-	-	100.85	0.606	0.510	0.011
MAN 29	Du	6	0.10	0.05	19.98	16.73	1.16	0.25	11.98	-	50.28	-	-	-	-	-	100.51	0.562	0.628	0.007
MAN 30	Hz	3	0.05	0.03	28.12	15.06	1.81	0.25	13.86	-	41.11	-	-	-	-	-	100.28	0.623	0.495	0.011
MAN 32	Hz	4	-	0.04	42.09	12.36	1.97	0.19	16.85	-	25.81	0.16	0.02	0.01	0.00	0.02	99.52	0.710	0.292	0.012
MAN 33	Du	3	0.02	0.03	40.75	13.66	2.04	0.12	15.96	-	26.91	-	-	-	-	-	99.49	0.677	0.295	0.013
MAN 34	Hz	5	0.10	0.05	35.36	13.46	1.93	0.19	15.61	0.02	33.08	0.11	0.02	-	0.06	0.03	100.02	0.676	0.386	0.007
MAN 37	Hz	4	-	0.04	34.52	14.32	2.54	0.19	14.85	-	32.81	0.07	0.02	-	0.02	0.01	99.37	0.651	0.390	0.012
MAN 39	Hz	4	0.00	0.03	21.91	16.59	2.78	0.19	12.16	0.00	46.28	0.12	0.03	0.00	0.01	-	100.12	0.568	0.586	0.011
MAN 40	Hz	4	-	0.03	22.34	15.93	2.77	0.27	12.44	0.01	45.13	0.03	0.01	-	0.01	0.04	99.02	0.584	0.575	0.023
MAN 41	Du	3	0.02	0.05	25.75	16.29	2.37	0.25	12.67	-	42.27	0.05	0.02	0.00	-	0.01	99.75	0.583	0.524	0.034
MAN 42	Hz	5	0.02	0.04	31.83	14.43	2.67	0.15	14.61	-	36.06	0.08	0.01	0.00	-	0.01	99.91	0.645	0.432	0.012
MAN 44	Hz	4	0.00	0.03	21.22	16.39	1.36	0.22	12.21	0.01	48.36	0.12	0.01	-	0.04	0.04	100.01	0.572	0.605	0.019
MAN 48	Hz	4	0.03	0.06	24.07	15.43	3.80	0.25	13.01	0.01	42.66	0.08	0.01	0.01	0.01	0.00	99.43	0.602	0.543	0.017
MAN 50	Hz	4	0.01	0.02	21.32	16.11	2.40	0.21	12.08	-	46.23	0.13	0.02	0.03	0.04	0.00	98.61	0.574	0.593	0.006
MAN 55	Du	3	0.01	0.03	20.89	15.97	2.50	0.23	12.36	0.02	47.64	0.08	0.02	0.03	0.02	0.02	99.83	0.582	0.611	0.036
MAN 56	Hz	4	0.04	0.04	25.91	15.29	1.84	0.16	13.71	-	44.07	0.12	0.05	-	0.05	-	101.29	0.617	0.533	0.019
MAN 57	Du	4	0.00	0.06	23.29	15.95	2.94	0.28	12.55	0.00	44.25	0.10	0.03	0.02	0.04	-	99.55	0.586	0.560	0.010
MAN 58	Hz	3	0.01	0.05	17.35	16.77	1.92	0.25	11.50	-	51.72	0.10	0.03	0.01	0.03	-	99.75	0.552	0.667	0.004
MAN 59	Hz	3	-	0.02	26.71	15.83	1.25	0.22	13.16	0.02	42.79	0.12	0.01	-	0.02	-	100.15	0.599	0.549	0.013
MAN 60	Du	4	-	0.04	22.16	16.12	2.03	0.28	12.44	0.04	46.85	0.14	0.03	-	-	-	100.13	0.581	0.587	0.019
MAN 62	Hz	4	0.02	0.04	23.28	15.88	1.85	0.19	12.64	0.00	45.33	0.08	0.03	-	-	-	99.34	0.588	0.566	0.006
MAN 63	Du	4	0.04	0.05	24.60	15.93	1.17	0.27	12.78	-	44.60	0.16	-	0.00	0.08	-	99.68	0.590	0.549	0.015
MAN 67	Hz	5	0.02	0.04	41.14	13.13	1.73	0.19	16.20	-	26.81	0.20	0.02	0.06	-	-	99.54	0.689	0.304	0.007
MAN 68	Du	4	0.00	0.02	35.04	13.02	2.11	0.11	15.86	-	33.61	0.14	0.02	0.00	0.02	-	99.96	0.686	0.392	0.006
MAN 70	Hz	4	0.03	0.07	21.71	16.91	1.96	0.28	11.80	-	46.69	0.10	0.02	0.01	0.02	-	99.59	0.556	0.591	0.016
MAN 72	Du	6	0.05	0.07	27.86	15.77	1.44	0.23	13.49	0.02	41.62	0.13	0.03	0.00	0.05	-	100.76	0.606	0.501	0.008

Table 5. (continued)

Sample	Rock	N	SiO_2	TiO_2	Al_2O_3	FeO	Fe_2O_3	MnO	MgO	CaO	Cr_2O_3	NiO	Na_2O	K_2O	P_2O_5	SO_2	Total	Mg#	Cr#	SD
MAN 73	Hz	14	0.02	0.06	24.37	16.87	2.21	0.23	12.21	0.01	43.94	0.15	0.03	0.02	0.02	-	100.14	0.565	0.547	0.025
MAN 77	Hz	4	0.12	0.02	44.35	12.77	2.20	0.21	16.72	0.11	23.28	0.29	0.02	0.05	0.03	-	100.16	0.702	0.261	0.019
MAN 78	Du	4	0.04	0.03	22.42	16.78	2.52	0.24	11.91	0.04	45.20	0.10	0.05	0.01	0.06	-	99.40	0.560	0.575	0.015
MAN 79	Du	5	0.03	0.06	33.56	15.16	1.78	0.21	14.17	0.01	34.18	0.14	0.02	0.02	0.05	-	99.40	0.627	0.409	0.042
MAN 80	Hz	5	0.03	0.04	46.79	12.99	2.22	0.15	16.87	0.01	20.01	0.27	0.03	-	0.06	-	99.46	0.700	0.223	0.005
MAN 81	Hz	3	-	0.04	27.10	15.50	1.16	0.23	13.32	0.01	42.36	0.06	0.03	-	-	-	99.81	0.607	0.512	0.024
MAN 82	Hz	5	0.03	0.06	23.11	17.23	1.50	0.29	12.07	0.03	46.74	0.09	0.04	-	0.04	-	101.23	0.557	0.542	0.013
MAN 84	Du	6	0.04	0.05	22.68	17.37	2.85	0.21	12.06	0.04	46.28	0.17	0.01	-	0.05	-	101.81	0.555	0.578	0.032
MAN 85	Du	3	-	0.05	21.70	17.38	3.63	0.29	11.65	0.00	45.64	0.16	0.02	-	0.03	-	100.55	0.546	0.585	0.006
MAN 87	Du	3	0.03	0.03	26.69	14.87	2.47	0.21	13.69	0.04	41.55	0.14	0.04	0.01	0.04	-	99.78	0.623	0.511	0.007
MAN 89	Du	3	0.02	0.02	21.61	17.13	4.51	0.29	11.71	0.03	44.55	0.13	0.01	-	0.04	-	100.06	0.551	0.580	0.012
MAN 92	Hz	3	0.00	0.06	24.09	16.60	2.67	0.34	12.43	0.03	44.64	0.16	0.04	-	0.06	-	101.12	0.573	0.554	0.017
MAN 93	Hz	4	0.06	0.04	20.34	17.63	2.60	0.18	11.03	-	46.34	0.01	0.03	-	-	-	98.26	0.527	0.611	0.006
MAN 94	Hz	4	0.01	0.03	26.84	15.78	2.02	0.28	13.29	-	42.60	0.15	0.03	-	0.03	-	101.05	0.602	0.516	0.004
MAN 95	Hz	5	0.04	0.06	41.31	13.47	2.20	0.19	16.22	0.02	26.31	0.15	0.01	0.00	0.03	-	100.02	0.684	0.299	0.020
MAN 96	Du	3	0.02	0.06	24.36	17.43	3.53	0.34	11.90	0.02	42.84	0.06	0.02	0.02	0.03	-	100.63	0.551	0.541	0.014
MAN 98	Du	3	0.02	0.04	28.92	14.51	2.50	0.18	14.12	0.04	39.31	0.20	0.03	0.02	0.00	-	99.90	0.636	0.477	0.012
MAN 99	Hz	4	0.04	0.05	26.96	15.88	2.51	0.29	13.01	0.01	40.76	0.12	0.02	0.00	-	-	99.64	0.595	0.504	0.007
MAN 101	Hz	3	0.01	0.03	27.62	15.20	1.61	0.22	13.81	0.02	41.98	0.11	0.01	0.01	0.05	-	100.69	0.620	0.505	0.025
MAN 103	Hz	4	0.02	0.06	17.48	17.94	2.58	0.21	11.06	0.02	51.56	0.04	-	0.04	0.03	-	101.03	0.525	0.664	0.014
MAN 105	Hz	5	0.02	0.07	22.29	16.16	1.75	0.27	12.25	0.02	46.03	0.12	0.02	0.02	0.04	-	99.08	0.577	0.581	0.005
MAN 107	Hz	5	0.02	0.03	21.74	16.39	3.37	0.24	11.97	0.03	44.95	0.10	0.02	0.00	0.01	-	98.88	0.567	0.581	0.019
MAN 109	Hz	4	0.04	0.04	20.07	16.68	2.21	0.26	11.85	0.01	48.54	0.10	0.02	0.01	0.04	-	99.89	0.561	0.619	0.013
MAN 110	Hz	3	-	0.03	33.73	14.32	1.95	0.21	14.73	0.01	34.33	0.14	0.02	0.00	0.02	-	99.49	0.649	0.406	0.008
MAN 111	Hz	3	0.08	0.07	24.13	15.79	1.02	0.18	13.13	0.05	46.28	0.14	0.01	0.01	-	-	100.88	0.599	0.563	0.004
MAN 112	Hz	3	0.01	0.06	45.88	13.31	2.73	0.17	16.58	-	20.45	0.29	0.04	0.00	0.05	-	99.57	0.691	0.230	0.006
MAN 113	Hz	3	0.39	0.05	30.35	14.65	2.31	0.24	14.38	0.19	37.93	0.15	0.00	-	-	-	100.65	0.638	0.456	0.006
MAN 114	Du	14	0.04	0.06	33.88	14.09	1.44	0.19	15.12	0.01	35.53	0.15	0.02	0.01	0.02	-	100.55	0.658	0.413	0.002
MAN 115	Hz	3	0.02	0.04	37.12	14.12	1.63	0.18	15.43	-	31.52	0.12	0.04	0.02	0.06	-	100.29	0.662	0.363	0.016
MAN 116	Hz	3	0.01	0.11	30.92	15.30	2.43	0.19	13.90	-	37.09	0.24	0.02	-	-	-	100.21	0.620	0.446	0.002
MAN 149	Hz	4	0.03	0.06	24.04	16.64	3.53	0.23	12.36	-	43.58	-	-	-	-	-	100.46	0.571	0.550	0.008
MAN 150	Hz		0.00	0.10	27.42	15.05	2.81	0.24	13.49	-	39.88	-	-	-	-	-	98.98	0.617	0.467	0.004
MAN 151	Du	5	0.03	0.04	24.92	16.32	3.45	0.22	12.67	-	42.70	-	-	-	-	-	100.33	0.582	0.545	0.006
MAN 153	Hz	5	0.02	0.06	24.10	16.40	2.69	0.18	12.76	-	44.92	-	-	-	-	-	101.12	0.583	0.565	0.0100
MAN 155	Hz	6	0.03	0.07	22.59	17.66	4.01	0.21	11.46	-	43.97	-	-	-	-	-	100.00	0.538	0.563	0.020
MAN 157	Du	7	-	0.05	24.67	17.85	3.20	0.27	11.41	-	42.01	-	-	-	-	-	99.47	0.535	0.532	0.018
So_2	Hz	3	0.04	0.06	28.83	15.34	2.68	0.21	13.69	-	38.85	0.12	0.01	-	0.05	-	99.88	0.616	0.428	0.006
So_3	Hz	3	0.01	0.06	32.04	14.86	2.51	0.17	14.38	-	36.28	0.13	0.03	0.01	0.02	-	100.50	0.635	0.403	0.022
So_4	Lz	5	0.02	0.06	31.82	14.63	2.69	0.18	14.49	-	36.06	0.12	0.03	0.01	0.01	-	100.12	0.640	0.451	0.016
So_7	Hz	3	0.01	0.05	23.01	16.30	2.08	0.24	12.54	0.00	46.02	0.11	0.01	-	0.01	-	100.39	0.580	0.598	0.003
So_9	Hz	3	-	0.08	19.78	17.77	2.84	0.19	11.25	-	48.09	0.08	0.01	-	0.02	-	100.11	0.532	0.571	0.014
So_10	Du	6	0.01	0.03	25.69	16.57	2.66	0.14	12.60	-	42.15	0.08	0.03	0.01	0.04	-	100.01	0.577	0.520	0.010
So_11	Hz	4	0.04	0.05	23.63	15.97	2.10	0.31	12.62	-	45.03	0.10	0.03	0.00	0.00	-	99.88	0.587	0.569	0.023

Table 5. (continued)

Sample	Rock	N	SiO_2	TiO_2	Al_2O_3	FeO	Fe_2O_3	MnO	MgO	CaO	Cr_2O_3	NiO	Na_2O	K_2O	P_2O_5	SO_2	Total	Mg#	Cr#	SD
So_15	Hz	3	0.01	0.07	33.81	14.16	1.93	0.19	15.00	-	34.96	0.11	0.04	0.02	0.10	-	100.38	0.655	0.410	0.011
So_16	Hz	3	-	0.04	40.28	12.17	1.58	0.21	16.79	-	28.30	0.27	0.01	-	0.05	-	99.69	0.712	0.320	0.009
So_17	Hz	4	0.03	0.07	39.03	13.28	2.22	0.13	16.05	0.00	28.82	0.17	0.02	-	0.04	-	99.86	0.685	0.331	0.004
So_19	Du	4	-	0.05	27.02	15.66	2.67	0.13	13.42	-	41.50	0.13	0.03	-	0.02	-	100.62	0.606	0.508	0.015
So_21	Hz	4	-	0.06	22.22	16.91	2.52	0.24	11.93	-	45.99	0.17	0.02	-	0.01	-	100.07	0.559	0.581	0.012
So_24	Hz	4	0.03	0.04	24.96	14.48	1.32	0.23	13.87	0.00	45.07	0.10	0.05	0.02	0.03	-	100.19	0.632	0.548	0.010
So_25	Hz	3	-	-	29.21	14.68	1.83	0.23	14.23	-	40.07	0.04	0.02	0.01	0.03	-	100.35	0.635	0.480	0.006
So_56	Hz	4	0.04	0.05	29.88	16.24	2.64	0.24	13.16	0.01	37.27	0.08	0.02	0.04	0.05	-	99.71	0.593	0.456	0.006
So_57	Hz	5	0.04	0.02	24.15	17.83	2.01	0.28	12.51	0.02	47.88	0.12	0.03	0.03	0.01	-	104.91	0.558	0.572	0.006
So_58	Hz	3	0.02	0.04	21.87	16.54	2.04	0.26	12.34	-	47.39	0.03	0.03	0.02	0.09	-	100.66	0.573	0.592	0.003
So_59	Hz	4	0.04	0.05	26.64	15.53	3.17	0.18	13.20	-	40.79	0.13	0.04	0.00	0.01	-	99.80	0.604	0.507	0.010
So_60	Du	4	0.03	0.04	23.00	16.43	1.82	0.31	12.20	0.01	45.63	0.11	0.02	0.01	-	-	99.60	0.572	0.571	0.008
So_61	Hz	3	0.03	0.06	19.93	17.55	2.72	0.28	11.29	0.02	48.47	0.11	0.04	-	0.03	-	100.53	0.536	0.620	0.003
So_62	Hz	3	0.02	0.07	27.48	15.28	1.90	0.20	13.52	-	41.36	0.11	0.04	0.01	0.02	-	100.02	0.614	0.503	0.015
So_63	Hz	4	0.02	0.05	27.17	16.11	3.52	0.23	13.21	-	40.52	0.19	0.01	0.00	0.05	-	101.09	0.596	0.500	0.003
So_65	Hz	4	0.01	0.03	33.53	13.76	2.09	0.17	15.04	0.03	34.54	0.16	0.01	0.02	0.03	-	99.41	0.663	0.409	0.014
So_66	Hz	4	0.01	-	25.85	15.91	2.74	0.27	12.92	0.01	41.92	0.12	0.01	0.01	0.06	-	99.84	0.593	0.521	0.010
So_67	Hz	5	0.14	0.04	32.44	14.42	1.53	0.23	14.57	0.01	35.84	0.19	0.02	0.00	0.05	-	99.49	0.645	0.426	0.005
So_68	Hz	3	0.02	0.04	34.29	13.77	2.85	0.21	15.15	0.02	33.28	0.10	0.04		0.00	-	99.76	0.664	0.394	0.006
So_70	Lz	5	0.07	0.05	33.79	15.21	2.53	0.16	14.24	0.01	33.60	0.22	0.02	0.03	0.02	-	99.95	0.627	0.400	0.033
So_74	Hz	3	0.05	0.04	31.28	14.91	1.30	0.19	14.27	0.01	38.23	0.15	0.02	0.01	0.03	-	100.49	0.632	0.451	0.013
So_75	Hz	3	0.10	0.06	29.64	15.29	1.13	0.23	13.95	0.07	39.67	0.10	0.01	-	0.08	-	100.34	0.621	0.473	0.017
So_76	Hz	3	0.05	0.05	27.78	15.29	1.80	0.16	13.57	0.01	40.73	0.15	0.04	-	0.04	-	99.68	0.615	0.496	0.005
So_80	Du	3	0.01	0.12	29.31	13.97	1.18	0.14	14.72	0.04	40.44	0.06	0.03	0.02	0.00	-	100.05	0.654	0.481	0.008
So_81	Hz	3	0.00	0.03	32.78	14.00	1.41	0.20	14.95	0.00	36.74	0.25	0.01	0.01	-	-	100.39	0.657	0.429	0.013
So_82	Hz	4	0.10	0.04	32.18	14.70	1.46	0.22	14.32	0.02	36.26	0.06	0.02	0.01	0.02	-	99.41	0.636	0.431	0.004
So_83	Hz	3	0.04	0.05	25.46	16.09	2.38	0.26	12.84	-	42.61	0.07	0.01	-	0.01	-	99.81	0.589	0.529	0.007
So_84	Hz	3	0.01	0.05	22.83	16.53	2.32	0.24	12.34	-	45.88	0.09	0.01	-	0.02	-	100.33	0.573	0.597	0.012
So_85	Hz	4	0.01	0.06	20.38	16.26	2.17	0.29	12.08	0.03	48.27	0.13	0.03	0.01	0.11	-	99.83	0.572	0.711	0.013
So_87	Du	6	0.07	0.04	22.46	15.89	2.42	0.24	12.53	0.06	45.74	0.14	0.02	0.03	0.04	-	99.68	0.586	0.577	0.007
So_88	Hz	3	0.03	0.03	41.65	13.42	1.39	0.21	16.16	0.02	26.55	0.23	0.03	-	0.06	-	99.78	0.684	0.300	0.016
So_89	Du	6	0.02	0.02	20.69	17.18	2.46	0.31	11.51	0.01	47.34	0.08	0.02	-	0.05	-	99.70	0.546	0.606	0.016
So_90	Hz	3	0.02	0.05	23.50	15.96	1.91	0.24	12.73	0.01	45.49	0.14	0.01	0.01	0.03	-	100.12	0.589	0.565	0.007
So_91	Hz	4	0.02	0.04	29.13	14.87	1.99	0.22	13.90	0.00	39.45	0.12	0.04	0.02	0.03	-	99.86	0.627	0.476	0.004
So_92	Hz	4	0.02	0.04	38.55	13.90	1.51	0.15	15.53	0.02	29.54	0.18	0.02	0.01	0.05	-	99.51	0.667	0.340	0.006
So_94	Hz	5	0.02	0.08	29.03	15.49	2.11	0.30	13.72	0.03	39.96	0.11	0.02	0.03	0.03	-	100.93	0.614	0.480	0.017
So_95	Du	4	0.04	0.02	36.14	13.98	2.15	0.19	15.19	0.04	31.31	0.10	0.02	0.00	0.02	-	99.20	0.661	0.368	0.028
So_96	Lz	4	0.03	0.05	45.88	12.68	1.23	0.19	17.01	0.01	22.23	0.21	0.02	-	0.00	-	99.55	0.707	0.245	0.024
So_100	Du	6	0.03	0.06	16.77	18.35	2.78	0.27	10.32	0.01	50.60	0.19	0.03	0.01	0.03	-	99.45	0.503	0.669	0.012
So_101	Hz	3	0.03	0.05	41.10	12.18	2.22	0.19	16.99	-	27.30	0.24	0.03	0.00	0.02	-	100.33	0.715	0.308	0.045
So_102	Hz	3	-	0.04	32.21	15.76	3.50	0.24	13.82	-	34.75	0.08	0.02	0.01	-	-	100.43	0.612	0.420	0.007
So_104	Hz	4	0.04	0.01	21.25	16.37	1.32	0.31	12.26	0.01	48.98	0.10	0.04	0.02	0.06	-	100.79	0.574	0.608	0.007
So_105	Hz	3	0.04	0.07	29.04	15.16	2.44	0.18	13.87	-	39.14	0.11	0.04	0.05	0.06	-	100.19	0.622	0.475	0.016

Table 5. (continued)

Sample	Rock	N	SiO_2	TiO_2	Al_2O_3	FeO	Fe_2O_3	MnO	MgO	CaO	Cr_2O_3	NiO	Na_2O	K_2O	P_2O_5	SO_2	Total	Mg#	Cr#	SD
So_106	Hz	3	0.03	0.08	24.19	16.28	4.00	0.17	12.76	0.04	42.81	0.11	-	-	0.06	-	100.52	0.585	0.543	0.031
So_107	Hz	4	0.05	0.08	22.78	17.12	3.40	0.27	11.67	0.01	43.76	0.16	0.04	0.02	-	-	99.37	0.551	0.563	0.016
So_108	Hz	5	0.04	0.04	22.60	17.93	3.60	0.22	11.43	0.02	44.50	0.12	0.02	0.01	0.06	-	100.57	0.534	0.569	0.024
So_109	Hz	3	0.02	0.03	24.40	15.70	4.13	0.23	13.02	0.03	42.88	0.13	0.04	-	0.03	-	100.63	0.598	0.541	0.015
So_110	Hz	4	0.05	0.05	24.11	15.72	3.21	0.21	12.86	-	43.41	0.15	0.04	-	0.01	-	99.81	0.595	0.547	0.010
So_112	Du	4	0.04	0.04	29.57	14.87	1.19	0.30	13.99	-	39.60	0.17	0.03	0.02	0.04	-	99.85	0.628	0.473	0.007
So_113	Du	3	0.02	0.03	23.93	16.52	3.75	0.14	12.51	0.01	43.58	0.17	0.02	-	0.01	-	100.67	0.576	0.550	0.010
So_114	Hz	3	-	0.07	21.06	17.75	3.03	0.22	11.30	0.03	46.26	0.11	0.01	0.00	0.03	-	99.87	0.533	0.609	0.011
So_115	Du	3	0.03	0.05	18.44	17.54	2.41	0.21	11.24	0.05	50.55	0.12	0.04	0.03	-	-	100.70	0.535	0.648	0.040
So_116	Hz	5	0.06	0.03	21.91	17.19	3.24	0.17	11.66	-	44.76	0.08	-	0.00	0.03	-	99.11	0.549	0.578	0.029
So_118	Hz	4	0.03	0.07	24.55	16.61	3.41	0.30	12.34	0.01	42.49	0.03	0.04	0.03	0.03	-	99.93	0.572	0.537	0.006
So_119	Hz	3	0.03	0.05	21.55	17.42	3.97	0.33	11.59	0.02	45.54	0.10	0.03	-	0.02	-	100.64	0.544	0.586	0.005
So_122	Hz	4	0.07	0.05	21.64	16.07	2.78	0.27	12.32	0.02	46.02	0.09	0.03	0.01	0.03	-	99.38	0.579	0.588	0.010
So_124	Hz	4	0.02	0.06	28.01	16.53	2.30	0.17	12.72	0.04	39.71	0.25	0.02	0.03	0.07	-	99.96	0.580	0.488	0.003
So_125	Hz	5	0.10	0.04	25.70	16.07	3.03	0.24	12.83	0.01	41.87	0.17	0.04	-	-	-	100.10	0.589	0.522	0.006
So_126	Hz	3	0.02	0.04	30.17	15.53	2.97	0.20	13.82	0.01	37.45	0.07	0.03	0.01	0.03	-	100.36	0.615	0.454	0.016
So_127	Hz	4	0.01	0.06	26.91	15.52	2.30	0.27	13.44	0.04	42.18	0.19	0.03	-	0.01	-	100.96	0.609	0.513	0.015
So_128	Hz	3	0.03	0.07	34.87	13.96	2.33	0.19	15.28	-	33.55	0.14	0.03	-	0.06	-	100.51	0.663	0.392	0.012
So_130	Hz	3	0.02	0.07	33.91	14.44	2.70	0.21	14.97	0.04	34.45	0.23	0.02	-	0.06	-	101.13	0.651	0.405	0.009
So_132	Hz	5	0.02	0.03	29.90	15.17	3.22	0.21	14.01	0.01	37.87	0.13	0.02	0.05	0.04	-	100.68	0.624	0.459	0.010
So_134	Hz	4	0.04	0.10	20.57	17.38	2.87	0.19	11.65	0.02	47.46	0.06	0.03	0.00	-	-	100.36	0.546	0.608	0.012
So_135	Hz	4	0.02	0.10	28.68	14.73	2.59	0.24	13.98	0.03	39.62	0.21	0.04	-	-	-	100.22	0.630	0.481	0.018
So_136	Hz	5	0.05	0.06	29.81	14.67	2.56	0.20	14.02	-	37.68	0.26	0.01	0.01	-	-	99.33	0.632	0.459	0.004
So_137	Du	4	0.03	0.06	30.09	14.46	1.85	0.18	14.25	0.01	37.92	0.08	0.02	0.03	0.03	-	98.99	0.639	0.458	0.009
So_139	Hz	5	0.02	0.03	36.84	13.77	2.93	0.19	15.20	0.04	29.54	0.21	0.02	0.00	-	-	98.78	0.665	0.350	0.005
So_140	Hz	4	0.04	0.06	40.77	12.39	1.17	0.19	16.57	0.04	27.64	0.21	0.03	0.03	-	-	99.13	0.706	0.313	0.003
So_141	Hz	5	0.06	0.07	44.01	12.61	2.23	0.16	16.70	0.03	22.74	0.24	0.02	0.01	0.00	-	98.88	0.704	0.257	0.006
So_142	Lz	5	0.04	0.06	37.34	14.04	1.82	0.13	15.10	0.03	29.56	0.17	0.03	0.01	0.05	-	98.37	0.659	0.347	0.028
So_143	Du	6	0.02	0.06	25.06	16.07	1.55	0.25	12.56	-	42.92	0.06	0.03	0.02	0.03	-	98.63	0.584	0.535	0.009
So_144	Hz	5	0.05	0.03	47.64	12.55	2.81	0.16	17.16	0.03	18.48	0.33	0.02	0.00	0.03	-	99.30	0.711	0.207	0.006
So_145	Hz	4	0.01	0.09	29.22	15.59	3.68	0.21	13.41	0.04	36.87	0.17	0.02	-	0.04	-	99.36	0.607	0.458	0.013
So_148	Hz	4	0.04	0.06	25.91	15.43	3.71	0.17	13.14	-	40.62	0.17	0.03	-	0.04	-	99.33	0.605	0.513	0.008
94-46	Hz	7	0.01	0.06	26.55	15.38	2.70	0.25	13.13	-	40.80	-	-	-	-	-	98.87	0.605	0.508	0.010

[a] "N" and Mg# are the same as for Table 2. Cr# is Cr/(Cr + Al). No chemical zoning has been detected. Operating conditions and uncertainty: see Table 2 footnote.

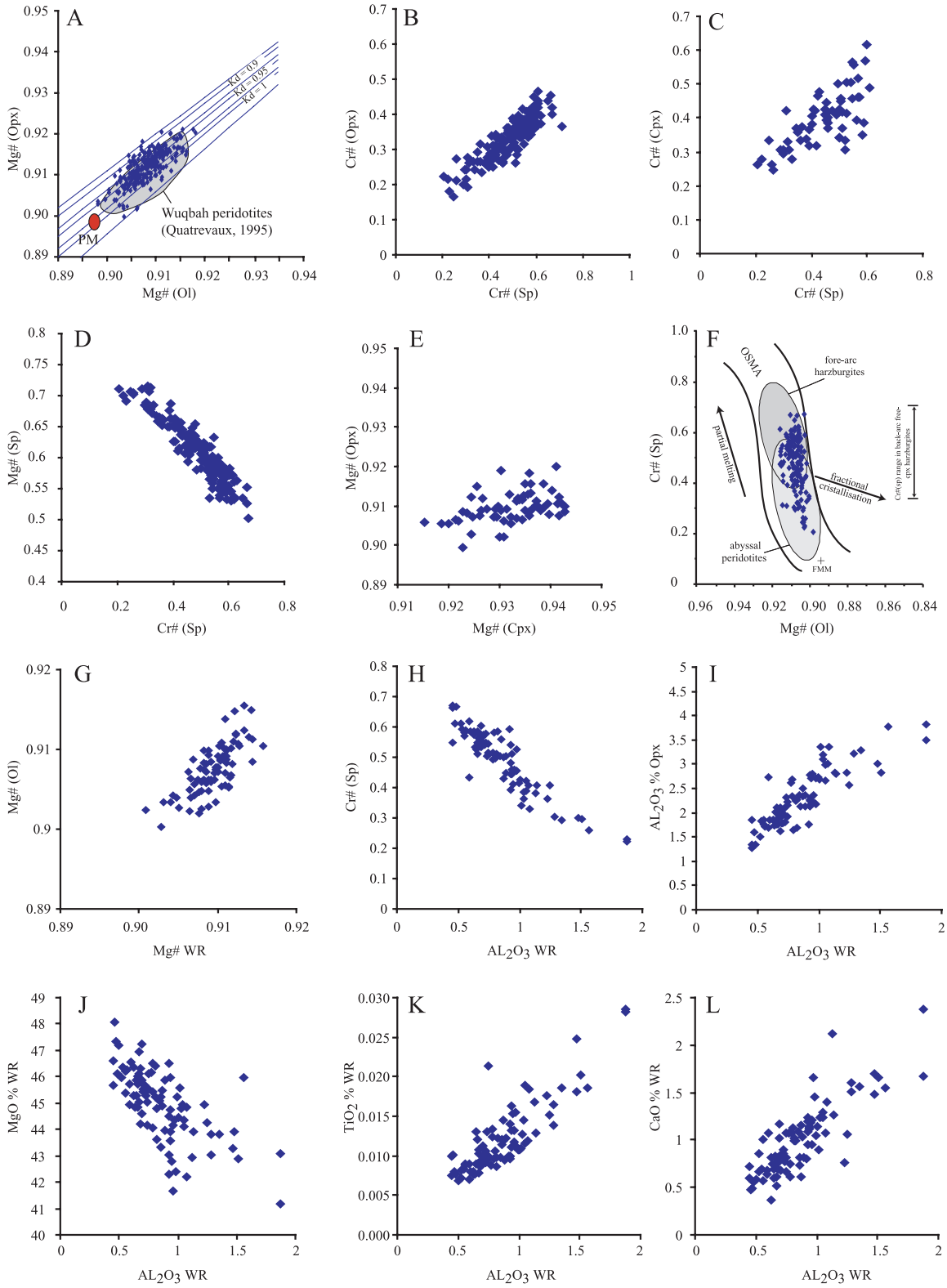
A
Mg# (Opx)
Mg# (Ol)
Kd = 0.9
Kd = 0.95
Kd = 1
Wuqbah peridotites
(Quatrevaux, 1995)
PM
B
Cr# (Opx)
Cr# (Sp)
C
Cr# (Cpx)
Cr# (Sp)
D
Mg# (Sp)
Cr# (Sp)
E
Mg# (Opx)
Mg# (Cpx)
F
Cr# (Sp)
Mg# (Ol)
OSMA
fore-arc
harzburgites
partial melting
fractional
cristallisation
Cr#(sp) range in back-arc fres-
tex harzburgites
abyssal
peridotites
+
FMM
G
Mg# (Ol)
Mg# WR
H
Cr# (Sp)
AL2O3 WR
I
AL2O3 % Opx
AL2O3 WR
J
MgO % WR
AL2O3 WR
K
TiO2 % WR
AL2O3 WR
L
CaO % WR
AL2O3 WR

Figure 4

1994b; *Jaques and Green*, 1980]. Also, there is a good Cr-Al partitioning between spinels and Opx (Figure 4b) and Cpx (Figure 4c).

[27] When considering the Al-Cr exchange reaction between coexisting Opx and spinel phases, we can calculate an average equilibrium temperature of 952°C ± 42°C [*Witt-Eickschen and Seck*, 1991], which is close to the values calculated using the Ca content of the pyroxenes: 947°C ± 68°C [*Bertrand and Mercier*, 1985]; 1027°C ± 64°C [*Brey and Kohler*, 1990]. As commonly seen in abyssal and ophiolitic peridotites, these temperature estimates are higher than those calculated with *Fabriès* [1979] and *Roeder et al.* [1979] thermometers, 790°C ± 10°C and 740°C ± 24°C, respectively, based on the partitioning of Fe^{2+} and Mg^{2+} between olivine and spinel.

4.5. Whole-Rock Chemistry

[28] The analyzed samples (90 rocks, Table 6) are serpentinized to different degrees as shown by the loss on ignition (LOI) values (0% < LOI < 15.67%) as already noted for the Sumail and Wadi Tayin peridotites [*Godard et al.*, 2000]. All peridotites have low CaO content, below 2.4%, with 87% of the samples below 1.5% as expected owing to the scarcity of the Cpx present in the study rocks. Few samples contain a small amount of secondary calcite crystallized in infra-millimeter scale fractures. Compared to the primitive mantle, the analyzed peridotites are particularly magnesium-rich (average $MgO\%_{(WR)} \approx 45\%$, SD = 1.3%), aluminum-poor (average $Al_2O_3\%_{(WR)} \approx 0.9\%$, SD = 0.3%) and alkali-poor (average $Na_2O\%_{(WR)} \approx 0.02\%$, SD = 0.01%). Their Al_2O content correlates positively with CaO and TiO_2 and anticorrelates with MgO (Figures 4l, 4k, and 4j, respectively), as theoretically expected during partial melting evolution [*Jagoutz et al.*, 1979; *Maaløe and Aoki*, 1977; *Ringwood*, 1975]. The samples show good correlations between mineral and bulk rock composition for Mg, Cr and Al (Figures 4g–4i).

[29] The Al_2O_3/SiO_2 ratios are lower than 0.04 and the MgO/SiO_2 higher than 0.95 (Figure 5), which makes the studied samples comparable to the most depleted part of the mantle fractionation array, as previously noted for peridotites from the southern part of the Oman ophiolite [*Godard et al.*, 2000]. However, the peridotites show large variations in MgO/SiO_2, which suggest that they suffered alteration, as commonly seen in abyssal peridotites [*Snow and Dick*, 1995; *Niu and Hékinian*, 1997a]. To test this hypothesis, we recalculate the primary chemistry of the whole rock using the equations developed for abyssal peridotites [*Snow and Dick*, 1995]. To do so, one must assume that major element compositions of primary unaltered minerals represent the primary rock chemistry before alteration [*Niu and Hékinian*, 1997a; *Snow and Dick*, 1995]. The bulk rock composition can be calculated from the mineral compositions and modal analysis corrected by the density of each phase. But this is only valid if the initial mode of the peridotite is perfectly reconstructed, which is not certain for the study peridotites that underwent 40–60% serpentinization. The calculation of MgO_R contents (R for "recalculated") before any secondary process as weathering and serpentinization was done as in equation (1) for the MgO example:

$$MgO_R = (mod_{olivine} \times MgO_{olivine}) + (mod_{opx} \times MgO_{opx}) + (mod_{cpx} \times MgO_{cpx}) + (mod_{spinel} \times MgO_{spinel}) \quad (1)$$

where MgO_R is recalculated $MgO\%_{(WR)}$ and mod is volumic abundance of each phase.

[30] Applying equation (1) to each oxide, we have compared the primary whole rock chemistry to the measured values. Rocks have undergone relative

Figure 4. Element partitioning between (a) olivine Mg# and Opx Mg#, (b) Opx Cr# and spinel Cr#, (c) Cpx Cr# and spinel Cr#, (d) spinel Mg# and spinel Cr#, (e) Opx Mg# and Cpx Mg#, (f) spinel Cr# and olivine Mg#, (g) olivine Mg# and whole rock Mg#, (h) Al_2O_3 whole rock versus spinel Cr#, (i) versus Al_2O_3 Opx, (j) versus whole rock MgO, (k) versus whole rock TiO_2, and (l) whole rock CaO. Figure 4a: After thermodynamic calculations [*Glücklich-Herbas*, 1992], we have drawn theoretical isothermal equilibrium lines for an exchange reaction with two ideal solutions. Kd represents the theoretical equilibrium Fe^{2+}/Mg^{2+} distribution coefficient. Each point stands for the average of Mg# in Opx versus the average of Mg# in olivine in a single sample. The gray area corresponds to 150 analyses of the Wuqbah peridotites [*Quatrevaux*, 1995]. Figure 4f: OSMA is the Olivine-Spinel Mantle Array [*Arai*, 1987, 1994a, 1994b]. The theoretical evolution after partial melting [*Arai*, 1994a] shows a trend beginning from the Fertile MORB Mantle (FMM). Domains represent mineral compositions of fore-arc harzburgites [*Ishii et al.*, 1992], abyssal peridotites [*Dick and Bullen*, 1984], and back-arc Cpx-free harzburgites [*Monnier et al.*, 1995, 1999a, 1999b, 2000, 2003].

Table 6. Major Element Analyses, Recalculated on a Free-Volatile Basis From 90 Analyses[a]

Samples	Rock	SiO_2	TiO_2	Al_2O_3	FeO	Fe_2O_3	MnO	MgO	CaO	Cr_2O_3	NiO	Na_2O	K_2O	P_2O_5	LOI	Total	Mg# RT
MAN 01	Hz	44.63	0.02	1.13	6.91	1.36	0.13	42.96	2.12	0.42	0.30	0.02	0.00	0.00	9.89	100.00	0.905
MAN 03	Hz	44.32	0.02	1.06	6.97	1.37	0.13	44.10	1.23	0.45	0.27	0.02	0.00	0.02	9.42	99.94	0.906
MAN 06	Du	43.71	0.01	0.71	7.03	1.38	0.13	45.51	0.68	0.53	0.29	0.02	0.00	0.00	10.06	100.00	0.908
MAN 07	Du	44.69	0.01	0.64	6.75	1.32	0.13	44.85	0.75	0.53	0.31	0.01	0.00	0.00	8.75	100.00	0.910
MAN 08	Du	44.48	0.01	0.65	6.80	1.33	0.12	45.26	0.59	0.42	0.33	0.01	0.00	0.00	10.01	100.00	0.911
MAN 09	Hz	44.93	0.01	0.74	6.85	1.34	0.13	44.16	1.08	0.44	0.30	0.01	0.00	0.00	9.16	100.00	0.908
MAN 10	Hz	45.48	0.01	0.93	6.59	1.29	0.13	43.59	1.19	0.49	0.30	0.00	0.00	0.00	6.99	100.00	0.910
MAN 11	Hz	43.19	0.01	0.79	6.68	1.31	0.12	46.52	0.61	0.44	0.31	0.02	0.00	0.00	9.14	100.00	0.914
MAN 13	Hz	44.19	0.01	0.74	6.91	1.36	0.13	45.06	0.77	0.49	0.32	0.01	0.01	0.00	7.56	100.00	0.909
MAN 14	Hz	44.62	0.01	0.66	6.86	1.35	0.13	44.84	0.75	0.46	0.31	0.01	0.00	0.00	7.81	100.00	0.909
MAN 20	Hz	43.85	0.02	0.94	7.01	1.37	0.13	44.72	1.15	0.49	0.29	0.01	0.00	0.02	7.79	100.00	0.907
MAN 23	Hz	43.73	0.01	1.03	6.97	1.37	0.14	44.78	1.23	0.41	0.32	0.01	0.00	0.01	4.35	100.00	0.908
MAN 25	Hz	43.72	0.01	0.65	6.78	1.33	0.13	45.89	0.70	0.45	0.33	0.01	0.00	0.00	7.49	100.00	0.912
MAN 27	Hz	43.45	0.01	0.89	6.72	1.32	0.13	45.89	0.81	0.57	0.30	0.01	0.00	0.02	0.72	100.12	0.913
MAN 28	Hz	43.70	0.01	0.81	6.95	1.36	0.13	45.22	1.02	0.43	0.30	0.01	0.00	0.02	7.43	99.96	0.909
MAN 30	Hz	43.57	0.01	0.81	6.07	1.19	0.13	46.41	1.12	0.47	0.30	0.01	0.00	0.01	15.67	100.09	0.921
MAN 32	Hz	43.83	0.02	1.35	7.12	1.40	0.13	43.83	1.56	0.46	0.29	0.02	0.00	0.00	8.26	100.00	0.904
MAN 33	Du	44.91	0.02	1.51	6.78	1.33	0.14	42.89	1.66	0.44	0.30	0.02	0.00	0.00	0.27	100.00	0.906
MAN 34	Hz	43.82	0.01	1.04	6.71	1.32	0.12	44.96	1.26	0.43	0.32	0.02	0.00	0.00	3.27	100.00	0.911
MAN 35	Hz	44.95	0.01	1.28	6.91	1.35	0.14	43.02	1.61	0.40	0.31	0.01	0.00	0.00	5.96	100.00	0.905
MAN 37	Hz	44.08	0.01	1.05	6.99	1.37	0.14	44.34	1.29	0.40	0.31	0.02	0.00	0.00	4.09	100.00	0.907
MAN 39	Hz	44.46	0.01	0.82	6.69	1.31	0.13	44.79	0.99	0.46	0.32	0.02	0.00	0.00	6.79	100.00	0.911
MAN 40	Hz	43.94	0.01	0.63	7.03	1.38	0.13	45.26	0.82	0.45	0.34	0.01	0.00	0.00	8.36	100.00	0.908
MAN 41	Du	46.41	0.01	0.98	6.58	1.29	0.14	42.38	1.45	0.45	0.30	0.01	0.00	0.00	−0.17	100.00	0.908
MAN 42	Hz	43.70	0.01	0.59	7.04	1.38	0.13	45.72	0.68	0.42	0.32	0.01	0.00	0.01	0.13	100.00	0.909
MAN 44	Hz	44.96	0.01	0.69	6.84	1.34	0.14	44.21	0.81	0.69	0.30	0.01	0.00	0.00	5.60	100.00	0.908
MAN 48	Hz	44.04	0.01	0.67	6.48	1.27	0.12	46.09	0.62	0.36	0.32	0.01	0.00	0.00	6.48	100.00	0.916
MAN 50	Hz	43.30	0.01	0.53	6.90	1.35	0.13	46.36	0.67	0.41	0.32	0.02	0.00	0.00	1.39	100.00	0.911
MAN 55	Du	43.53	0.01	0.52	6.92	1.36	0.13	45.98	0.86	0.37	0.31	0.01	0.00	0.00	1.24	100.00	0.910
MAN 56	Hz	42.25	0.01	0.69	6.76	1.33	0.12	47.26	0.78	0.45	0.34	0.01	0.00	0.00	9.36	100.00	0.914
MAN 57	Du	45.83	0.01	0.86	6.80	1.33	0.13	43.32	0.81	0.41	0.29	0.19	0.01	0.00	11.44	100.00	0.907
MAN 58	Hz	43.58	0.01	0.49	6.88	1.35	0.13	46.12	0.55	0.56	0.32	0.02	0.00	0.00	9.02	100.00	0.911
MAN 59	Hz	43.56	0.01	0.72	6.83	1.34	0.13	45.68	0.89	0.51	0.32	0.01	0.00	0.00	5.05	100.00	0.911
MAN 60	Du	42.44	0.01	0.60	7.00	1.37	0.14	46.56	1.08	0.41	0.31	0.01	0.00	0.02	0.07	99.94	0.911
MAN 62	Hz	43.01	0.01	0.69	6.96	1.36	0.13	45.88	1.17	0.46	0.31	0.01	0.00	0.00	8.48	100.00	0.910
MAN 63	Du	43.42	0.01	0.65	6.82	1.34	0.12	46.01	0.83	0.45	0.31	0.02	0.00	0.02	11.50	100.00	0.912
MAN 67	Hz	44.71	0.02	1.29	6.49	1.27	0.12	43.83	1.51	0.47	0.28	0.02	0.01	0.01	9.24	100.03	0.912
MAN 68	Du	42.52	0.01	0.93	6.84	1.34	0.12	46.50	0.95	0.59	0.31	0.01	0.00	0.02	9.10	100.14	0.912
MAN 70	Hz	43.43	0.01	0.56	6.90	1.35	0.12	46.25	0.56	0.47	0.30	0.02	0.00	0.01	11.07	100.00	0.911
MAN 72	Du	43.84	0.01	0.87	6.52	1.28	0.13	45.46	1.15	0.52	0.30	0.01	0.00	0.01	7.71	100.09	0.914
MAN 73	Hz	41.80	0.01	0.46	6.93	1.36	0.12	48.06	0.48	0.40	0.33	0.01	0.00	0.01	10.37	99.96	0.914
MAN 77	Hz	41.60	0.02	1.57	6.98	1.37	0.13	45.98	1.54	0.46	0.29	0.02	0.00	0.01	8.30	99.97	0.910
MAN 78	Du	43.76	0.01	0.71	6.97	1.37	0.13	45.41	0.85	0.46	0.30	0.01	0.00	0.01	8.50	99.98	0.909
MAN 79	Du	44.57	0.02	1.25	6.63	1.30	0.13	44.27	1.05	0.47	0.30	0.02	0.00	0.00	0.35	100.00	0.911
MAN 80	Hz	44.09	0.03	1.88	6.92	1.36	0.13	43.10	1.67	0.49	0.28	0.03	0.00	0.01	8.86	100.00	0.905
MAN 81	Hz	44.90	0.01	0.94	6.85	1.34	0.13	43.91	1.12	0.42	0.29	0.01	0.00	0.01	9.14	99.94	0.907
MAN 82	Hz	46.46	0.01	0.93	6.37	1.25	0.13	43.04	1.09	0.59	0.33	0.01	0.00	0.01	6.39	100.21	0.912
MAN 83	Hz	43.30	0.02	0.75	6.88	1.35	0.12	46.11	0.66	0.44	0.30	0.02	0.01	0.01	10.84	99.98	0.911
MAN 84	Du	44.14	0.01	0.72	6.75	1.32	0.12	45.28	0.86	0.46	0.30	0.02	0.01	0.01	11.53	100.02	0.911
MAN 85	Du	43.40	0.01	0.63	6.95	1.36	0.13	46.37	0.37	0.47	0.31	0.02	0.00	0.01	12.05	100.01	0.911
MAN 86	Hz	43.05	0.01	0.68	6.70	1.31	0.13	46.94	0.52	0.36	0.31	0.01	0.00	0.00	11.91	100.00	0.915
MAN 89	Du	42.52	0.01	0.50	6.91	1.35	0.13	47.20	0.58	0.42	0.32	0.02	0.00	0.01	12.29	99.97	0.913
MAN 92	Hz	43.33	0.01	0.68	6.77	1.33	0.13	46.31	0.70	0.44	0.30	0.01	0.00	0.00	11.84	100.00	0.913
MAN 93	Hz	42.57	0.01	0.47	6.87	1.35	0.13	47.32	0.49	0.40	0.32	0.01	0.00	0.01	12.50	99.96	0.913
MAN 94	Hz	43.86	0.01	0.79	6.91	1.35	0.13	45.44	0.75	0.44	0.30	0.01	0.00	0.00	10.16	100.00	0.910
MAN 95	Hz	43.90	0.02	1.47	6.76	1.33	0.14	43.90	1.70	0.47	0.29	0.02	0.01	0.01	10.83	100.01	0.909
MAN 96	Du	43.36	0.01	0.71	7.05	1.38	0.13	45.67	0.85	0.51	0.31	0.01	0.00	0.00	8.35	100.00	0.908
MAN 98	Du	42.83	0.01	0.77	6.90	1.35	0.13	46.15	1.07	0.45	0.31	0.01	0.00	0.01	8.91	100.00	0.911
MAN 99	Hz	44.89	0.01	0.89	6.95	1.36	0.14	43.94	1.04	0.47	0.32	0.01	0.00	0.00	4.48	100.00	0.906
MAN 101	Hz	44.03	0.01	0.84	6.70	1.31	0.13	45.11	1.09	0.44	0.30	0.01	0.00	0.01	7.19	100.00	0.911
MAN 103	Hz	43.04	0.01	0.45	6.91	1.36	0.13	46.59	0.72	0.42	0.31	0.01	0.01	0.01	6.38	99.97	0.912
MAN 105	Hz	44.18	0.01	0.55	6.90	1.35	0.13	45.37	0.69	0.40	0.31	0.02	0.00	0.01	2.77	99.94	0.910

Table 6. (continued)

Samples	Rock	SiO_2	TiO_2	Al_2O_3	FeO	Fe_2O_3	MnO	MgO	CaO	Cr_2O_3	NiO	Na_2O	K_2O	P_2O_5	LOI	Total	Mg# RT
MAN 107	Hz	45.44	0.01	0.79	6.48	1.27	0.13	44.05	1.08	0.56	0.29	0.01	0.00	0.01	6.16	100.13	0.912
MAN 109	Hz	44.54	0.01	0.59	6.99	1.37	0.13	44.93	0.63	0.43	0.31	0.01	0.00	0.01	9.49	99.96	0.908
MAN 110	Hz	44.46	0.01	1.14	6.93	1.36	0.13	43.92	1.26	0.47	0.31	0.01	0.00	0.00	5.98	100.00	0.907
MAN 111	Hz	43.72	0.00	0.66	6.90	1.35	0.13	45.71	0.73	0.46	0.33	0.01	0.00	0.00	8.92	100.00	0.910
MAN 112	Hz	45.34	0.03	1.88	6.94	1.36	0.14	41.17	2.38	0.46	0.29	0.03	0.01	0.00	3.31	100.00	0.901
MAN 113	Hz	43.81	0.02	0.98	6.87	1.35	0.13	44.36	1.66	0.51	0.30	0.01	0.00	0.00	8.85	100.00	0.908
MAN 114	Du	43.61	0.01	0.99	6.84	1.34	0.13	45.23	1.04	0.48	0.31	0.01	0.01	0.00	6.29	100.00	0.910
MAN 115	Hz	43.84	0.02	1.23	7.00	1.37	0.13	44.94	0.77	0.40	0.28	0.02	0.01	0.00	7.66	100.00	0.908
MAN 116	Hz	42.68	0.01	0.94	7.03	1.38	0.13	45.96	1.12	0.42	0.30	0.02	0.01	0.00	7.97	100.00	0.909
MAN 117	Hz	44.76	0.02	1.47	6.76	1.33	0.12	43.29	1.48	0.43	0.29	0.02	0.02	0.00	11.19	100.00	0.907
So_2	Hz	44.83	0.01	0.87	6.61	1.30	0.12	44.89	0.61	0.47	0.30	0.01	0.00	0.01	9.62	100.04	0.912
So_11	Hz	44.60	0.01	0.70	6.82	1.34	0.14	44.60	1.02	0.39	0.30	0.01	0.01	0.01	4.47	99.93	0.909
So_15	Hz	45.76	0.02	0.95	7.02	1.38	0.13	42.77	1.18	0.39	0.30	0.01	0.00	0.01	7.27	99.91	0.903
So_17	Hz	46.21	0.02	1.08	6.83	1.34	0.13	42.20	1.40	0.38	0.30	0.01	0.01	0.01	1.55	99.93	0.904
So_19	Du	45.64	0.01	0.82	6.69	1.31	0.12	43.63	0.99	0.44	0.30	0.02	0.00	0.01	9.23	99.99	0.909
So_21	Hz	44.57	0.01	0.67	6.79	1.33	0.13	45.02	0.71	0.49	0.31	0.01	0.00	0.01	8.99	100.05	0.910
So_25	Hz	47.06	0.01	0.93	6.35	1.25	0.12	42.30	1.24	0.46	0.29	0.01	0.01	0.01	8.99	100.05	0.911
So_56	Hz	47.44	0.01	0.96	6.54	1.28	0.13	41.67	1.21	0.45	0.28	0.01	0.01	0.01	5.65	100.00	0.907
So_58	Hz	45.16	0.01	0.92	6.46	1.27	0.13	44.51	0.80	0.49	0.30	0.01	0.01	0.01	8.18	100.07	0.913
So_59	Hz	43.77	0.01	0.75	6.88	1.35	0.13	45.51	0.81	0.46	0.31	0.01	0.01	0.01	7.26	100.00	0.910
So_60	Du	42.75	0.01	0.56	7.14	1.40	0.13	46.20	1.00	0.50	0.32	0.01	0.01	0.01	9.40	100.03	0.908
So_62	Hz	43.76	0.01	0.74	6.90	1.35	0.13	45.55	0.78	0.39	0.31	0.02	0.00	0.01	4.27	99.93	0.910
So_65	Hz	43.95	0.01	1.07	6.81	1.33	0.13	44.82	1.07	0.43	0.30	0.02	0.01	0.01	7.14	99.97	0.910
So_67	Hz	44.33	0.01	1.01	6.82	1.34	0.13	44.43	1.15	0.46	0.30	0.01	0.01	0.01	6.95	100.00	0.909
So_92	Hz	42.52	0.01	1.01	7.51	1.47	0.14	45.58	0.89	0.33	0.31	0.01	0.01	0.01	7.90	99.81	0.903
So_100	Du	43.93	0.01	0.45	7.02	1.38	0.13	45.69	0.59	0.45	0.31	0.01	0.01	0.01	8.22	99.98	0.909
So_145	Hz	44.83	0.01	0.96	6.81	1.34	0.13	44.17	0.96	0.48	0.30	0.02	0.00	0.01	8.09	100.02	0.908
So_148	Hz	44.14	0.01	0.86	6.75	1.32	0.13	45.25	0.74	0.48	0.29	0.02	0.01	0.01	8.74	100.02	0.911

[a] Major element analysis results are in oxide weight %. ICP-AES average uncertainties: SiO_2 (Standard Deviation < 1%); TiO_2 (SD < 20%); Al_2O_3 (SD < 10%); Fe_2O_3 total (SD < 1%); MnO (SD < 5%); MgO (SD < 1%); CaO (SD < 10%); Na_2O (SD < 10%); K_2O (SD < 10%); P_2O_5 (SD < 10%). Mg# is the molar ratio Mg/(Mg + Fe total).

magnesium (average $MgO_R \approx 47.1\%$, meaning 2.1% loss) and iron (average $FeO^*_R \approx 8.5\%$, meaning 0.4% loss) losses and relative Si, Al, Ca and Cr enrichment (respectively +1.1%, +0.5%, +0.6% and +0.3%). Hence the Oman peridotites have been altered less than abyssal peridotites [*Snow and Dick*, 1995]. Because Na_2O_R and K_2O_R are on average similar to actual Na_2O and K_2O contents, we think that Oman peridotites do not record significant alkali gain or loss.

[31] The REE patterns are given in Table 7 and illustrated in Figure 6. They are well below chondritic values with the normalized Lu values ($0.08 < (Lu)_N < 0.77$). Each pattern can be divided in two parts, a first one from Lu to Sm and a second from Sm to La. The first part is characterized by a linear or slightly convex upward decrease from the Heavy REE to the Middle REE (Figure 6). The second part corresponds to extremely low Light REE values (between 1 and 100 ppb) close to the detection limits (see Table 7). But the very good correlation that exists between La/Yb versus Ce/Yb (no correlation exhibit between La and Yb contents) indicates that the LREE measurements are actually quite good for most of the samples. The LREE distribution is characterized by a relatively flat or concave increase from the MREE to the LREE, which appears clearly enriched in most of the rocks (Figure 6).

[32] A large amount of REE patterns is also characterized by strong positive Eu anomalies. This is generally interpreted as an indication that the rock includes cumulate (or residual) plagioclase. However, in the studied peridotites, we never found traces of plagioclase, possibly because it has been transformed in secondary minerals during the serpentinization and late alteration process. On the other hand, we observe no clear correlation between the Eu content and the LREE enrichments but a weak negative correlation between the Eu content and the spinel Cr# suggests that the plagioclase had a primary origin. However, the fact that the Eu/Eu* ratio (with $Eu/Eu^* = Eu_N/\mathrm{sqrt}(Sm_N*Gd_N)$) displays >1 and <1 values, may indicate that some of the expected plagioclase had a cumulative origin.

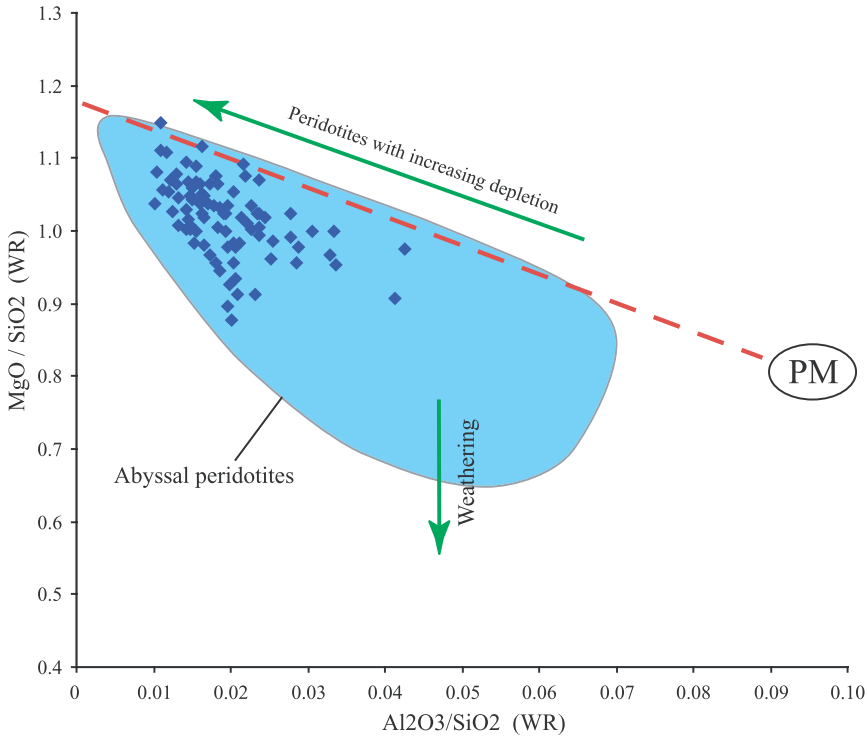

Figure 5. Whole rock MgO and Al_2O_3 contents normalized by SiO_2 contents. The Silicate Earth differentiation trend [*Snow and Dick*, 1995] begins in the Primitive Mantle (PM) zone [*Jagoutz et al.*, 1979; *Maaløe and Aoki*, 1977; *Ringwood*, 1975] and shows an increasing Al_2O_3/SiO_2 ratio. Published data concern abyssal peridotites [*Baker and Beckett*, 1999; *Niu et al.*, 1997; *Snow and Dick*, 1995].

[33] The HREE concentrations and HREE/MREE ratios are well correlated to the spinel Cr#, as illustrated for the Yb contents and Yb/Er ratio in Figures 7a and 7b. This is a main argument for considering them as reliable partial melting indexes and to use them as such.

4.6. Effects of Serpentinization and of Weathering on the Peridotite Primary Chemistry

[34] A few elements may have been modified during a late weathering stage or during serpentinization [*Niu and Hékinian*, 1997a]. These chemical modifications are expected to be correlated with LOI. If H_2O and CO_2 are low in primary minerals, they are significant in primary amphiboles and in secondary hydrous minerals such as serpentines. The fact that there is no correlation between LOI and modified elements in the whole rock, such as Mg, Fe, Si and Al indicates that the loss or gain of major elements was not related to serpentinization as noted in other peridotites [*Hostetler et al.*, 1966; *Komor et al.*, 1985; *Snow and Dick*, 1995]. The effects of serpentinization and weathering have been tested for the LREE and the LREE/MREE ratios which are plotted versus LOI in Figure 8. They do not display any clear correlation.

5. Chemical Evolution of the Oman Peridotites

[35] One of our main objectives was to quantify the evolution of the mantle and to locate the intense melting zones along ridge. We had to distinguish the chemical variations related to the melting processes from those caused by other processes. Therefore it was necessary to determine elements that were modified by postmelting processes and the accurate chemical tracers that could be used to best characterize the melting variations.

5.1. Evidence for Melt/Rock Interaction

[36] Melt-rock interactions are known to modify in some degree the chemistry of the initial rock and magma. This has been shown in abyssal peridotites using textural (e.g., interstitial Cpx and plagioclase, resorbed Opx...) and/or chemical arguments (e.g., Ti and Na enrichment) [*Allan and Dick*, 1996; *Arai and Matsukage*, 1996; *Arai et al.*, 1997; *Dijkstra et*

Table 7. Trace Element Analyses[a]

Samples		La	Ce	Pr	Nd	Sm	Eu	Gd	Tb	Dy	Ho	Er	Tm	Yb	Lu
Quantification Limit		2.35	3.13	1.01	5.87	2.37	1.13	2.65	0.51	1.85	0.51	1.46	0.31	1.44	0.38
JP-1 Average		27.83	60.46	7.57	30.75	8.67	2.16	8.91	1.57	12.31	2.93	10.74	2.03	17.65	3.58
JP-1 SD	Rock	4.42	6.32	0.65	2.80	1.96	0.80	1.65	0.22	1.09	0.33	0.66	0.35	1.48	0.40
MAN 01	Hz	3.09	7.84	1.54	7.99	6.75	1.61	16.56	4.90	45.07	13.39	44.33	8.16	64.72	11.29
MAN 03	Hz	7.28	18.01	2.19	10.48	3.61	1.67	7.77	2.46	27.81	8.36	33.85	6.16	54.18	10.04
MAN 06	Du	7.12	16.66	2.27	9.88	1.76	1.55	3.06	1.01	9.17	3.14	12.71	3.42	29.11	5.70
MAN 07	Du	14.03	4.26	0.49	3.92	2.00	-	-	-	2.15	0.67	5.18	1.10	16.94	3.57
MAN 08	Du	-	-	-	-	-	-	-	-	-	-	-	-	-	-
MAN 09	Hz	12.39	26.20	3.39	14.13	2.22	1.05	2.86	0.37	7.49	1.95	9.50	2.12	23.25	3.85
MAN 10	Hz	8.17	9.74	1.96	5.78	2.11	-	2.28	0.92	14.44	4.78	22.36	3.88	39.20	7.48
MAN 11	Hz	8.03	11.72	1.53	3.08	1.62	1.18	3.05	1.02	9.14	2.61	12.34	2.46	24.95	4.85
MAN 13	Hz	75.51	135.60	16.41	62.61	11.17	3.85	7.31	1.55	10.68	2.40	10.06	2.38	20.76	3.78
MAN 14	Hz	6.10	8.74	0.87	4.38	1.89	-	2.21	0.59	9.80	2.66	10.96	2.30	23.57	3.68
MAN 20	Hz	-	-	-	-	-	-	-	-	-	-	-	-	-	-
MAN 23	Hz	11.44	26.73	1.01	6.76	1.89	-	7.92	2.71	28.04	7.85	33.93	6.74	56.79	11.21
MAN 25	Hz	8.51	1.28	-	1.57	0.60	-	2.06	0.31	6.53	2.57	12.66	2.10	23.73	4.43
MAN 32	Hz	10.61	19.09	1.05	3.62	6.36	7.06	26.14	5.89	60.85	17.03	58.19	11.24	82.95	14.41
MAN 33	Du	6.77	1.26	-	0.88	2.55	-	7.58	3.02	36.40	10.79	43.58	8.05	69.49	13.40
MAN 34	Hz	0.46	0.66	-	0.92	0.91	0.31	6.80	2.23	27.59	8.09	32.67	6.69	49.09	8.24
MAN 35	Hz	9.16	-	-	0.73	0.37	0.11	7.43	2.03	30.92	9.69	42.84	6.72	63.51	10.76
MAN 37	Hz	9.95	6.80	0.39	0.51	0.15	0.30	4.96	1.50	19.67	6.78	28.84	5.96	50.24	9.33
MAN 39	Hz	2.23	3.85	0.31	1.90	0.14	-	-	-	3.12	1.22	6.93	1.10	22.05	4.77
MAN 40	Hz	9.88	12.61	1.25	2.88	1.63	0.55	1.99	0.14	4.28	1.33	9.12	2.11	19.89	4.65
MAN 41	Du	44.26	40.75	3.32	12.10	1.95	1.84	4.60	0.97	13.65	4.40	20.15	4.65	40.02	7.73
MAN 42	Hz	1.89	2.63	0.47	3.38	0.24	-	2.36	1.05	15.10	4.81	22.15	3.97	40.60	7.04
MAN 44	Hz	9.49	27.19	3.29	12.04	1.86	1.05	2.18	0.55	3.34	1.39	6.19	1.38	16.25	3.22
MAN 48	Hz	2.54	4.63	0.30	2.06	0.92	0.40	0.97	0.28	7.16	2.44	11.53	2.20	24.91	4.54
MAN 50	Hz	2.81	4.40	0.31	3.71	0.71	-	0.42	-	2.98	1.19	9.18	1.79	24.90	4.43
MAN 55	Du	4.71	7.04	0.79	4.10	0.49	-	1.45	-	2.29	0.87	5.09	0.90	17.34	2.78
MAN 56	Hz	4.64	7.52	0.53	2.96	0.92	-	-	-	4.16	2.32	10.64	1.63	25.38	4.00
MAN 57	Du	4.58	5.41	0.51	2.34	0.57	-	1.13	0.15	5.64	2.52	14.12	2.28	29.17	5.19
MAN 58	Hz	2.06	4.63	0.20	1.74	0.79	-	0.37	0.33	2.08	0.85	4.99	1.11	13.64	2.99
MAN 59	Hz	1.18	2.58	0.17	1.61	0.44	0.21	0.95	0.44	5.44	1.91	8.19	1.48	15.73	3.39
MAN 60	Du	4.81	8.71	0.82	4.23	0.66	0.63	0.73	0.18	5.39	1.92	8.56	2.21	21.31	4.88
MAN 62	Hz	13.70	1.46	0.11	3.15	1.02	-	2.79	0.18	3.93	1.76	11.90	1.82	29.63	5.15
MAN 63	Du	3.58	7.06	0.79	2.59	0.38	0.63	1.56	0.50	5.19	2.23	10.69	2.41	21.78	4.55
MAN 67	Hz	1.95	3.78	0.42	4.53	1.79	0.44	10.54	3.27	37.64	11.45	45.74	8.23	67.42	11.83
MAN 68	Du	2.06	4.81	0.27	2.30	0.34	-	1.07	0.74	11.61	4.12	18.29	4.25	36.89	6.90
MAN 70	Hz	2.18	4.13	0.42	2.21	0.39	-	-	0.09	2.17	0.94	5.59	1.65	16.24	3.38
MAN 72	Du	3.75	8.16	1.11	4.21	0.60	0.41	2.76	0.83	10.62	3.82	18.87	3.92	37.10	7.03
MAN 73	Hz	1.60	4.22	0.56	1.90	-	0.34	1.32	0.41	7.13	2.35	10.39	2.36	21.23	4.80
MAN 77	Hz	7.38	10.93	1.04	4.82	2.88	3.65	21.00	5.85	60.77	17.63	66.03	11.09	89.78	15.38
MAN 78	Du	2.18	5.18	0.48	2.28	0.34	-	0.50	0.42	5.07	2.17	9.73	2.70	24.25	5.01
MAN 79	Du	1.61	3.48	0.30	1.51	2.43	4.30	8.12	2.61	25.21	7.38	30.27	5.77	47.60	8.90
MAN 80	Hz	0.96	4.42	0.42	4.81	9.38	3.58	37.88	10.68	94.86	25.99	91.36	15.80	124.75	21.45
MAN 81	Hz	0.44	1.03	0.11	1.09	0.74	-	-	0.31	7.00	3.29	16.37	3.79	36.72	7.46
MAN 82	Hz	0.45	1.62	-	0.68	0.88	0.24	0.51	0.14	3.62	1.40	8.75	2.15	24.60	5.24
MAN 83	Hz	5.59	10.84	1.31	5.53	0.95	0.72	1.90	0.81	13.61	5.03	20.85	4.30	32.30	6.02
MAN 84	Du	5.24	11.40	1.08	7.97	2.36	1.12	0.68	0.23	3.65	1.40	8.34	1.92	21.53	4.13
MAN 85	Du	2.04	9.81	0.61	3.07	1.62	-	0.52	0.20	3.42	1.22	7.48	1.87	19.38	4.16
MAN 86	Hz	-	-	-	1.51	1.03	-	-	-	4.95	1.76	11.70	1.16	26.51	4.88
MAN 89	Du	1.01	2.75	0.14	1.51	0.84	0.60	-	-	2.23	0.69	5.14	1.20	14.66	3.01
MAN 92	Hz	1.20	1.96	-	2.50	1.42	-	-	-	2.71	1.04	9.10	1.09	25.19	4.56
MAN 93	Hz	0.87	2.86	0.43	1.27	0.59	0.74	0.32	0.09	1.97	1.03	5.29	1.34	15.63	3.52
MAN 94	Hz	5.37	0.60	-	1.39	0.29	-	1.28	0.20	8.08	3.01	17.80	3.07	37.99	7.09
MAN 95	Hz	5.13	8.99	1.39	6.18	8.01	4.11	23.72	7.40	70.65	19.34	69.53	11.82	93.59	15.78
MAN 96	Du	1.70	3.72	0.37	2.42	0.31	-	1.20	0.21	5.17	2.12	10.15	1.87	23.32	4.39
MAN 98	Du	1.46	3.00	0.26	2.06	0.64	0.48	1.43	0.34	7.05	2.78	14.28	3.27	27.77	5.60
MAN 99	Hz	1.64	3.98	0.22	1.05	0.38	-	0.82	0.18	7.32	2.97	14.73	2.97	30.73	6.27
MAN 101	Hz	1.66	4.05	0.29	1.46	0.73	0.22	0.42	0.36	8.33	3.55	17.70	3.75	35.89	7.08
MAN 103	Hz	2.12	4.40	0.51	1.76	0.48	0.68	0.44	0.11	1.48	0.65	4.87	1.20	13.52	3.29
MAN 105	Hz	1.40	4.91	-	2.86	1.64	1.31	-	0.07	3.19	1.74	8.57	1.96	23.62	4.88

Table 7. (continued)

Samples		La	Ce	Pr	Nd	Sm	Eu	Gd	Tb	Dy	Ho	Er	Tm	Yb	Lu
Quantification Limit		2.35	3.13	1.01	5.87	2.37	1.13	2.65	0.51	1.85	0.51	1.46	0.31	1.44	0.38
JP-1 Average		27.83	60.46	7.57	30.75	8.67	2.16	8.91	1.57	12.31	2.93	10.74	2.03	17.65	3.58
JP-1 SD	Rock	4.42	6.32	0.65	2.80	1.96	0.80	1.65	0.22	1.09	0.33	0.66	0.35	1.48	0.40
MAN 107	Hz	5.02	9.77	1.35	5.09	0.14	0.14	1.40	0.22	3.49	1.37	6.30	1.57	15.58	3.68
MAN 109	Hz	0.94	2.89	0.20	0.73	-	0.21	0.24	0.08	2.52	1.14	6.48	1.61	17.61	3.55
MAN 110	Hz	1.40	3.77	-	0.94	1.08	-	1.80	1.09	16.20	5.67	25.29	5.07	46.81	7.89
MAN 111	Hz	0.91	2.58	-	0.97	0.55	-	0.63	0.11	4.17	1.74	8.68	2.00	19.22	4.08
MAN 112	Hz	2.11	1.37	0.23	3.31	8.08	6.21	40.05	10.37	100.14	26.59	97.83	15.32	131.52	26.31
MAN 113	Hz	1.50	1.44	0.17	1.78	1.13	1.33	7.94	2.18	26.27	7.62	32.32	5.89	52.76	9.40
MAN 114	Du	5.02	9.94	0.77	3.97	1.11	0.24	1.74	0.85	11.12	3.06	16.36	3.06	28.79	5.73
MAN 115	Hz	4.11	7.98	1.07	3.69	1.86	-	3.89	1.27	17.46	5.88	25.30	4.08	46.15	8.41
MAN 116	Hz	12.02	28.62	2.82	12.55	4.23	-	4.89	1.29	17.60	5.78	20.80	4.76	38.80	6.87
MAN 117	Hz	0.61	9.42	1.03	8.32	3.49	0.59	11.54	4.48	43.53	12.86	52.23	9.01	72.04	12.61
So_2	Hz	0.64	1.99	0.18	0.58	0.43	0.20	2.60	0.99	10.67	3.53	15.23	2.94	28.68	5.38
So_3	Hz	7.42	16.80	2.14	10.54	2.38	0.34	8.01	2.49	27.69	8.46	32.72	6.57	56.85	10.26
So_4	Lz	6.02	6.62	0.50	2.96	1.70	1.05	4.30	1.55	16.29	4.95	21.51	4.09	36.17	5.69
So_7	Hz	0.80	2.19	0.10	0.48	0.21	0.10	1.97	0.35	7.23	2.18	13.04	3.00	29.97	6.21
So_9	Hz	2.25	3.15	0.18	1.06	0.38	0.03	0.37	0.11	5.07	1.77	11.08	2.68	26.71	5.26
So_10	Du	0.95	1.57	0.42	1.04	1.06	-	-	0.59	8.55	3.38	15.97	3.24	32.38	6.59
So_11	Hz	4.69	8.86	0.96	4.96	0.48	0.29	0.97	0.46	5.62	2.57	11.41	2.49	25.00	5.51
So_15	Hz	0.83	2.36	0.12	0.86	3.14	3.44	6.67	2.26	25.57	7.39	32.03	5.72	50.73	10.41
So_16	Hz	4.50	9.84	0.94	6.26	8.19	7.24	31.00	8.30	77.61	21.49	78.35	12.18	96.54	15.60
So_17	Hz	0.25	1.74	0.35	2.33	3.88	1.46	14.27	4.28	46.86	14.23	53.35	8.73	78.38	13.95
So_19	Du	3.14	5.52	0.24	1.98	0.66	1.17	1.62	0.87	10.57	3.44	17.25	3.80	34.86	6.22
So_21	Hz	3.01	8.22	0.50	2.08	0.12	0.28	0.59	0.15	2.88	1.17	7.27	1.91	19.87	4.68
So_24	Hz	1.22	2.10	0.34	0.44	2.70	-	1.07	0.02	3.08	1.00	6.54	1.38	15.17	3.61
So_25	Hz	1.53	2.59	0.25	0.81	0.19	0.55	0.50	0.27	6.91	2.70	15.14	3.02	31.39	6.65
So_56	Hz	6.03	12.44	1.19	7.09	1.99	1.27	3.16	0.81	13.79	4.69	23.70	5.35	44.40	8.64
So_57	Hz	1.51	10.66	0.31	2.71	-	0.66	1.23	0.18	3.85	1.76	8.81	2.07	22.16	4.83
So_58	Hz	3.69	4.55	0.31	4.00	-	0.63	0.58	0.18	3.71	1.39	8.12	1.55	20.30	4.04
So_59	Hz	9.06	30.18	2.58	9.98	3.44	3.10	2.96	0.49	6.31	2.19	11.49	2.47	24.03	5.17
So_60	Du	12.22	6.64	0.54	2.28	-	0.70	1.12	0.33	4.29	1.72	8.62	1.98	20.22	4.77
So_61	Hz	4.58	9.29	1.42	5.01	3.47	-	0.70	0.26	3.58	1.23	7.48	1.88	17.56	4.03
So_62	Hz	3.75	7.32	0.35	2.90	2.78	0.53	0.69	0.90	9.46	3.25	14.51	3.73	24.79	5.75
So_63	Hz	5.04	11.23	0.99	6.44	2.89	0.95	4.97	0.93	11.56	4.05	16.93	3.72	32.14	6.77
So_65	Hz	9.76	20.01	2.20	10.97	3.67	1.29	3.84	1.13	13.36	4.66	17.14	3.22	28.46	6.25
So_66	Hz	18.35	35.26	3.41	14.62	1.87	1.50	2.41	0.26	4.05	1.11	6.77	1.45	13.40	3.24
So_67	Hz	1.99	5.59	-	2.00	1.22	1.71	0.92	0.32	7.20	2.83	14.12	3.02	26.02	5.05
So_68	Hz	1.35	3.08	0.34	2.47	0.70	0.74	3.92	1.58	16.73	5.50	22.74	4.26	35.80	6.60
So_70	Lz	7.12	14.97	1.78	7.26	1.46	1.23	4.66	1.25	16.35	5.25	21.97	4.07	34.43	6.51
So_71	Hz	-	2.84	0.31	0.79	0.31	0.13	1.45	0.66	6.58	2.38	11.85	2.99	27.54	5.48
So_72	Hz	-	3.33	0.42	0.66	0.72	-	0.80	0.82	10.13	3.89	16.79	3.92	31.99	6.34
So_74	Hz	4.10	5.51	0.57	2.03	0.23	0.15	1.54	0.95	12.88	4.64	20.20	4.15	37.18	7.14
So_75	Hz	2.88	3.68	0.37	1.19	1.08	-	1.83	0.86	11.02	4.35	18.73	3.65	33.96	7.35
So_76	Hz	3.88	2.43	0.25	1.42	0.23	0.25	1.14	0.62	8.16	2.73	14.32	3.26	27.31	6.32
So_77	Hz	-	2.95	0.37	1.80	0.19	0.86	2.24	0.44	5.44	2.27	10.05	2.72	26.10	5.37
So_78	Hz	-	1.95	0.37	1.28	-	0.77	4.06	0.96	14.57	4.94	23.69	4.53	39.92	7.90
So_79	Hz	-	9.54	1.39	4.36	-	0.51	2.44	0.46	6.40	1.94	8.94	2.02	18.41	4.00
So_80	Du	1.12	2.29	-	0.68	0.70	0.19	0.80	0.35	8.31	2.50	15.50	2.79	27.21	5.11
So_81	Hz	1.00	1.35	0.26	1.72	2.17	0.38	1.23	0.36	9.05	3.93	17.52	4.10	36.66	7.38
So_82	Hz	1.16	2.69	0.37	0.69	1.42	0.52	2.28	0.90	14.04	4.25	21.31	4.52	37.74	7.83
So_83	Hz	0.60	1.07	-	1.25	0.59	0.88	1.09	0.63	7.43	2.92	13.90	2.90	30.75	6.91
So_84	Hz	1.03	3.37	0.22	0.71	-	0.12	0.29	0.19	2.37	1.28	7.47	1.85	19.86	4.36
So_85	Hz	1.91	2.82	0.29	1.04	0.25	0.45	-	-	1.35	0.59	4.35	1.33	16.24	3.29
So_87	Du	2.63	4.39	0.89	2.36	0.42	0.89	0.47	0.14	3.12	1.13	6.65	1.82	16.56	3.16
So_88	Hz	1.92	4.29	0.46	2.26	2.88	2.23	13.45	4.55	48.50	13.55	53.54	9.95	77.26	14.01
So_89	Du	1.51	1.98	0.70	1.95	1.02	0.33	2.07	0.66	5.68	2.20	8.09	1.53	18.61	4.04
So_90	Hz	3.50	7.04	1.11	3.57	1.40	0.91	1.62	0.41	5.61	1.85	9.15	1.86	20.18	4.19
So_91	Hz	6.51	11.45	1.22	5.29	1.10	0.52	4.59	1.41	15.04	5.61	22.53	5.16	42.15	8.01
So_92	Hz	3.37	7.14	0.37	2.03	0.73	0.75	3.44	1.25	15.52	4.71	22.46	4.43	39.08	6.98
So_94	Hz	1.72	2.73	0.38	3.52	0.91	1.84	1.89	1.00	11.06	4.12	20.25	4.38	38.67	6.63
So_95	Du	0.88	2.34	0.31	1.73	0.56	-	3.46	1.21	16.70	5.63	23.45	4.76	42.46	7.75

Table 7. (continued)

Samples		La	Ce	Pr	Nd	Sm	Eu	Gd	Tb	Dy	Ho	Er	Tm	Yb	Lu
Quantification Limit		2.35	3.13	1.01	5.87	2.37	1.13	2.65	0.51	1.85	0.51	1.46	0.31	1.44	0.38
JP-1 Average		27.83	60.46	7.57	30.75	8.67	2.16	8.91	1.57	12.31	2.93	10.74	2.03	17.65	3.58
JP-1 SD	Rock	4.42	6.32	0.65	2.80	1.96	0.80	1.65	0.22	1.09	0.33	0.66	0.35	1.48	0.40
So_96	Lz	1.50	3.45	0.32	5.27	11.32	5.49	49.13	12.55	98.96	28.28	91.44	15.19	126.46	23.91
So_100	Du	3.77	8.01	0.71	2.52	1.25	2.14	2.09	0.39	2.90	1.67	6.51	1.75	18.32	4.48
So_101	Hz	4.92	22.34	4.70	40.65	27.38	12.29	55.77	11.67	91.17	22.47	74.46	11.95	84.53	12.75
So_102	Hz	3.34	7.75	0.65	3.90	3.89	0.59	12.19	3.68	31.37	10.36	35.51	7.61	57.87	10.73
So_104	Hz	1.60	4.89	0.45	1.61	-	0.55	0.82	0.34	1.45	1.14	5.64	1.20	16.73	3.72
So_105	Hz	1.72	5.89	0.81	3.01	1.26	-	0.34	0.41	6.57	2.96	13.96	2.77	30.26	5.73
So_106	Hz	18.03	34.85	3.44	16.24	3.29	0.71	1.53	0.20	5.42	1.89	9.58	2.39	27.57	5.01
So_107	Hz	2.33	5.21	0.37	0.90	0.34	-	1.10	0.26	3.37	1.49	8.39	1.91	21.14	4.84
So_108	Hz	2.59	5.02	0.36	3.68	1.12	1.07	1.14	0.27	5.02	1.56	9.31	2.04	21.21	3.86
So_109	Hz	4.28	9.33	0.80	4.58	1.42	-	2.25	0.03	2.17	1.19	6.27	1.57	15.92	3.79
So_110	Hz	0.73	1.67	0.35	1.61	0.66	0.54	0.37	0.15	2.85	1.61	8.93	2.11	21.29	4.65
So_111	Hz	0.58	2.17	0.09	1.47	-	0.22	-	0.18	2.84	1.44	8.04	2.18	19.64	4.46
So_112	Du	1.60	3.57	0.16	0.80	-	0.19	0.24	-	4.23	1.46	10.13	2.16	23.33	4.74
So_113	Du	2.30	4.16	0.44	2.68	0.31	-	0.30	0.28	2.83	1.41	8.42	1.99	23.47	4.51
So_114	Hz	1.16	4.17	0.44	2.86	0.40	0.85	0.35	0.15	2.39	0.96	5.17	1.51	16.41	3.92
So_115	Du	1.96	4.82	0.11	1.66	0.47	0.74	0.51	0.01	2.46	0.90	6.54	1.34	16.62	3.49
So_117	Du	0.58	1.66	-	1.22	0.89	0.20	0.42	0.06	2.92	1.82	8.42	2.25	20.59	4.30
So_118	Hz	0.88	2.76	-	1.06	-	-	-	0.11	3.47	1.52	10.96	2.17	24.63	5.27
So_119	Hz	1.06	2.26	0.38	5.28	0.89	0.91	1.86	0.40	4.46	1.61	8.80	2.08	22.51	4.94
So_120	Du	0.57	0.95	-	0.94	0.38	0.07	1.19	0.33	3.81	1.78	10.67	2.39	24.59	4.98
So_122	Hz	0.56	3.87	-	0.64	-	-	-	-	1.93	1.17	7.08	1.80	17.09	3.33
So_124	Hz	1.27	2.79	0.00	1.16	-	0.67	0.99	0.61	15.11	5.13	24.06	4.67	44.60	7.66
So_125	Hz	2.84	3.35	0.66	2.95	-	1.74	1.47	0.42	6.10	2.13	12.11	2.62	24.39	5.44
So_126	Hz	1.80	3.44	0.47	2.48	2.09	2.26	6.04	1.85	21.75	7.20	28.01	5.36	48.50	8.51
So_127	Hz	1.60	2.33	0.56	0.71	-	1.88	1.29	0.24	1.84	1.13	6.68	1.48	16.05	3.33
So_128	Hz	0.24	2.21	0.18	1.47	1.46	0.90	4.31	1.79	23.41	7.79	31.57	5.76	48.62	8.33
So_130	Hz	0.90	1.69	0.12	1.13	2.58	-	4.47	1.92	25.26	7.71	32.04	6.37	52.40	10.02
So_132	Hz	1.55	5.35	0.64	3.98	0.75	0.79	2.46	1.03	13.00	4.77	17.69	4.20	35.88	7.17
So_134	Hz	1.80	3.82	0.30	2.08	0.99	-	0.35	0.17	6.17	2.00	10.46	2.06	23.08	4.84
So_135	Hz	2.76	5.52	0.62	2.28	2.10	-	1.84	0.99	9.85	2.85	14.92	3.53	28.65	5.64
So_136	Hz	0.91	2.92	-	1.48	0.88	0.36	0.80	1.05	14.52	4.73	22.70	4.12	42.10	8.04
So_137	Du	6.81	16.24	1.81	6.47	2.07	0.65	2.72	0.68	10.38	2.97	15.62	3.34	26.91	5.75
So_139	Hz	1.94	4.53	0.75	3.19	0.44	1.47	10.92	2.88	30.22	9.33	36.45	6.36	54.55	10.67
So_140	Hz	2.98	6.29	0.54	5.96	5.69	1.82	32.86	8.61	80.05	22.91	80.12	13.29	106.17	17.39
So_141	Hz	1.81	3.06	0.60	5.04	6.66	3.19	26.74	7.41	75.22	20.67	77.63	13.39	98.80	16.06
So_142	Lz	1.96	4.59	0.63	3.72	7.17	1.20	23.57	7.25	71.31	18.90	70.34	12.31	87.30	14.94
So_143	Du	1.67	3.11	0.16	2.94	-	0.74	1.40	0.64	6.14	2.30	10.43	2.94	22.59	4.88
So_144	Hz	3.25	5.79	1.08	5.55	7.76	4.48	28.43	8.93	85.08	22.87	88.91	13.59	110.74	18.89
So_145	Hz	3.21	7.83	1.66	7.11	3.49	0.93	6.57	1.26	15.07	5.60	22.46	4.60	42.06	7.32
So_148	Hz	4.16	8.97	0.96	6.26	0.89	2.02	3.98	1.13	10.71	3.36	14.38	2.65	29.12	5.79

[a] Trace element analyses were obtained by ICP-MS and are given in ppb. The REE detection limit is given at the top of the table (calculated as 10 times standard deviation on 30 blank analyses), the average composition of standard JP-1 as measured in our laboratory, with its standard deviation (13 duplicate analyses). The procedure for sample can be obtained on request to the authors.

al., 2002, 2003; *Girardeau and Francheteau*, 1993; *Seyler and Bonatti*, 1997; *Wang et al.*, 2001].

[37] But the studied rocks do not display any textural evidence of melt crystallization such as the presence of poikilitic interstitial minerals, possibly with magmatic twins, that could have been seen in thin sections. This is possibly a consequence of the alteration process. But this is not very surprising as the samples were systematically taken in visually homogeneous zones, away from visible impregnated areas (see section 3.2). A few samples however contain Opx crystals with resorbed shapes which can indicate interaction of the harzburgite with a low-silica activity melt [*Bodinier*, 1988; *Bodinier et al.*, 1990; *Kelemen*, 1990; *Kelemen et al.*, 1995, 1997a; *Nicolas*, 1986a; *Quick*, 1981].

[38] The phase chemistry also does not show any effects common to melt/solid phase interactions, in contrast with what can be seen for instance in some of the Hess Deep harzburgites where the Cpx and mostly the spinels are clearly enriched in incom-

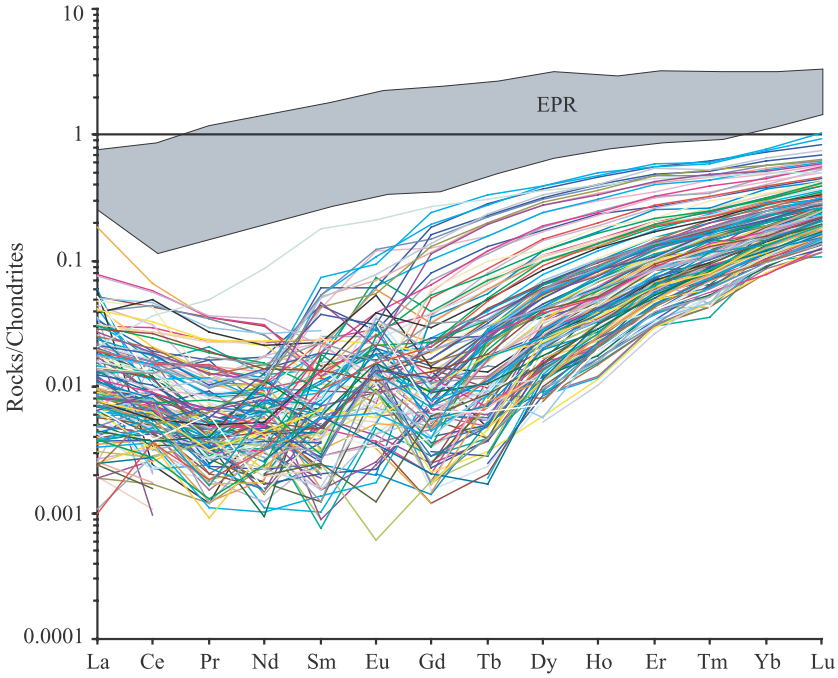

Figure 6. Chondrite-normalized REE patterns of the Oman peridotites. The field of EPR peridotites (dark gray area) is also shown for comparison [*Niu and Hékinian*, 1997b]. Normalization values are from *Sun and McDonough* [1989].

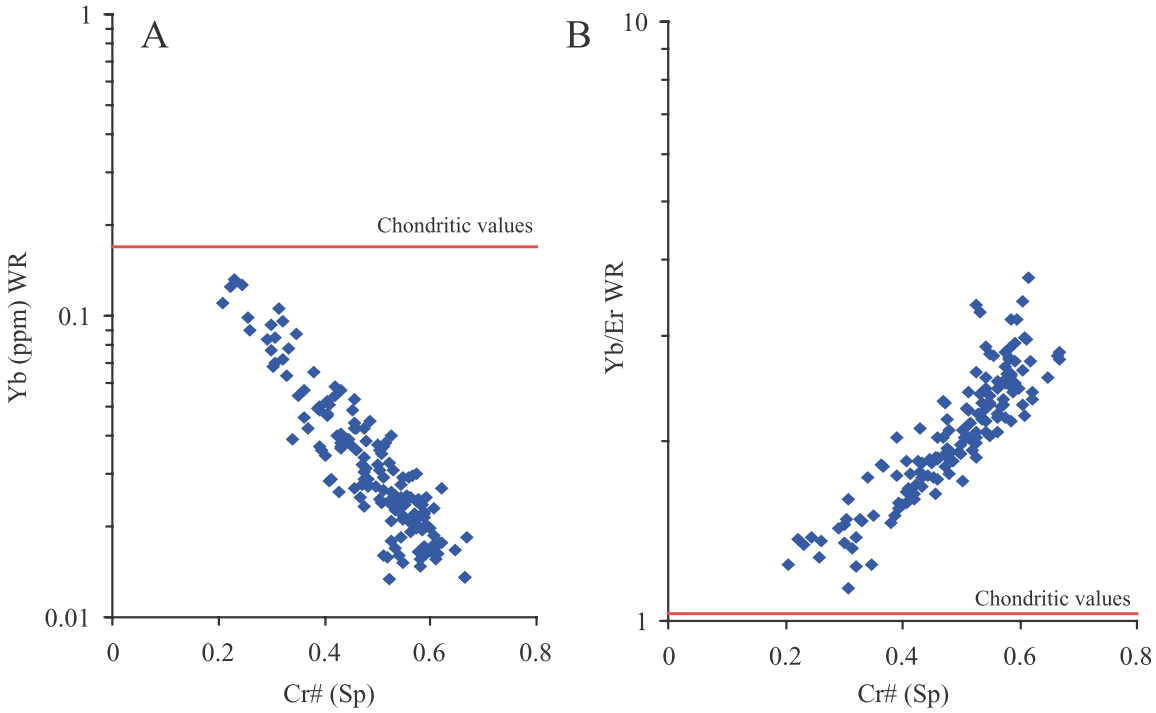

Figure 7. (a) Cr# ratio in spinel versus whole rock Yb concentrations (in ppm) and (b) Cr# ratio in spinel versus whole rock Yb/Er ratio. Chondritic and primitive mantle values are from *Sun and McDonough* [1989].

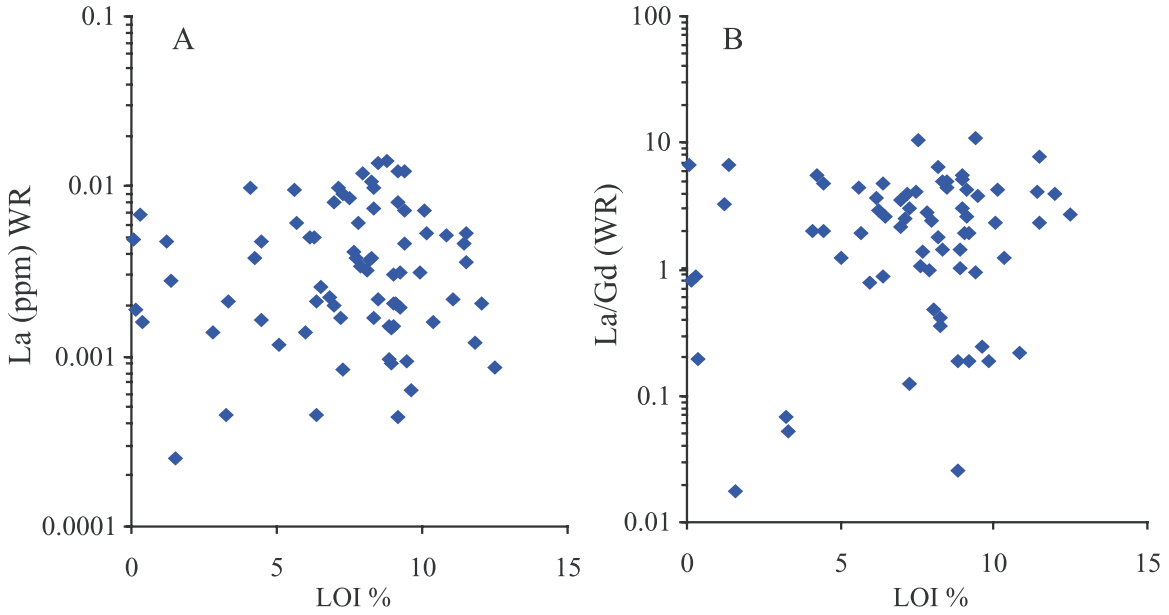

Figure 8. (a) Whole rock La (in ppm) versus loss on ignition (%) and (b) La/Gd ratio in whole rock versus loss on ignition (%).

patible elements, such as in Ti or Na [*Allan and Dick*, 1996; *Arai et al.*, 1997; *Dick and Natland*, 1996; *Girardeau and Francheteau*, 1993; *Hekinian et al.*, 1993; *Kelemen*, 1990; *Monnier et al.*, 2003]. In the studied peridotites, no significant enrichment in Ti has been observed either in spinels (TiO_2 maximum value: 0.17% versus 0.4% to 0.5% at Hess Deep) or in the other phases, Cpx for instance (Table 4; see other mineral compositions in Tables 2, 3, and 5). This is consistent with the whole rocks $TiO_{2(WR)} < 0.3\%$ contents, even after recalculation of the primary major element contents (as discussed in section 4.5).

[39] Data on whole rock REE concentrations have to be discussed with caution as they generally record both partial melting and melt-rock interaction processes, as discussed in recent studies [e.g., *Godard et al.*, 1995, 2000; *Kelemen et al.*, 1990, 1992; *Ozawa and Shimizu*, 1995; *Takazawa et al.*, 1992]. This is perhaps the case for the studied peridotites whose LREE concentrations have probably been modified as they commonly increase from the MREE to the LREE giving the typical spoon-shaped patterns already described in the South Oman peridotites [*Godard et al.*, 2000]. Many authors ascribed the LREE enrichments to postmelting metasomatism, due to fluid or magma percolation [e.g., *Wilshire*, 1984] or to chromatographic effects [e.g., *Navon and Stolper*, 1987]. This is commonly invoked to explain the observed LREE patterns that are thought to mark partial "refertilization" of the depleted mantle [*Bodinier and Godard*, 2003; *Bodinier et al.*, 1991; *Bonatti et al.*, 1992; *Gervilla and Remaidi*, 1993; *Johnson and Dick*, 1992; *Johnson et al.*, 1990; *Kelemen et al.*, 1990, 1992, 1995, 1997a; *Suhr*, 1999; *Tartarotti et al.*, 2002].

[40] Some authors [e.g., *Dixon et al.*, 1988] have also proposed that the high LREE concentrations (e.g., La, Ce) observed in some oceanic basalts were related to the presence of small amounts of H_2O during the melting process of the mantle sources. Because the partial melting in Oman probably did not occur in the presence of large and ubiquitous amounts of H_2O (see following section), the LREE–rich fluid phases were probably channeled within specific areas.

[41] Meanwhile, the clear correlations between the LREE/MREE ratios and the Cr# of spinels or Yb contents in the whole rock (Figures 9a and 9b, respectively), indicate that these enrichments were probably gained during the latest stage of melting or through interaction with influxed fluid after melting [*Ozawa and Shimizu*, 1995]. These enrichments can be explained by an open-system melting model, which involves continuous influx of LREE-enriched fluid/melt into the mantle peridotite inducing its melting and melt extraction from the melting region as melting proceeds [*Ozawa and Shimizu*, 1995].

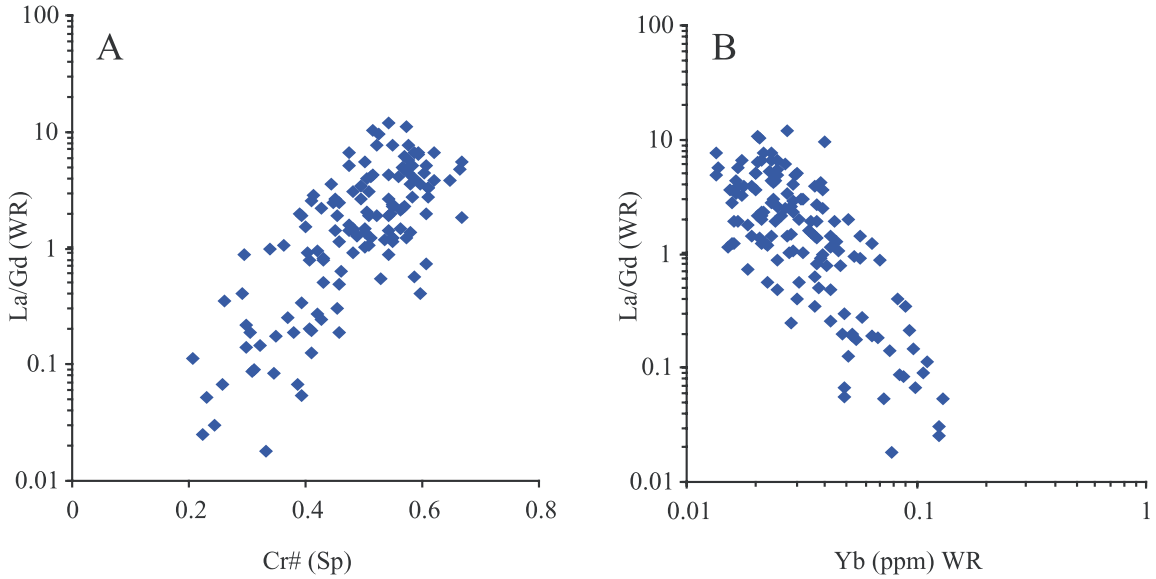

Figure 9. (a) Cr# ratio of spinel versus whole rock La/Gd ratio and (b) whole rock Yb concentrations (in ppm) versus La/Gd ratio.

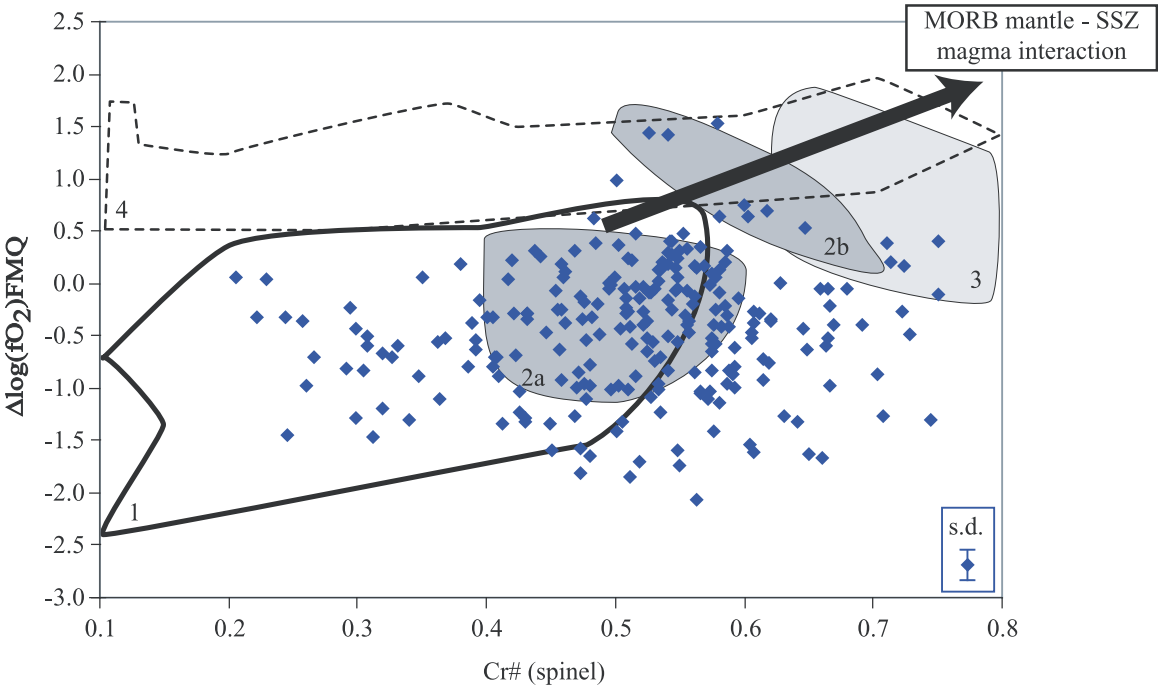

Figure 10. Plot of $\Delta\log fO_2$ (FMQ) versus Cr# in spinel for the Oman peridotites. For comparison, five different fields corresponding to peridotites from various contexts are given: 1, abyssal domains from previous calculations [*Bryndzia and Wood*, 1990] or from previous data integrated in our calculations [*Arai and Matsukage*, 1996; *Dick and Natland*, 1996; *Johnson and Dick*, 1992; *Snow and Dick*, 1995]; 2a and 2b, harzburgites from fore-arc domains from IBM [*Parkinson and Pearce*, 1998]; 3, dunites from the same location as 2; and 4, arc domains [*Parkinson and Arculus*, 1999]. The large black arrow shows the melt-rock interaction trend in supra-subduction zone SSZ involving increases in both oxygen fugacity and Cr# in spinel [*Pearce et al.*, 2000]. The standard deviation, s.d., includes the error due to calculation of the oxygen fugacity.

[42] However, we can be more confident with the M- and HREE elements which are excellent indicators of degree of melting [*Bodinier et al.*, 1990; *Gerbert-Gaillard*, 2002; *Godard et al.*, 1995; *Gruau et al.*, 1998; *Parkinson et al.*, 1992; *Vernières et al.*, 1997] even if a significant amount of exotic material influxes [*Ozawa and Shimizu*, 1995]. Recent studies demonstrate that modifications of the HREE to MREE during refertilization, if they exist, are modest in quantity and probably the same for all elements [*Bodinier et al.*, 1990; *Godard et al.*, 1995; *Vernières et al.*, 1997].

5.2. Oxygen Fugacity Conditions During Melting

[43] To better characterize the conditions of the melting process, we have calculated the fO_2 (oxygen fugacity). The Oman ophiolite is well known for the complexity of its lava sequence, and particularly for the presence of V2 and V3 lavas with ''subduction related'' major and trace element characteristics, over the Geotimes lavas [e.g., *Alabaster et al.*, 1982; *Einaudi et al.*, 2003; *Ernewein et al.*, 1988; *Pearce*, 1980; *Umino et al.*, 1990]. We used the oxybarometer based on the Fe-Mg olivine-spinel exchange [*Ballhaus et al.*, 1990] to calculate fO_2. Results are illustrated in Figure 10, which plots the oxygen fugacity deviation from QFM (i.e., Quartz-Fayalite-Magnetite) buffer versus the Cr# in the spinels. According to the Cr# in spinel, the Oman peridotites belong to the abyssal and fore-arc fields as already discussed in section 4.3 (Figure 4f). The spinels suggest a relatively low oxygen fugacity, with values between −2 and 0.6 log units away from QFM, similar to that already proposed for peridotites from the southern part of the Oman ophiolite [*Godard*, 2003]. In terms of fO_2, the Oman peridotites are very different from arc (Figure 10, field 4) and some fore-arc peridotites (fields 2b and 3). But their degree of oxidation is quite similar to abyssal peridotites (field 1) and IBM (Izu-Bonin-Mariana) fore-arc harzburgites (field 2a); considered to be equivalent to the present-day reduced oceanic mantle [*Parkinson and Arculus*, 1999]. However, there is no obvious correlation between fO_2 and spinel Cr# in our samples, contrary to what is seen in the IBM reduced oceanic mantle after channeling of the subduction zone melts [*Parkinson and Arculus*, 1999; *Pearce et al.*, 2000]. This shows that melting of the Oman peridotites did not occur in the presence of large amount of H_2O, as expected for the formation of island arc lavas (field 4 in Figure 10). But, this does not mean that there was no water during the melting process. To better characterize the origin of water present in these rocks, a specific study should be done on the rare cpx present in some of the peridotites, using stable isotopes for instance, or on fluid inclusions, if present in some of the primary phases.

5.3. Partial Melting Estimates

[44] Our petrological data indicate that the Oman peridotite phases and whole rock chemistry have preserved most of their primary characteristics, except for the LREE (see section 5.1) and for some major elements whose primary concentration can be recalculated. To characterize the extent of melting of the mantle rocks, we mostly used the Cr# in primary spinel which has long been thought to well reflect the melting process of its host peridotites as seen from experimental studies [*Barnes and Roeder*, 2001; *Bonatti and Michael*, 1989; *Bonatti et al.*, 1992; *Dick*, 1977; *Dick and Bullen*, 1984; *Evans and Frost*, 1975; *Hellebrand et al.*, 2001; *Irvine*, 1965, 1967; *Michael and Bonatti*, 1985; *Sack and Ghiorso*, 1991; *Seyler et al.*, 2003].

[45] To calculate the maximum extent of melting, F_{max} value of *Langmuir et al.* [1992], we have used the equation from *Hellebrand et al.* [2001], where $F_{max} = 10*Ln(Cr\#)+24$. This yields F_{max} estimates ranging from 8.2% to 20.5% for the Oman peridotites, with a mean value of about 16.5%. The 12.3% range of the F_{max} values given here is significantly smaller than the 23% range (7–30%) already proposed by *Le Mée et al.* [2004]. Le Mee et al.'s estimate was calculated using Fe/Mg fractionation between olivine and spinel which was not appropriate since the rocks probably underwent some late Fe/Mg exchange [*Le Mée*, 2004]. The estimated 16.5% F_{max} mean value we have calculated for the Oman peridotites is consistent with the mean extent of melting ($F_{mean} \approx F_{max}/2 \approx 8\%$) deduced from present-day oceanic basalts [*Langmuir et al.*, 1992].

[46] The good correlation between the HREE bulk-rock concentrations and the Cr# of spinels (Figures 7a and 7b) makes that theoretical HREE concentrations can be calculated. This has been done using a fractional modal melting model [*Gast*, 1968; *Johnson et al.*, 1990; *Shaw*, 1970] for Yb, using partition coefficients from *Kelemen et al.* [1993] and a starting peridotite similar in composition to that of the spinel lherzolite of *Takazawa et al.* [2000], with olivine (70%), Opx (16%), Cpx (10%) and spinel (4%). Figure 11 shows that such a model, red line, provides a good fit to the trend

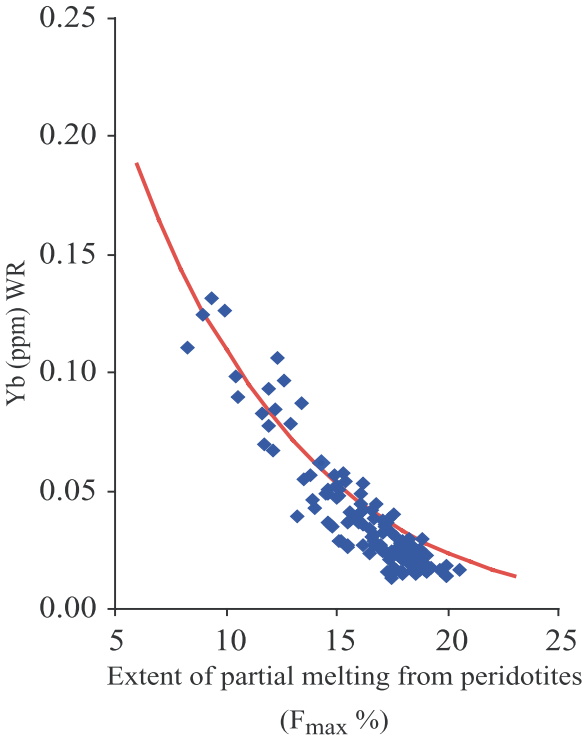

Figure 11. Yb concentrations (in ppm) from whole rocks of Oman peridotites versus the extent of melting calculated from Cr# of spinel with the equation from *Hellebrand et al.* [2001]. The red line is obtained using the fractional no modal melting model [*Johnson et al.*, 1990], partition coefficients from *Kelemen et al.* [1993], and as starting peridotite the spinel lherzolite described by *Takazawa et al.* [2000], with olivine (70%), Opx (16%), Cpx (10%), and spinel (4%).

defined by the measured Yb concentrations versus the calculated degree of partial melting that was calculated using the equation from *Hellebrand et al.* [2001]. This observation, again, corroborates the idea that the Cr# of spinels reflects the peridotite melting history well.

5.4. Efficiency of Melt Extraction

[47] We have argued in the preceding sections that the study peridotites underwent a high extent of melting (F_{max}), from 8.2% to 20.5% with a mean value at about 16%. A central question is to know if these estimates reflect the actual extent of melting as implied in preceding sections or the efficiency of the melt extraction [e.g., *Kelemen et al.*, 1995]. This is not trivial as the total melt extraction also depends of the initial composition of the peridotite and of the depth at which it will begin to melt. Whatever the situation is, the melt produced by partial melting can be continuously extracted, maintained in the rock for a period of time and then extracted, partly extracted or never extracted. As in the studied peridotites there is no petrographic evidence for secondary "magmatic" clinopyroxene or plagioclase that could have crystallized from the melt; we can consider that most of the melt was extracted. However, the existence of the strong enrichments in LREE within most of the samples, indicate that the peridotites encountered fluid/melt-related modifications during the latest stage of melting or after the melting process.

5.5. Crust Thickness Estimates

[48] It has been proposed that the crustal thickness is directly correlated to the magma budget and therefore to the peridotite melt extraction at the 10–20 km scale [*Cannat et al.*, 1995; *Sempéré et al.*, 1993; *Shaw*, 1992; *Sinton and Detrick*, 1992; *Whitehead et al.*, 1984]. Our work shows that, at the scale of the whole Oman ophiolite, there is a correlation (Figure 12) between the mean extent of melting F_{mean} ($F_{mean} \approx F_{max}/2$) as inferred from the

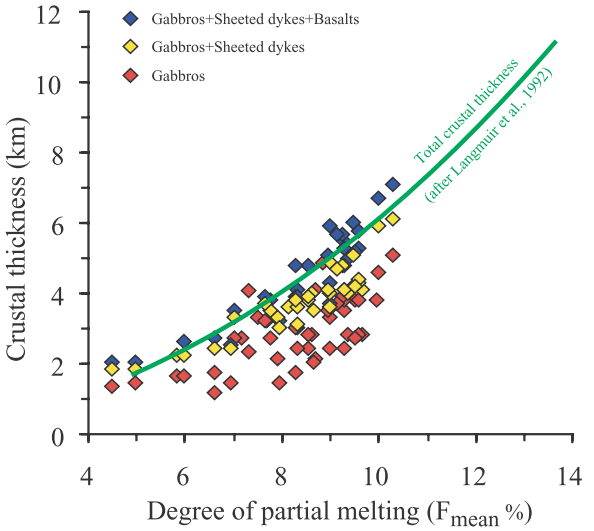

Figure 12. Mean extent of melting versus crustal thicknesses (in km) in the Oman ophiolite. The gabbro thicknesses (red diamonds), the gabbros + sheeted dykes thicknesses (yellow diamonds), and the total crust (gabbros + sheeted dykes + basalts) thicknesses (blue diamonds) are deduced from *Dahl* [1984], *Juteau et al.* [1988a], *Nicolas and Boudier* [2000], and *Nicolas et al.* [1996] and from the geological maps. The mean extent of melting F_{mean} is inferred from the spinel Cr# (raw data), where $F_{mean} \approx F_{max}/2$ [*Langmuir et al.*, 1992] and $F_{max} = 10*\text{Ln}(\text{Cr\#}) + 24$ [*Hellebrand et al.*, 2001]. The green line plots to the variation of the crustal oceanic thickness after the theoretical model of *Langmuir at al.* [1992].

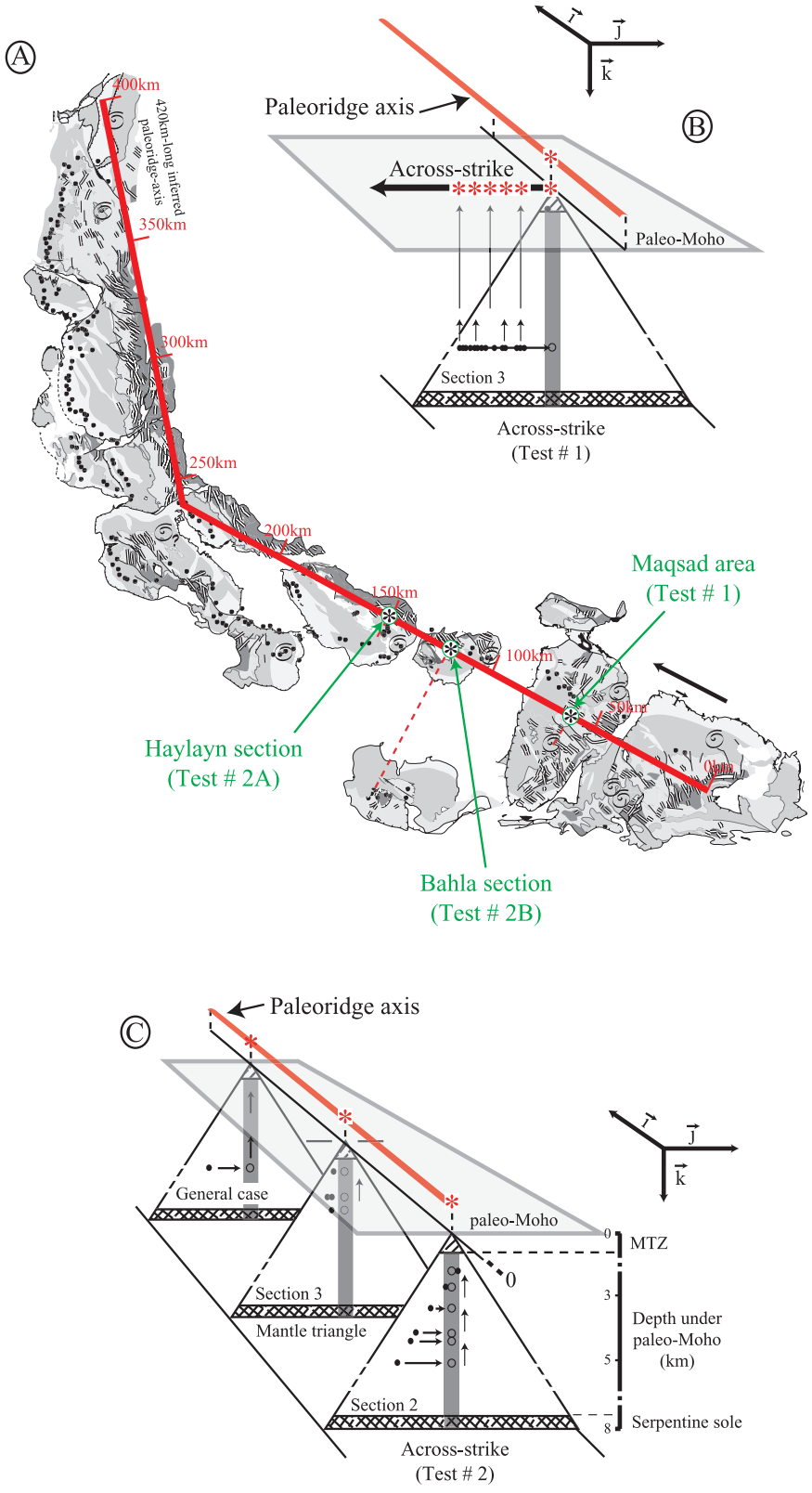
Ⓐ
400km
420km-long inferred paleoridge-axis
350km
300km
250km
200km
150km
100km
50km
0km
Haylayn section
(Test # 2A)
Maqsad area
(Test # 1)
Bahla section
(Test # 2B)
Ⓑ
Paleoridge axis
Across-strike
Paleo-Moho
Section 3
Across-strike
(Test # 1)
Ⓒ
Paleoridge axis
General case
paleo-Moho
MTZ
0
3
5
8
Depth under paleo-Moho (km)
Serpentine sole
Section 3
Mantle triangle
Section 2
Across-strike
(Test # 2)

Figure 13

spinel Cr# (our data) and the crustal thickness (as deduced from previous works [*Dahl*, 1984; *Juteau et al.*, 1988a; *Nicolas and Boudier*, 2000; *Nicolas et al.*, 1996] and measurements obtained from 1:25000 and 1:500000 scale geological maps (this work). Note that a 4.30 km thick crust (which is the average thickness of the Oman ophiolite crust with 3 km thick gabbro, 0.8 km sheeted dykes and 0.5 km basalts) corresponds to an extent of melting (F_{mean}) of about 8%. Figure 12 also shows that the data plots within the evolution curve of the whole oceanic crust which indicates that the Oman mantle evolution is coherent with the global ridge system for a rather cold to standard mantle [*Langmuir et al.*, 1992].

[49] This good correlation between the estimates of partial melting ($\sim$4% < F_{mean} < $\sim$10%) and the estimated Oman crust thickness (ranging from $\sim$2 km to $\sim$7 km) is for us another strong argument to consider the spinel Cr# as a reliable indicator to describe the partial melting process, as previously stated.

6. Sample Comparability

[50] As seen previously, the Oman peridotites display a wide range of compositions that can be interpreted in terms of extent of melting variations. To understand the meaning of these chemical variations, we had to verify that they did not result from a biased sampling. First we verified that the samples were indeed representative of the whole mantle section beneath the ridge, even if this parameter has not been yet considered for abyssal peridotites [e.g., *Seyler et al.*, 2003]. This was very important as samples were taken at an horizontal distance of 1 to up than 10 km from the geological paleoaxis trace, and at a vertical distances of 1 to 7 km from the paleo-Moho (Figure 13). We have defined an orthogonal reference frame $(O, \vec{i}, \vec{j}, \vec{k})$ within which each sample has three coordinates (x, y, z) which give its 3D location with respect to the paleo-ridge (Figure 13). Their representativity has been studied first in the direction orthogonal to the ridge-axis (across-strike test # 1), then in the vertical section beneath the ridge-axis (depth tests # 2A and #2B).

6.1. Across-Strike Test

[51] We have developed in section 2.1 a set of structural arguments stressing that the mantle rocks were probably formed in the same span of time, which means that they likely were molten at the same time. Independently and to ensure that the horizontal distance to the paleoaxis has no major influence on the chemical characteristics of our samples, we have studied the variability of the chemical indicators across-strike, i.e. across-time (Figure 13b). Thus we have selected 22 samples of peridotite, distributed in 12 sites (we have commonly 3 samples per site taken a few meters apart) over a distance of about 9.5 km, perpendicular to the paleo-ridge. The samples, located by red dots on the map (Figure 14b), come from the Maqsad area in the south of the Oman ophiolite (Figure 14a), which is the best place for such a test as the paleo-Moho is nearly flat. They include 20 harzburgites and two dunites (91OQ57 and 91OQ58) from the center part of the Maqsad diapir.

[52] Results are given in Figure 15a, which presents the variation of the Cr# in spinels versus the across-strike distance. The error bars stand for the variability at the scale of the sample (if one per site) or the sampling site (if more). In these 22 samples, Cr# ranges from 0.51 to 0.57 which is nearly 6 times smaller than the range at the ophiolite scale (0.2 to 0.7). This indicates that, in the Maqsad area, there is very small across-ridge chemical variability. This lets us conclude that a peridotite can be considered as representative of the mantle whatever the distance at which it has been picked from the paleo-ridge axis. In other words, these results show that sampling off-axis or close to the axis is not a key parameter, at least for the Maqsad area.

6.2. Depth Tests

[53] Samples used to test the homogeneity of the peridotites along a vertical section under the paleo-

Figure 13. Sampling location and projection method. (a) Definition of the orthogonal frame $(O, \vec{i}, \vec{j}, \vec{k})$ represented virtually as in accretion context. Each sample defines a specific mantle triangle orthogonal to the inferred 400 km long paleo-ridge. (b) Sketch of the "across-strike" test #1. (c) Sketch of the "depth tests" #2A (Haylayn sector) and #2B (Bahla massif). Projection method (general case): each sample (solid circle) has been vertically projected on the ridge axis plane (open circle), so that it is represented by only one point on the ridge (star). Sections 2 and 3 illustrate cases where, in a single triangle, several samples were collected at increasing distances from the paleo-Moho to test the vertical homogeneity of the mantle.

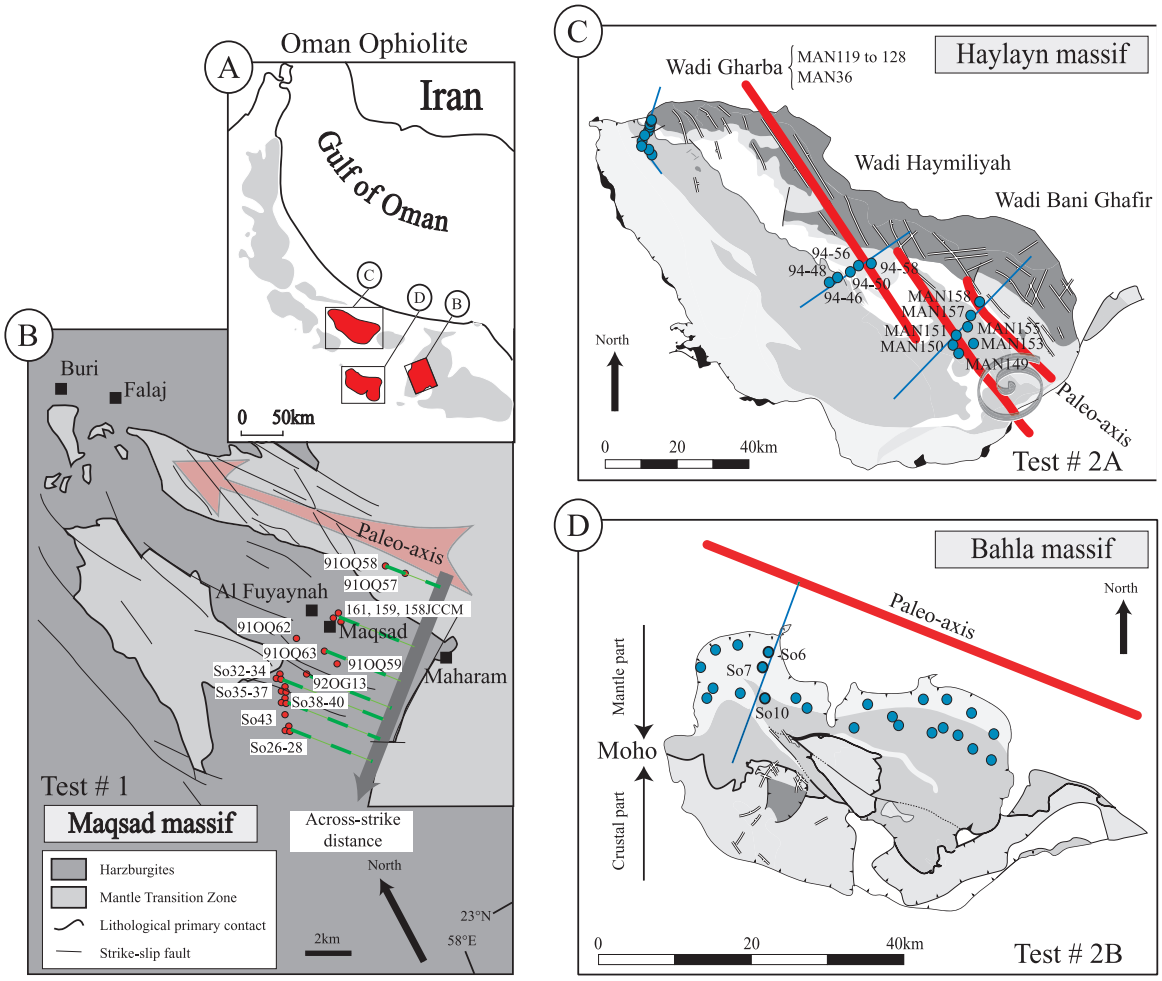

Figure 14. (a) Location of test sampling areas. (b) Test #1 sampling area (22 peridotites) to test the across-strike chemical variability (map after *Quatrevaux* [1990]; modified after I. Amri and G. Ceuleneer, personal communication, 2002). Each red point stands for a peridotite sample, with 3 samples taken at a few meters distance for most sampling sites. This has allowed us to identify 12 different sampling sites over a 9.5 km distance perpendicular to the Maqsad paleo-ridge. (c) Test #2A sampling for the depth homogeneity. Samples have been taken along 3 wadis (Gharba, Haymiliyah, and Bani Ghafir). Samples whose numbers begin with "94-" are from a field campaign in 1994 (T. Juteau, personal communication, 1999). (d) Depth test #2B sampling.

Moho come from the Haylayn massif in the central part of the ophiolite (Figure 14a), in a domain where the paleo-ridge axis is well located [*Juteau et al.*, 1988a; *Reuber et al.*, 1989, 1991]. They were picked in 3 wadis allowing the sampling of 3 $(\vec{j}, \vec{k})$ sections of mantle (Figure 14c). The data (test # 2A) show that there is no significant variation of the melting indices in a single section. This is for instance well exemplified by the spinel Cr# variations (Figure 15b) in the wadis Gharba (average = 0.54, SD = 0.02), Haymiliyah (average = 0.55, SD = 0.06) and Bani Ghafir (average = 0.55, SD = 0.01) for which variations are at least 5 times smaller than that measured at the ophiolite scale (average SD = 0.48). Such homogeneity in the primary phase compositions is also recorded by the whole-rock trace element content as seen in the Bahla samples (Figure 14d) for which we have the whole-rock chemistry (test # 2B). It can be shown with the Yb/Er ratio (Figure 15c) whose variations at the section scale ($1.9 < Yb/Er < 2.3$) are nearly 7 times smaller than at the ophiolite scale ($1.1 < Yb/Er < 3.8$).

[54] The fact that we do not observe any significant variations in the chemistry of the samples whatever their positions along the $\vec{j}$ and $\vec{k}$ directions over distances of up to 10 km across strike and a few km in depth, allows us to conclude that our sampling is representative of the mantle accreted

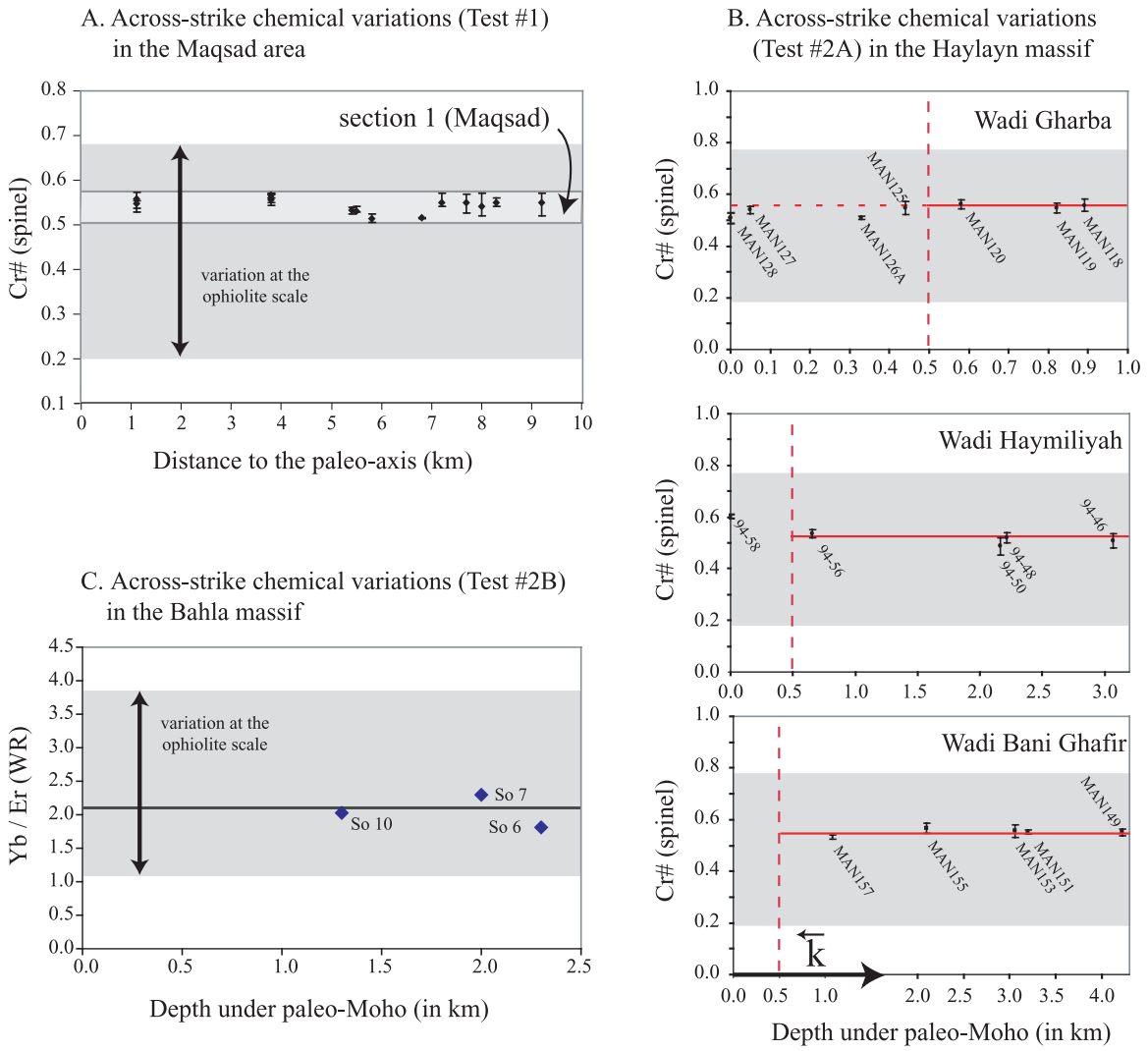

Figure 15. (a) Variation of spinel Cr# for the across-strike distance test #1 (Maqsad samples). The light gray bands have to be compared to the darker one (all ophiolite samples), the thickness of which is several times greater than that observed in each test. (b) Cr# in spinels variations for depth test #2A (Haylayn samples; see map in Figure 12c). (c) Yb/Er ratio in whole rock for the depth test #2B (Bahla samples).

beneath the Oman paleo-ridge. In the next section, we show that the large chemical variability is in fact well organized when analyzed over 400 km long paleo-axis.

7. Along-Axis Variations of Cr# in Spinel

7.1. Methods Used to Characterize the Variations

[55] To characterize the along-ridge axis variations, the location of each sample has been projected on the 400 km long (i) direction of the $(\vec{i}, \vec{j}, \vec{k})$ reference frame, the zero coordinate having been placed at the south end of the reference line (Figure 13a). This kind of presentation is similar to the one that has been used to study the chemical variations recorded along present-day mid-oceanic ridges [e.g., *Dosso et al.*, 1991, 1999; *Langmuir et al.*, 1992; *Seyler et al.*, 2003]. In our study however, the density of sampling is much larger, as on average 45 samples were collected per 100 km compared to 5 samples per 100 km for the Mid-Atlantic Ridge study [*Langmuir et al.*, 1992] and 1 sample for the South-West Indian Ridge [*Seyler et al.*, 2003].

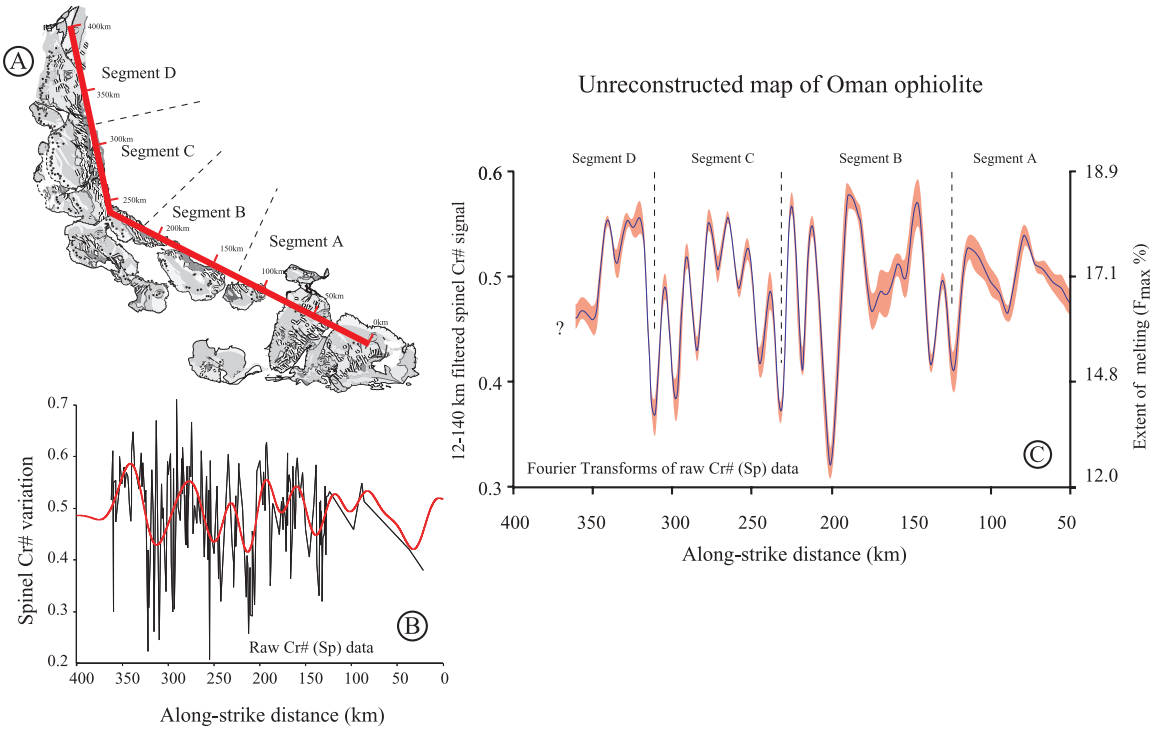

Figure 16. (a) Map of the Oman ophiolite where the mean spinel Cr# for each sample transect has been projected onto the inferred ridge axis trend (red line). (b) Spinel Cr# signal without any statistical processing plotted versus along-strike distance (in km) and (c) 12–100 km filtered spinel Cr# signal (blue line). The red field corresponds to the standard deviation (2 sigma) for each sample.

[56] We first present the along-axis variations using the ophiolite map without any reconstruction (Figure 16a), and then illustrate distance within the reconstructed ophiolite (Figure 17a) obtained by reassembling its different parts assuming that massifs have been separated by tectonic extension, with no erosional gaps [*Nicolas et al.*, 2000a].

[57] For both cases, we also choose to only display the Cr# of spinel variations because of the strong correlations existing between this partial melting index and the HREE (see preceding discussions). In this paper, we first present spinel Cr# versus the longitudinal profile along which rocks have been sampled, without any statistical processing (Figures 18b and 19b).

[58] We also present the same set of data processed using Fourier Transforms (Figures 18c and 19c) and not the seven point running average used in the *Nature* paper.

[59] However, comparison of the results obtained using these two methods (red and green lines in Figure 18a obtained by Fourier Transform and 7 running average, respectively) shows that there are no significant differences in the chemical variation pattern, which indicates that the 7 point running average smoothing method [*Le Mée et al.*, 2004] is accurate.

7.2. Raw Cr# Variations

[60] When plotted along the ridge of the unreconstructed ophiolite (Figure 16b), the spinel Cr# displays chemical variations, with a relatively short wavelength and variable amplitudes. Along the ridge axis the lowest values are concentrated in three narrow areas, with pronounced variations around points 320 km and 210 km, and weaker variations around 320 km, delimitating four larger zones marked by higher values of the index. A similar distribution is found in the case of the reconstructed ophiolite (Figure 15b), which differs only by the exact positions of the lowest values that are located at about 320 km, 240 km and 170 km. In this later case, the Cr# "spectrum" between 170 and 240 km (corresponding to the southern part of the ophiolite) is less "chaotic" than what is observed for the southern area of the unreconstructed ophiolite (Figure 16b). It clearly resembles to the Cr# "spectrum" between 240 and 320 km, which corresponds to the northern part of the ophiolite that did not undergo as much tectonic dismemberment during ophiolite obduction. This suggests that

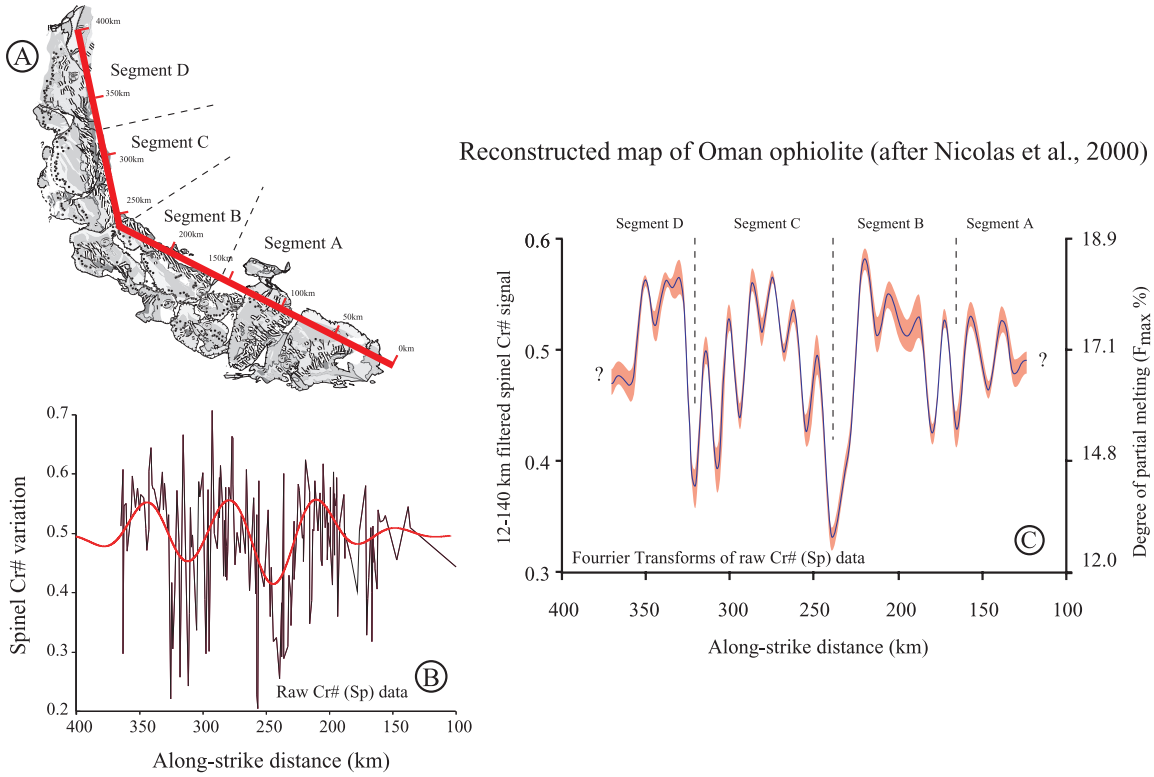

Figure 17. The same as Figure 13 but with the reconstructed map of Oman ophiolite [after *Nicolas et al.*, 2000a].

the reconstructed ophiolite better describes the segmentation pattern than the unreconstructed one.

[61] The three zones defined by the lowest Cr# values delimit four large domains with the highest values concentrated around their centers (Figure 15c). With this said, there are a few low values in the central parts of the larger zones and high values near the discontinuities. We will see in the following section that these four segments will be better defined after processing the data.

7.3. Cr# Variation Distribution After Smoothing

[62] Smoothed data are shown for Cr# in Figure 18a that presents the amplitude of chemical variations versus the along-strike distance. Four large domains marked by high values of Cr# are visually detected in the rough signal (Figure 18a) as it was graphically outlined by the raw data, the forth domain between 130 and 170 km being more badly defined because of the scarcity of the data The long-wavelength aspect of the Cr# signal can be also seen in the spectral domain, as shown in Figure 18b. Clearly, the low frequency amplitudes corresponding to wavelengths between 50 km to 100 km (70 km in average) compose the major part of the signal. To verify this last point, we have processed a set of random signals generated with our computer. Figure 18c shows that the amplitudes do not vary significantly along-strike distance and that there is no obvious organization in the signal. In the spectral domain of the random data set, it is impossible to distinguish any clear long-wavelength segments (Figure 18d).

[63] To conclude, if our spinel Cr# were randomly distributed, they should display approximately the same amplitude at all wavelengths as seen in Figure 18d. This is not the case, and instead the Fourier transforms of spinel Cr# clearly exhibit dominant amplitudes at wavelengths lying between 50 and 100 km (70 km in average) for the large domains, and between 10 and 20 km for the shortest wavelengths (Figure 18b). This demonstrates that the chemical variations that we are describing in this paper do not represent artifacts.

8. Discussion

8.1. Characteristics of the Chemical Segmentation Pattern

[64] Plots of the spinel Cr# signal along ridge (Figure 19c) well display the two types of variations

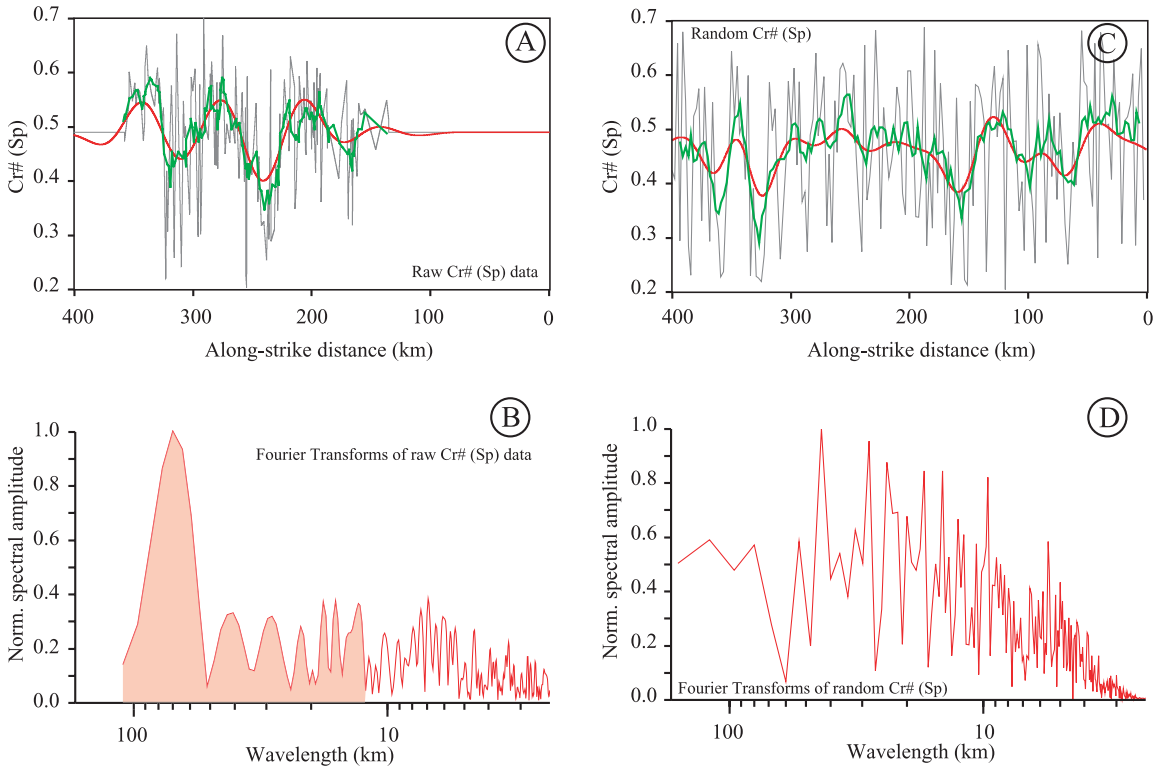

Figure 18. Comparison between the running average and the long-wavelength filtered signal. (a) The raw spinel Cr# data set is plotted in gray; the signal filtered between 50 and 100 km (70 km in average) corresponds to the red line and the running average method used by *Le Mée et al.* [2004] to the green line. (b) The same as in Figure 18a but for a random signal matching the amplitudes of the spinel Cr# signal. After performing a Fourier Transform, the normalized amplitudes of the spinel Cr# signal are plotted as a function of (c) wavelength and (d) the random signal shown in Figure 18b.

seen in the spectral domain (Figure 18b): one with a long wavelength and the other with a shorter one:

[65] 1. The large wavelength corresponds to the 50–100 km long segments (70 km on average, Figure 18b). Four of them have been defined, labeled A, B, C and D from South to North. Each segment displays its highest Cr# values in its center and the lowest ones at its extremities. These characteristics are typical of the segments defined in the present ridges whose centers corresponds to topographic domes formed by a thick magmatic crust over a depleted mantle and whose edges are characterized by the presence of relatively fertile rocks and by major morphological discontinuities. By analogy with present oceanic ridges [e.g., *MacDonald et al.*, 1988a], it can be considered that this type of segment likely correspond to a large asthenospheric mantle upwellings (Figure 19c). The geodynamic significance of the segments will be discussed in the section 8.4.

[66] 2. At a shorter wavelength, scale of 10–20 km, 14 narrow undulations marked by pronounced variations of the spinel Cr# signal have been distinguished within the larger segments. They have been labeled A#, B#, C# and D# in Figure 19c. This short wavelength may not be statistically significant in segments A and B that correspond to the reconstructed part of the ophiolite, but the distribution of short segments is probably significant for segment C (Fizh-Hilti area) which is complete and underwent no reconstruction. The amplitude variations between two adjacent shorter wavelengths are also significant because variations of Cr#, represented by its standard deviation (red narrow fields bordering the compositional line in Figure 1c) is lower than the variation of Cr # between two shorter wavelengths. As we do not observe any correlation between the raw Cr# of spinel and the standard deviation (2 sigma), we can consider that the shorter wavelengths describe true chemical variations. From the

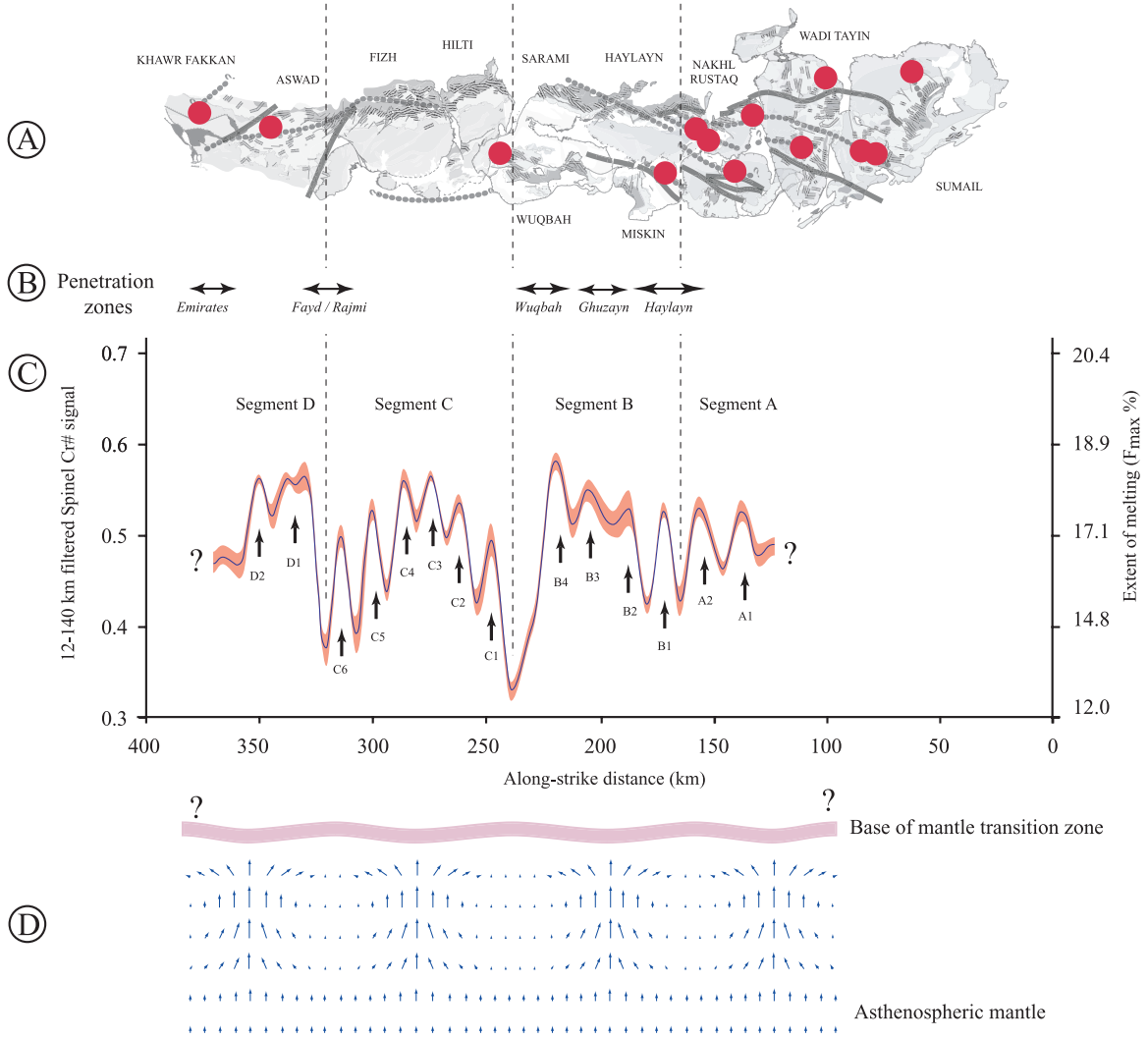

Figure 19. Along-strike comparison between our segmentation model (B) and previously published segmentation features. (a) Location of the structural mantle diapirs (red circles) defined by peridotites foliations and lineations [*Nicolas and Boudier*, 2000]. (b) Location of dike penetration zones [*MacLeod and Rothery*, 1992] mentioned with their original names. (c) Filtered spinel Cr# signal between 12–100 km (blue line). The red field corresponds to the standard deviation (2 sigma) for each sample. This diagram displays four 100–50 km long wavelengths (labeled A, B, C, and D) with 14 shorter 10–20 km wavelengths (labeled A#, B#, C# and D#), making undulations within the larger ones. Note that Segment C, which corresponds to the Fizh-Hilty area, is complete. (d) Geometry of the mantle flow associated with the large-scale upwellings [after *Choblet and Parmentier*, 2001]. Melt productivity is maximum at the centers of upwelling. Solid flow (blue arrows).

filtered Cr# signal, it can be estimated that they represent between 1 and 3% variations of the extent of melting within the larger mantle upwellings. They may relate the rise of shallow mantle instabilities associated with melt buoyancy and possibly correspond to the small structural diapirs (Figure 19a) already described in the ophiolite [*Ceuleneer*, 1986; *Ceuleneer et al.*, 1988; *Nicolas et al.*, 1988a; *Rabinowicz*, 1987]. These zones of melt focusing may also correspond to cryptic flow field patterns controlled by diffuse porous flow heterogeneities or to the feeding zones of the magma plumbing systems of the third-order volcanic segmentation described at 9°–10°N on EPR [*White et al.*, 2002].

8.2. Comparison With Structural Segmentation Features

[67] In the Oman ophiolite, we do not have any morpho-structural data concerning the basalts that could be used to define the segmentation geometry

as for the present-day mid-oceanic segmentation classification. Also, there is no field evidence for the existence of major paleo-transform faults except in the northern part of the Aswad massif to the north for which we unfortunately lack chemical data [*Gnos and Nicolas*, 1996]. The Aswan area discontinuity is possibly recorded by our data (Figure 19). As discussed in section 2.3, the ophiolite also displays some other discontinuity features like zones of dyke inter-penetration (Figure 19b) considered as extremities of magma chambers or segments [*MacLeod and Rothery*, 1992]. We note that these zones generally stand near the edges of the large segments defined in this study and never in their central parts (Figure 19b). The structural diapirs, which may be good indicators of paleo-ridge dynamics [e.g., *Nicolas and Boudier*, 2000] are abundant (about 7) in segment A to the south of the ophiolite (Figure 19a). It is difficult to say if the correlation between the chemical discontinuities and the structural diapirs is significant or not, but it can be noted that, in the northern and central part of the ophiolite, most of the structural diapirs could correspond to chemical ones. Our petrological data from the southern part of the ophiolite (Semail and Wadi Tayin massifs) are too rare to confirm or rule out the presence of correlations.

[68] As the crustal thickness is thought to be directly correlated to the melt productivity and therefore to the peridotite extent of melting [*Cannat et al.*, 1995; *Shaw*, 1992; *Sinton and Detrick*, 1992; *Whitehead et al.*, 1984], the most depleted zones of our chemical segments should correlate positively with the thicker parts of the magmatic crust. We have seen in section 5.5 that such relationships exists at the scale of the whole Oman ophiolite (Figure 12). This points to vertical magma transport from the zones of intense partial melting to zones where the crust crystallizes, as already proposed for present-day oceanic ridge models [e.g., *Sauter et al.*, 2001; *Sempéré et al.*, 1993].

8.3. Comparison With Present Oceanic Ridge Segmentation Features

[69] The chemical segmentation pattern defined for the Oman fossil oceanic ridge can be compared to the general one defined from the seafloor morphology [e.g., *MacDonald et al.*, 1988a; *Sempéré and MacDonald*, 1987; *Sinton et al.*, 1991] (see section 1.1 for references). Although we have no new data to confirm or rule out the possible existence of first-order discontinuities at the extremities of the Oman Ophiolite [*Ceuleneer*, 1986; *Gnos and Nicolas*, 1996], our data do suggest the existence of large segments that can be interpreted as second-order structures. At least of two segments (B and C) are about 70 km long. They are shorter than the first-order segments described along the EPR (300–900 km) and MAR (200–800 km), but quite similar to second-order discontinuities (EPR: 30–300 km; MAR: 10–100 km). On the other hand, the shortest Oman segments are on average 10 to 20 km long which is equivalent to the third-order segmentation distance for present-day ridges. Such small segments could be limited by simple deviations of their axis in zones where two generations of dykes exist [*MacLeod and Rothery*, 1992] or by OSCs (Over Spreading-Centers) with small offsets as the one already described in the Wuqbah massif [*Girardeau et al.*, 2002b].

8.4. Implications for the Dynamics of the Deep Oceanic Mantle

[70] The segmentation pattern we proposed in section 8.1 is based on the study of the shallower part of the mantle section of the Oman ophiolite, i.e., the uppermost 10 km under the paleo-Moho where magma extraction is the highest. This is still very shallow, but much deeper than what is accessible along in present-day mid-oceanic ridges.

[71] Data on the spinel Cr# allow us to estimate at 12% (F_{max}) the variation in the extent of melting that occurred beneath the ridge, varying from 20.5% in the central parts to 8.2% in their borders. A difference of F_{max} of ~12%, at 1.2% melting per kilobar [e.g., *Ahern and Turcotte*, 1979], requires a 10 kb or ~30 km difference in the thickness of the conductive boundary layer in the shallow mantle and a temperature variation of about 150°C, which is an unrealistically temperature gradient over only 50 km along strike.

[72] This indicates that temperature variations were not the appropriate parameter to explain the extent of melting variations we have evidenced. An alternative explanation is to consider that the observed variations in the extent of melting reflect along ridge variations of the fluid/melt contents within the peridotites. Indeed, even if fluids were not present in huge amounts during melting of the Oman mantle (as seen in section 5.2), it can be considered that they were all preferentially channeled in specific zones, which could therefore have undergone (1) a higher degree of melting as the fluids lower the melting solidus and change the

melting mechanisms, (2) large viscosity variations and therefore buoyant rise. In these zones of focusing rise of the mantle, fluid-flux melting is probably the dominant process to explain the melt formation. Such a scheme well explains the variations in the degree of melting, estimated at maximum 5% (F_{max}) with the raw Cr# in spinel and at 1 to 3% (F_{max}) from the filtered signal (Figure 19), observed in the neighboring samples that define the 10–20 km long short segments. The extremely large jumps of the melting rates marking the large-scale instabilities, 50–100 km wavelength (70 km in average), probably also relate some along ridge variations of temperature linked to the presence of major ridge discontinuities like transform faults.

[73] The development of the 50–100 km scale instabilities is consistent with results obtained by numerical modeling of present ridge mantle dynamics which show that 3D upwellings can develop in a low viscosity mantle [e.g., *Choblet*, 1999; *Choblet and Parmentier*, 2001; *Hirth and Kohlstedt*, 1996; *Jha et al.*, 1994; *Parmentier and Morgan*, 1990], particularly when the viscosity varies due to partial melting and water content [*Choblet and Parmentier*, 2001]. In recent models that take into account rheology variations due to melting and magma production, a 3D structure is observed at shallow depth for accretion rates below 6 cm/year and up to 20 cm/year full rate, with formation of segments 40 to 150 km long [*Choblet and Parmentier*, 2001]. This segmentation size is similar to that of the large segments we are describing in the Oman ophiolite.

[74] To date, there are very few observational constraints on the geometry of mantle upwellings. Meanwhile, it has been proposed that they have almost circular shapes as suggested by field observations of mantle diapirs in the Oman ophiolite [*Nicolas et al.*, 1988a], and that their presence at depth was generating topographic domes deepening in both the directions parallel and transverse to the ridge. Because of the lateral variations of the velocity of the flow, there must be substantiate dynamic flow along the ridge. This likely causes the transport from the center of the upwelling toward its periphery of some hot fluid/melt-rich mantle, in which the 10–20 km long upwellings can form. However, the lateral transport of the asthenospheric mantle (along strike), even if it cannot be neglected, must be rapidly deflected by the main mantle flows (across strike), due to the vicinity of the other segments. Concerning the exact 3D geometry of the mantle flow, which is not the topic of this paper, we believe that we still need more detailed, fine-scale, structural studies, particularly in zones considered as "structurally homogeneous."

8.5. Geodynamic Setting

[75] As our data on fO_2 (see section 5.2) show that the melting episode occurred in reduced conditions and therefore in the absence of large amounts of H_2O, it is quite unlikely that melting was produced above a subduction zone [*Ahmed and Arai*, 2002; *Beurrier*, 1987; *Gealey*, 1977; *Lippard et al.*, 1986; *Pearce et al.*, 1984; *Pearce*, 1980, 1982, 1991; *Schiano et al.*, 1997; *Shervais*, 2001; *Welland and Mitchell*, 1977]. It also probably did not occurred beneath a typical mid-oceanic ridge like those observed in the Atlantic and Pacific oceans as can be seen on palinspastic reconstructions of the western end of the Tethys which suggest that the ophiolite formed in a paleo-oceanic domain bounded to the SW and NE by continents and that was narrowing to the NW [e.g., *Dercourt et al.*, 1986]. This suggests that the Oman paleo-ridge was propagating in a narrow ocean or, possibly, in a marginal basin as was already proposed [*MacLeod and Rothery*, 1992; *Taylor and Karner*, 1983; *Taylor et al.*, 1996; *Weissel*, 1977, 1981]. These two settings are potentially favorable for the development of the observed segmentation features since major border effects that can channel the mantle flow are expected in the two environments, providing that they were marked by high heat flows.

9. Conclusions

[76] The main results of our petrological study on the Oman peridotites are the following:

[77] 1. Most of the studied peridotites are harzburgites. Their primary phase chemistries and REE bulk-rocks concentrations suffered only minor transformation during serpentinization and weathering and mostly display their primary petrological features.

[78] 2. Although a few harzburgites display fertile primary minerals and bulk-rock chemistries, most of the studied samples have depleted characteristics with very low concentrations Ti and Na whole rock and high Cr# ratio in spinels and low Al_2O_3 contents in orthopyroxenes. Accordingly, the harzburgites are dominantly magnesium-rich, alumi-

num and alkali poor, and strongly depleted in HREE.

[79] 3. Most of the studied harzburgites display light REE enrichments giving typical spoon-shaped patterns. Because of the strong correlation existing between the LREE/MREE ratios and spinel Cr# or Yb contents in the whole rock, these enrichments, which can be explained by an open-system melting model, was likely gained during the latest stage of melting or through interaction with influxed fluid after melting.

[80] 4. Oxygen fugacity estimates show that melting occurred in reduced conditions. On the basis of this Cr# ratio and in agreement with Yb concentrations in the bulk rocks, a F_{max} average of about 16.5% of partial melting is estimated, with variations ranging between 8.3 and 20.5% ($4\% < F_{mean} < 10\%$).

[81] 5. To study the along-ridge chemical variation of the spinel Cr#, data have been processed using Fourier Transforms. Results are similar to those obtained previously using a seven point running average method [*Le Mée et al.*, 2004].

[82] 6. When plotted along ridge, the spinel Cr# display two types of variation with very distinctive wavelengths. They define four long segments, 50–100 km long (70 km in average) and numerous 10–20 km shorter ones making undulations within the long ones. All segments, whatever their wavelength, have a center marked by high values of spinel Cr# ($\approx F_{max}$) and edges corresponding to the lowest values. Only segment C that corresponds to the Fizh-Hilti area is complete, while the rest have been tectonically dismembered to some extent.

[83] 7. The large, 50–100 km segments (70 km in average), may correspond to large asthenospheric mantle upwellings between major deep mantle discontinuities while the smaller ones possibly relate more superficial mantle instabilities similar to the structural diapirs of *Nicolas et al.* [1988a]. We consider that the variation in extent of melting in the short-scale instabilities relates fluid/melt flux melting variations.

[84] 8. By comparison to mid-oceanic ridge segmentation features, it is proposed that the long Oman segments correspond to second-order type segments, and that the smallest are of third- to fourth-order type. The petrological and segmentation features suggest that the Oman paleo-ridge was active in a small ocean with intermediate-spreading rates.

[85] Our chemical data set on the peridotites from the Oman ophiolite constrains a large-scale segmentation model for a fossil oceanic lithosphere. The data suggest the mantle residues have perfectly recorded the segmentation process and well correspond to the morphological segmentation defined at present-day mid-oceanic ridges. This work also brings new data on the geometry of the melting zones that should be used to constrain numerical modeling and for further characterization of the segments in the Oman ophiolite.

Acknowledgments

[86] Financial support was provided by the Centre National de la Recherche Scientifique (CNRS) through the Intérieur de la Terre program and by the French Ministère de la Recherche. The manuscript was greatly enhanced by the exhaustive and constructive comments of Peter Kelemen, who also suggested many useful modifications, and by the useful remarks by Jean Bédard, Vincent Salters, Glenn Gaetani, and the anonymous reviewer. The authors also thank Eric Beucler and Antoine Mocquet for the Fourier Transforms data processing and Eric Humler for stimulating discussions and suggestions. We thank Hilal Al Azri and Jean-Paul Breton for their logistic support on the field, E. Boeuf and H. Loyen, who made the thin sections, Bernard Reynier, Michel Valladon, and Jo Cotten for their help during ICP-MS and ICP-AES analyses, and Marcel Bohn, who is in charge of the microprobe.

References

Ahern, J. L., and D. L. Turcotte (1979), Magma migration beneath an ocean ridge, *Earth Planet. Sci. Lett.*, *45*(1), 115–122.

Ahmed, A., and S. Arai (2002), Unexpectedly high-PGE chromitite from the deeper mantle section of the northern Oman ophiolite and its tectonic implications, *Contrib. Mineral. Petrol.*, *143*(3), 263–278.

Alabaster, T., J. A. Pearce, and J. Malpas (1982), The volcanic stratigraphy and petrogenesis of the Oman ophiolite complex, *Contrib. Mineral. Petrol.*, *81*(3), 168–183.

Allan, J. F., and H. J. B. Dick (1996), Cr-rich spinel as a tracer for melt migration and melt-wall rock interaction in the mantle: Hess Deep, Leg 147, in *Hess Deep Rift Valley: Leg 147, Sites 894–895*, *Proc. Ocean Drill. Program Sci. Results*, vol. 147, edited by C. Mével et al., pp. 157–172, Ocean Drill. Program, College Station, Tex.

Arai, S. (1987), An estimation of the least depleted spinel peridotites on the basis of olivine-spinel mantle array, *Jahrb. Mineral. Monatsh.*, *8*, 347–357.

Arai, S. (1994a), Characterization of spinel peridotites by olivine-spinel compositional relationships: Review and interpretation, *Chem. Geol.*, *113*(3–4), 191–204.

Arai, S. (1994b), Compositional variation of olivine-chromian spinel in Mg-rich magmas as a guide to their residual spinel peridotites, *J. Volcanol. Geotherm. Res.*, *59*(4), 279–293.

Arai, S., and K. Matsukage (1996), Petrology of the gabbro-troctolite-peridotite complex from Hess Deep, equatorial Pacific: Implication for mantle-melt interaction within the oceanic lithosphere, in *Hess Deep Rift Valley: Leg 147, Sites 894–895*, *Proc. Ocean Drill. Program Sci. Results*, vol. 147, edited by C. Mével et al., pp. 135–155, Ocean Drill. Program, College Station, Tex.

Arai, S., K. Matsukage, E. Isobe, and S. Vysotskiy (1997), Concentration of incompatible elements in oceanic mantle: Effect of melt/wall interaction in stagnant or failed melt conduits within peridotite, *Geochim. Cosmochim. Acta*, *61*(3), 671–675.

Augé, T. (1982), Petrology and geochemistry of some chromitiferous bodies within the Oman ophiolite, *Ofioliti*, *2/3*, 133–154.

Augé, T. (1987), Chromite deposits in the northern Oman ophiolite: Mineralogical constraints, *Miner. Deposita*, *22*, 1–10.

Baker, M. B., and J. R. Beckett (1999), The origin of abyssal peridotites: A reinterpretation of constraints based on primary bulk compositions, *Earth Planet. Sci. Lett.*, *171*(1), 49–61.

Ballhaus, C., R. F. Berry, and D. H. Green (1990), Oxygen fugacity controls in the Earth's upper mantle, *Nature*, *348*, 437–440.

Barnes, S. J., and P. L. Roeder (2001), The range of spinel compositions in terrestrial mafic and ultramafic rocks, *J. Petrol.*, *42*(12), 2279–2302.

Batiza, R. (1996), Magmatic segmentation of mid-ocean ridges: A review, in *Tectonic, Magmatic, Hydrothermal and Biological Segmentation of Mid-ocean Ridges*, edited by C. Mc Leod, *Geol. Soc. Spec. Publ.*, *118*, 103–130.

Benoit, M., M. Polve, and G. Ceuleneer (1996), Trace element and isotopic characterization of mafic cumulates in a fossil mantle diapir (Oman ophiolite), *Chem. Geol.*, *134*, 199–214.

Bertrand, P., and J. C. Mercier (1985), The mutual solubility of coexisting ortho- and clinopyroxene toward an absolute geothermometer for the natural system, *Earth Planet. Sci. Lett.*, *76*, 109–122.

Beurrier, M. (1987), Géologie de la nappe ophiolitique de Samail dans les parties orientale et centrale des montagnes d'Oman, Thèse Doctorat d'Etat, 426 pp., Paris VI, Paris.

Bodinier, J.-L. (1988), Geochemistry and petrogenesis of the Lanzo peridotite body, western Alps, *Tectonophysics*, *149*, 67–88.

Bodinier, J.-L., and M. Godard (2003), Orogenic, ophiolitic, and abyssal peridotites, in *Treatise on Geochemistry*, edited by R. W. Carlson, pp. 103–170, Elsevier, New York.

Bodinier, J.-L., G. Vasseur, J. Vernières, C. Dupuy, and J. Fabriès (1990), Mechanisms of mantle metasomatism: Geochemical evidence from the Lherz orogenic peridotite, *J. Petrol.*, *31*, 597–628.

Bodinier, J.-L., M. A. Menzies, and M. F. Thirlwall (1991), Continental to oceanic mantle transition—REE and Sr-Nd isotopic geochemistry of the Lanzo lherzolite massif, in *Orogenic Lherzolites and Mantle Processes*, *J. Petrol.*, spec. issue, 191–210.

Bonatti, E., and P. J. Michael (1989), Mantle peridotites from continental rifts to ocean basins to subduction zones, *Earth Planet. Sci. Lett.*, *91*(3–4), 297–311.

Bonatti, E., A. Peyve, P. Kepezhinskas, N. Kurentsova, M. Seyler, S. Skolotnev, and G. Udintsev (1992), Upper mantle heterogeneity below the Mid-Atlantic Ridge, 0°–15°N, *J. Geophys. Res.*, *97*, 4461–4476.

Boudier, F., and R. G. Coleman (1981), Cross-section through the peridotite in the Samail ophiolite, Southeastern Oman Mountains, *J. Geophys. Res.*, *86*, 2573–2592.

Boudier, F., G. Ceuleneer, and A. Nicolas (1988), Shear zones, thrusts and related magmatism in the Oman ophiolite: Initiation of thrusting on an oceanic ridge, *Tectonophysics*, *151*, 275–296.

Boudier, F., A. Nicolas, B. Ildefonse, and D. Jousselin (1997), EPR microplates, a model for the Oman ophiolite, *Terra Nova*, *9*(2), 79–82.

Braun, M. G., and P. B. Kelemen (2002), Dunite distribution in the Oman Ophiolite: Implications for melt flux through porous dunite conduits, *Geochem. Geophys. Geosyst.*, *3*(11), 8603, doi:10.1029/2001GC000289.

Brey, G. P., and T. P. Kohler (1990), Geothermobarometry in four-phase lherzolites II. New thermobarometers, and practical assessment of existing thermobarometers, *J. Petrol.*, *31*, 1353–1378.

Bryndzia, L. T., and B. J. Wood (1990), Oxygen thermobarometry of abyssal spinel peridotites: The redox state and the C-O-H volatile composition of the Earth's sub-oceanic mantle, *Am. J. Sci.*, *290*, 1093–1116.

Cannat, M. (1996), How thick is the magmatic crust at slow spreading ridges?, *J. Geophys. Res.*, *101*, 2847–2857.

Cannat, M., C. Mével, and M. Maia (1995), Thin crust, ultramafic exposures, and rugged faulting patterns at the Mid-Atlantic Ridge (22°–24°N), *Geology*, *23*, 49–52.

Ceuleneer, G. (1986), Structure des ophiolites d'Oman: flux mantellaire sous un centre d'expansion océanique et charriage à la dorsale, Thèse de Doctorat d'Univ., 338 pp., Univ. de Nantes, Nantes, France.

Ceuleneer, G. (1991), Evidence for a paleo-spreading center in the Oman Ophiolite: Mantle structures in the Maqsad area, in *Ophiolite Genesis and Evolution of Oceanic Lithosphere*, edited by T. Peters, pp. 147–173, Springer, New York.

Ceuleneer, G., and M. Rabinowicz (1992), Mantle flow and melt migration beneath oceanic ridge: Models derived from observations in ophiolites, in *Mantle Flow and Melt Generation at Mid-ocean Ridges*, *Geophys. Monogr. Ser.*, vol. 71, edited by J. Phipps Morgan, D. Blackman, and J. Sinton, pp. 123–154, AGU, Washington, D. C.

Ceuleneer, G., A. Nicolas, and F. Boudier (1988), Mantle flow patterns at an oceanic spreading centre: The Oman peridotites record, *Tectonophysics*, *151*, 1–26.

Choblet, G. (1999), Dynamique interne des planètes: apport de la modélisation 3D pour un fluide à rhéologie complexe, Doctorat d'Univ., 268 pp., Univ. de Rennes 1, Rennes, France.

Choblet, G., and E. M. Parmentier (2001), Mantle upwelling and melting beneath slow spreading centers: Effects of variable rheology and melt productivity, *Earth Planet. Sci. Lett.*, *184*(3–4), 589–604.

Coleman, R. G. (1981), Tectonic setting for ophiolite obduction in Oman, *J. Geophys. Res.*, *86*(B4), 2497–2508.

Coleman, R. G. (1984), Ophiolites and the tectonic evolution of the arabian peninsula, in *Ophiolites and Oceanic Lithosphere*, edited by I. G. Gass, S. J. Lippard, and A. W. Shelton, pp. 359–366, Blackwell Sci., Malden, Mass.

Dahl, R. (1984), Etude géométrique, pétrologique et géochimique de la séquence crustale de l'ophiolite d'Oman, massif de Rustaq (Bloc d'Haylayn). Un modèle tridimentionnel de zone d'accrétion, Thèse Doctorat 3ème Cycle, 264 pp., Univ. de Nantes, Nantes, France.

Dercourt, J., et al. (1986), Geological evolution of the tethys belt from the Atlantic to the pamirs since the LIAS, *Tectonophysics*, *123*(1–4), 241–315.

Dick, H. J. B. (1977), Partial melting in the Josephine peridotite, I., *Am. J. Sci.*, *277*(7), 801–832.

Dick, H. J. B., and T. Bullen (1984), Chromian spinel as a petrogenetic indicator in abyssal and alpine-type peridotites and spatially associated lavas, *Contrib. Mineral. Petrol.*, *86*, 54–76.

Dick, H. J. B., and J. H. Natland (1996), Late-stage melt evolution and transport in the shallow mantle beneath the East Pacific Rise, in *Hess Deep Rift Valley: Leg 147, Sites 894–895*, *Proc. Ocean Drill. Program Sci. Results*, vol. 147, edited by C. Mével et al., pp. 103–134, Ocean Drill. Program, College Station, Tex.

Dijkstra, A. H., M. R. Drury, R. L. M. Vissers, and J. Newman (2002), On the role of melt-rock reaction in mantle shear zone formation in the Othris Peridotite Massif (Greece), *J. Struct. Geol.*, *24*(9), 1431–1450.

Dijkstra, A. H., M. G. Barth, M. R. Drury, P. R. D. Mason, and R. L. M. Vissers (2003), Diffuse porous melt flow and melt-rock reaction in the mantle lithosphere at a slow-spreading ridge: A structural petrology and LA-ICP-MS study of the Othris Peridotite Massif (Greece), *Geochem. Geophys. Geosyst.*, *4*(8), 8613, doi:10.1029/2001GC000278.

Dilek, Y., E. Moores, D. Elthon, and A. Nicolas (2000), *Ophiolites and Oceanic Crust: New Insights From Field Studies and the Ocean Drilling Program*, 552 pp., Geol. Soc. of Am., Boulder.

Dixon, J. E., E. Stolper, and J. R. Delaney (1988), Infrared spectroscopic measurements of CO_2 and H_2O in Juan de Fuca Ridge basaltic glasses, *Earth Planet. Sci. Lett.*, *90*(1), 87–104.

Dosso, L., B. B. Hanan, H. Bougault, J.-G. Schilling, and J.-L. Joron (1991), Sr-Nd-Pb geochemical morphology between 10° and 17°N on the Mid-Atlantic Ridge: A new MORB isotope signature, *Earth Planet. Sci. Lett.*, *106*(1–4), 29–43.

Dosso, L., H. Bougault, C. H. Langmuir, C. Bollinger, O. Bonnier, and J. Etoubleau (1999), The age and distribution of mantle heterogeneity along the Mid-Atlantic Ridge (31–41°N), *Earth Planet. Sci. Lett.*, *170*(3), 269–286.

Einaudi, F., M. Godard, P. Pezard, J.-J. Cochemé, C. Coulon, T. Brewer, and P. Harvey (2003), Magmatic cycles and formation of the upper oceanic crust at spreading centers: Geochemical study of a continuous extrusive section in the Oman ophiolite, *Geochem. Geophys. Geosyst.*, *4*(6), 8608, doi:10.1029/2002GC000362.

Ernewein, M., C. Pflumio, and H. Whitechurch (1988), The death of an accretion zone as evidenced by the magmatic history of the Sumail ophiolite (Oman), *Tectonophysics*, *151*, 247–274.

Evans, B. W., and B. R. Frost (1975), Chrome-spinel in progressive metamorphism—A preliminary analysis, *Geochim. Cosmochim. Acta*, *39*(6–7), 959–972.

Fabriès, J. (1979), Spinel-olivine geothermometry in peridotites from ultramafic complexes, *Contrib. Mineral. Petrol.*, *69*, 329–336.

Gast, P. W. (1968), Trace element fractionation and the origin of tholeiitic and alkaline magma types, *Geochim. Cosmochim. Acta*, *32*, 1057–1086.

Gealey, W. K. (1977), Ophiolite obduction and geologic evolution of the Oman mountains and adjacent areas, *Geol. Soc. Am. Bull.*, *88*, 1183–1191.

Gerbert-Gaillard, L. (2002), Caractérisation géochimique des péridotites de l'ophiolite d'Oman: Processus magmatiques aux limites lithosphère/asthénosphère, Thèse Doctorat 3ème Cycle, 217 pp., Univ. de Montpellier II, Montpellier, France.

Gervilla, F., and M. Remaidi (1993), Field trip to the Ronda ultramafic massif: An example of asthenoshere-lithosphere interaction?, *Ofioliti*, *18*, 21–35.

Girardeau, J., and J. Francheteau (1993), Plagioclase-wehrlites and peridotites on the East Pacific Rise (Hess Deep) and the Mid-Atlantic Ridge (DSDP Site 334): Evidence for magma percolation in the oceanic upper mantle, *Earth Planet. Sci. Lett.*, *115*(1–4), 137–149.

Girardeau, J., C. Monnier, P. Launeau, and F. Quatrevaux (2002a), Kinematics of mantle flow beneath a fossil Overlapping Spreading Center: The Wuqbah massif case, Oman ophiolite, *Geochem. Geophys. Geosyst.*, *3*(7), 1043, doi:10.1029/2001GC000228.

Girardeau, J., C. Monnier, L. Le Mée, and F. Quatrevaux (2002b), The Wuqbah peridotite, central Oman ophiolite: Petrological characteristics of the mantle in a fossil overlapping ridge setting, *Mar. Geophys. Res.*, *23*(1), 43–56.

Glücklich-Herbas, M. (1992), Caractérisation pétrochimique du manteau lherzolitique sous-continental., Ph.D. thesis, 453 pp., Univ. de Paris VII (IPGP), Paris.

Gnos, E., and A. Nicolas (1996), Structural evolution of the northern end of the Oman Ophiolite and enclosed granulites, *Tectonophysics*, *254*(1–2), 111–137.

Godard, M. (2003), Petrogenesis of a propagating segment at a fast spreading ridge: Geochemistry of peridotites from the Maqsad segment, Oman Ophiolite, *Geophys. Res. Abstr.*, *5*, 12,324.

Godard, M., J.-L. Bodinier, and G. Vasseur (1995), Effects of mineralogical reactions on trace element redistributions in mantle rocks during percolation processes: A chromatographic approach, *Earth Planet. Sci. Lett.*, *133*(3–4), 449–461.

Godard, M., D. Jousselin, and J.-L. Bodinier (2000), Relationships between geochemistry and structure beneath paleo-spreading centre: A study of the mantle section in the Oman ophiolite, *Earth Planet. Sci. Lett.*, *180*, 133–148.

Grindlay, N. R., P. J. Fox, and P. R. Vogt (1992), Morphology and tectonics of the mid-atlantic ridge (25°–27°30′S) from sea beam and magnetic data, *J. Geophys. Res.*, *97*(B5), 6983–7010.

Gruau, G., J. Bernard-Griffiths, and C. Lecuyer (1998), The origin of U-shaped rare earth patterns in ophiolite peridotites: assessing the role of secondary alteration and melt/rock reaction, *Geochim. Cosmochim. Acta*, *62*(21–22), 3545–3560.

Hacker, B. R., and J. L. Mosenfelder (1996), Metamorphism and deformation along the emplacement thrust of the Samail ophiolite, Oman, *Earth Planet. Sci. Lett.*, *144*(3–4), 435–451.

Harte, B. (1977), Rock nomenclature with particular relation to deformation and recrystallization textures in olivine-bearing xenoliths, *J. Geol.*, *85*, 279–288.

Hekinian, R., D. Bideau, J. Francheteau, J.-L. Cheminée, R. Armijo, P. Lonsdale, and N. Blum (1993), Petrology of the East Pacific Rise crust and upper mantle exposed in the Hess Deep (eastern equatorial Pacific), *J. Geophys. Res.*, *98*, 8069–8094.

Hellebrand, E., J. E. Snow, and H. J. B. Dick (2001), Coupled major and trace elements as indicators of the extent of melting in mid-ocean-ridge peridotites, *Nature*, *410*, 677–681.

Hirth, G., and D. L. Kohlstedt (1996), Water in the oceanic upper mantle: Implications for rheology, melt extraction and the evolution of the lithosphere, *Earth Planet. Sci. Lett.*, *144*(1–2), 93–108.

Hopson, C. A., R. G. Coleman, and R. T. Gregory (1981), Geologic section through the Samail Ophiolite and asso-

ciated rocks along a Muscat-Ibra transect, southeastern Oman mountains, *J. Geophys. Res.*, *86*, 2527–2544.
Hostetler, P. B., R. G. Coleman, F. A. Mumpton, and B. W. Evans (1966), Brucite in alpine serpentinites, *Am. Mineral.*, *51*, 75–98.
Irvine, T. N. (1965), Chromian spinel as a petrogenetic indicator, 1: Theory, *Can. J. Earth Sci.*, *2*, 648–672.
Irvine, T. N. (1967), Chromian spinel as a petrogenetic indicator. 2: Petrologic applications, *Can. J. Earth Sci.*, *4*, 71–103.
Ishii, T., P. T. Robinson, H. Maekawa, and R. Fiske (1992), Petrological studies of peridotites from diapiric serpentinite seamounts in the Izu-Ogasawara-Mariana Forearc, Leg 125, *Proc. Ocean Drill. Program Sci. Results*, *125*, 445–485.
Jagoutz, E., H. Palme, and H. Baddenhausen (1979), The abundances of major, minor and trace elements in the Earth's primitive mantle as derived from primitive ultramafic nodules, *Proc. Lunar Planet. Sci. Conf. 10th*, 2031–2050.
Jaques, A. L., and D. H. Green (1980), Anhydrous melting of peridotite at 0–15 kb pressure and the genesis of tholeitic basalts, *Contrib. Mineral. Petrol.*, *73*, 287–310.
Jha, K., E. M. Parmentier, and M. J. Phipps (1994), The role of mantle-depletion and melt-retention buoyancy in spreading-center segmentation, *Earth Planet. Sci. Lett.*, *125*(1–4), 221–234.
Johnson, K. M., and H. J. B. Dick (1992), Open system melting and the temporal and spatial variation of peridotite and basalt compositions at the Atlantis II Fracture Zone, *J. Geophys. Res.*, *97*(B6), 9219–9241.
Johnson, K. M., H. J. B. Dick, and N. Shimizu (1990), Melting in the oceanic upper mantle: An ion microprobe study of diopsides in abyssal peridotites, *J. Geophys. Res.*, *95*, 2661–2678.
Jousselin, D., and A. Nicolas (2000), The Moho transition zone in the Oman ophiolite-related with wehrlites in the crust and dunites in the mantle, *Mar. Geophys. Res.*, *21*, 229–241.
Juteau, T., M. Beurrier, R. Dahl, and P. Nehlig (1988a), Segmentation at a fossil spreading axis: The plutonic sequence of the Wadi Haymiliyah area (Haylayn Block, Sumail Nappe, Oman), *Tectonophysics*, *151*, 167–197.
Juteau, T., M. Ernewein, I. Reuber, H. Whitechurch, and R. Dahl (1988b), Duality of magmatism in the plutonic sequence of the Sumail nappe, Oman, *Tectonophysics*, *151*, 107–135.
Kelemen, P. (1990), Reaction between ultramafic rock and fractionating basaltic magma I. Phase relations, the origin of calc-alkaline magma series, and the formation of discordant dunite, *J. Petrol.*, *31*(1), 51–98.
Kelemen, P., G. Hirth, N. Shimizu, M. Spiegelman, and H. J. B. Dick (1997a), A review of melt migration processes in the adiabatically upwelling mantle beneath oceanic spreading ridges, *Philos. Trans. R. Soc. London, Ser. A*, *355*, 283–318.
Kelemen, P., K. Koga, and N. Shimizu (1997b), Geochemistry of gabbro sills in the crust-mantle transition zone of the Oman ophiolite: Implications for the origin of the oceanic lower crust, *Earth Planet. Sci. Lett.*, *146*, 475–488.
Kelemen, P. B., H. J. B. Dick, and J. E. Quick (1992), Formation of harzburgite by pervasive melt/rock reaction in the upper mantle, *Nature*, *358*, 635–641.
Kelemen, P. B., K. T. M. Johson, R. Kinzler, and A. J. Irving (1990), High field strength element depletions in arc basalts due to mantle: production of harzburgites by mantle-magma interaction, *Nature*, *358*, 635–640.
Kelemen, P. B., N. Shimizu, and T. Dunn (1993), Relative depletion of Nb in some arc magmas and the continental crust: Partitioning of K, Nb, La and Ce during melt/rock reaction in the upper mantle, *Earth Planet. Sci. Lett.*, *120*, 111–134.
Kelemen, P. B., N. Shimizu, and V. J. Salters (1995), Extraction of mid-oceanic-ridge basalt from the upwelling mantle by focused flow of melt in dunite channels, *Nature*, *375*, 747–753.
Komor, S. C., D. Elthon, and J. F. Casey (1985), Serpentinization of cumulate ultramafic rocks from the North Arm Mountain massif of the Bay of Islands ophiolite, *Geochim. Cosmochim. Acta*, *49*(11), 2331–2338.
Korenaga, J., and P. Kelemen (1997), Origin of gabbro sills in the Moho transition zone of the Oman ophiolite: Implications for magma transport in the oceanic lower crust, *J. Geophys. Res.*, *102*, 27,729–27,749.
Langmuir, C. H., J. F. Bender, and R. Batiza (1986), Petrological and tectonic segmentation of the East Pacific Rise, 5°30′–14°30′N, *Nature*, *322*, 422–429.
Langmuir, C. H., E. M. Klein, and T. Planck (1992), Petrological systematics of mid-ocean ridge basalts: Constraints on melt generation beneath ocean ridges, in *Mantle Flow and Melt Generation at Mid-Ocean Ridges*, *Geophysic Monogr. Ser.*, vol. 71, edited by J. Phipps Morgan, D. Blackman, and J. Sinton, pp. 183–280, AGU, Washington, D. C.
Launeau, P., and P.-Y. F. Robin (1996), Fabric analysis using the intercept method, *Tectonophysics*, *26*, 119–791.
Le Mée, L. (2004), Chemistry of the Oman ophiolite peridotites and along-strike segmentation of mid-oceanic ridges, Doctorat d'Univ.é, 374 pp., Univ. de Nantes, Nantes, France.
Le Mée, L., J. Girardeau, and C. Monnier (2004), Mantle segmentation along the Oman ophiolite fossil mid-ocean ridge, *Nature*, *432*, 167–172.
Lippard, S. J., A. W. Shelton, and I. G. Gass (1986), *The Ophiolite of Northern Oman*, *Geol. Soc. London Mem.*, vol. 11, 178 pp., Blackwell Sci., Malden, Mass.
Maaløe, S., and K. Aoki (1977), The major element composition of the upper mantle estimated from the composition of lherzolites, *Contrib. Mineral. Petrol.*, *63*, 161–173.
MacDonald, K. C., J. C. Sempéré, and P. J. Fox (1984), The East Pacific Rise from the Sequeiros to the Orozco fracture zones: along strike continuity of the axial neovolcanic zone and the structure and evolution of Overlapping Spreading Centers, *J. Geophys. Res.*, *89*, 6049–6069.
MacDonald, K. C., J. C. Sempéré, P. J. Fox, and R. Tyce (1987), Tectonic evolution of ridge-axis discontinuities by the meeting, linking, or self-decapitation of neighboring ridge segments, *Geology*, *15*, 993–997.
MacDonald, K. C., P. J. Fox, L. J. Perram, M. F. Eisen, R. M. Haymon, S. P. Miller, S. M. Carbotte, M.-H. Cormier, and A. N. Shor (1988a), A new view of the mid-ocean ridge from the behaviour of ridge-axis discontinuities, *Nature*, *335*(6187), 217–225.
MacDonald, K. C., R. M. Haymon, and S. P. Miller (1988b), Deep-tow and Sea Beam studies of dueling propagating ridges on the East Pacific Rise near 20°40′S., *J. Geophys. Res.*, *93*, 2875–2898.
MacLeod, C. J., and D. A. Rothery (1992), Ridge axial segmentation in the Oman ophiolite: Evidence from along-strike variations in the sheeted dyke complex, in *Ophiolites and Their Modern Oceanic Analogues*, edited by L. M. Parson, B. J. Murton, and P. Browning, *Geol. Soc. Spec. Publ.*, *60*, 39–63.
Mercier, J.-C., (1985), Olivine and pyroxenes, in *Preferred Orientation in Minerals and Rocks: An Introduction to Modern Texture Analysis*, edited by H. R. Wenk, pp. 407–430, Springer, New York.

Mercier, J.-C., and A. Nicolas (1975), Textures and fabrics of upper-mantle peridotites as illustrated by xenoliths from basalts, *J. Petrol.*, *16*(2), 454–487.

Michael, P. J., and E. Bonatti (1985), Peridotite composition from the North Atlantic: Regional and tectonic variations and implications for partial melting, *Earth Planet. Sci. Lett.*, *73*(1), 91–104.

Miyashiro, A. (1973), The Troodos ophiolitic complex was probably formed in an island arc, *Earth Planet. Sci. Lett.*, *19*, 218–224.

Monnier, C., J. Girardeau, R. Maury, and J. Cotten (1995), Back-arc basin origin for the East Sulawesi ophiolite (eastern Indonesia), *Geology*, *23*(9), 851–854.

Monnier, C., J. Girardeau, M. Pubellier, M. Polvé, H. Permana, and H. Bellon (1999a), Petrology and geochemistry of the Cyclops ophiolite (Irian Jaya - East Indonesia): Consequences for the evolution of the north Australian margin during Cenozoic, *Mineral. Petrol.*, *65*, 1–28.

Monnier, C., M. Polvé, J. Girardeau, M. Pubellier, R. C. Maury, H. Bellon, and H. Permana (1999b), Extensional to compressive Mesozoic magmatism at the SE Eurasian margin as recorded from the Meratus ophiolite (SE Borneo, Indonesia), *Geodin. Acta*, *12*, 43–55.

Monnier, C., J. Girardeau, M. Pubellier, and H. Permana (2000), L'ophiolite de la chãcirc;ne centrale (Irian Jaya, Indonésie): Evidences pétrologiques et géochimiques pour une origine dans un bassin arrière-arc, *C. R. Acad. Sci. Paris, Ser. II*, *2000*, 691–699.

Monnier, C., J. Girardeau, J.-P. Réhault, H. Permana, and H. Bellon (2003), Dynamics and age of formation of the Seram-Ambo ophiolites (Central Indonesia), *Bull. Soc. Geol. Fr.*, *174*(6), 529–543.

Navon, O., and E. Stolper (1987), Geochemical consequences of melt percolation: The uppermantle as a chromatographic column, *J. Geol.*, *95*, 285–307.

Nicolas, A. (1986a), A melt extraction model based on structural studies in mantle peridotites, *J. Petrol.*, *27*, 999–1022.

Nicolas, A. (1986b), Structure and petrology of peridotites: Clues to their geodynamic environment, *Rev. Geophys.*, *24*, 875–895.

Nicolas, A. (1989), *Structure of Ophiolites and Dynamics of Oceanic Lithosphere*, 367 pp., Springer, New York.

Nicolas, A., and F. Boudier (2000), Large mantle upwellings and related variations in crustal thickness in the Oman ophiolite, *Geol. Soc. Am. Bull.*, *349*(2), spec. publ., 67–74.

Nicolas, A., G. Ceuleneer, F. Boudier, and M. Misseri (1988a), Structural mapping in the Oman ophiolites: Mantle diapirism along an oceanic ridge, *Tectonophysics*, *151*, 27–56.

Nicolas, A., I. Reuber, and K. Benn (1988b), A new magma chamber model based on structural studies in the Oman ophiolite, *Tectonophysics*, *151*, 87–105.

Nicolas, A., F. Boudier, and B. Ildefonse (1994), Evidence from the Oman ophiolite for active mantle upwelling beneath a fast-spreading ridge, *Nature*, *370*, 51–53.

Nicolas, A., F. Boudier, and B. Ildefonse (1996), Variable crustal thickness in the Oman Ophiolite: Implication for oceanic crust, *J. Geophys. Res.*, *101*(B8), 17,941–17,950.

Nicolas, A., F. Boudier, B. Ildefonse, and E. Ball (2000a), Accretion of Oman and United Arab Emirates Ophiolites—Discussion of a new structural map, *Mar. Geophys. Res.*, *21*, 174–179.

Nicolas, A., B. Ildefonse, F. Boudier, X. Lenoir, and W. Ben Ismail (2000b), Dike distribution in the Oman-United Emirates ophiolites, *Mar. Geophys. Res.*, *21*, 269–287.

Niu, Y., and R. Hékinian (1997a), Spreading rate dependence of the extent of mantle melting beneath ocean ridges, *Nature*, *385*, 326–329.

Niu, Y., and R. Hékinian (1997b), Basaltic liquids and harzburgitic residues in the Garrett Transform: A case study at fast-spreading ridges, *146*, 243–258.

Niu, Y., C. H. Langmuir, and R. J. Kinzler (1997), The origin of abyssal peridotites: A new perspective, *Earth Planet. Sci. Lett.*, *152*(1–4), 251–265.

Ozawa, K., and N. Shimizu (1995), Open-system melting in the upper mantle: Constraints from the Hayachine-Miyamori ophiolite, northeastern Japan, *J. Geophys. Res.*, *100*(B11), 22,315–22,336.

Pallister, J. S. (1981), Structure of the sheeted dyke complex of the Samail ophiolite near Ibra, Oman, *J. Geophys. Res.*, *86*, 2661–2672.

Pallister, J. S., and C. A. Hopson (1981), Samail ophiolite plutonic suite: Field relations, phase variation, cryptic variation and layering, and a model of a spreading ridge magma chamber, *J. Geophys. Res.*, *86*, 2593–2644.

Parkinson, I. J., and R. J. Arculus (1999), The redox state of subduction zones: Insights from arc-peridotites, *Chem. Geol.*, *160*(4), 409–423.

Parkinson, I. J., and J. A. Pearce (1998), Peridotites from the IZU-Bonin-Mariana forearc (ODP Leg 125): Evidence for partial melting and melt-mantle interactions in a suprasubduction zone setting, *J. Petrol.*, *39*, 1577–1618.

Parkinson, I. J., J. A. Pearce, M. F. Thirlwall, K. T. M. Johnson, and C. Ingram (1992), Trace element geochemistry of peridotites from Izu-Bonin-Mariana Forearc, Leg 125, *Proc. Ocean Drill. Program Sci. Results*, *125*, 507–518.

Parmentier, E. M., and P. J. Morgan (1990), Spreading rate dependence of three dimensional structure in oceanic spreading centers, *Nature*, *348*, 325–328.

Parson, L. M., J. A. Pearce, B. J. Murton, R. A. Hodkinson, and R. C. D. S. Party (1990), Role of ridge jumps and ridge propagation in the tectonic evolution of the Lau back-arc basin, south-west Pacific, *Geology*, *18*, 470–473.

Pearce, J., S. J. Lippard, and S. Roberts (1984), Characteristics and tectonic significance of supra-subduction zone ophiolites, in *Marginal Basin Geology: Volcanic and Associated Sedimentary and Tectonic Processes in Modern and Ancient Marginal Basins*, edited by B. P. Kokelaar and M. F. Howells, *Geol. Soc. Spec. Publ.*, *16*, 77–94.

Pearce, J. A. (1980), Geochemical evidence for the genesis and eruptive setting of lavas from Tethyan ophiolites, in *Ophiolites: Proceedings of the International Ophiolite Symposium*, edited by A. Panayiotou, pp. 261–272, Cyprus Geol. Surv. Dep, Lefkosia, Cyprus.

Pearce, J. A. (1982), Trace element characteristics of lavas from destructive plate boundaries, in *Andesites*, edited by R. S. Thorpe, pp. 525–548, John Wiley, Hoboken, N. J.

Pearce, J. A. (1991), Ocean floor comes ashore, *Nature*, *354*, 110–111.

Pearce, J. A., T. Alabaster, A. W. Shelton, and M. Searle (1981), The Oman Ophiolite as a Cretaceous arc-basin complex: Evidence and implications, *Philos. Trans. R. Soc. London, Ser. A*, *300*(1454), 299–317.

Pearce, J. A., P. F. Barker, S. J. Edwards, I. J. Parkinson, and P. T. Leat (2000), Geochemistry and tectonic significance of peridotites from the South Sandwich arc-basin system, South Atlantic, *Contrib. Mineral. Petrol.*, *139*(1), 36–53.

Python, M., and G. Ceuleneer (2003), Nature and distribution of dykes and related melt migration structures in the mantle section of the Oman ophiolite, *Geochem. Geophys. Geosyst.*, *4*(7), 8612, doi:10.1029/2002GC000354.

Quatrevaux, F. (1990), Etude des hétérogénéités texturales et chimiques dans les harzburgites du diapir de Maqsad (ophiolite d'Oman), DEA, 50 pp., Univ. de Paris VII, Paris.

Quatrevaux, F. (1995), Etude pétrologique des péridotites des massifs de Maqsad et Wuqbah, ophiolite d'Oman, Thèse de Doctorat d'Univ., 536 pp., Paris VII, Paris.

Quick, J. E. (1981), The origin and significance of large, tabular dunite bodies in the Trinity peridotite, northern California., *Contrib. Mineral. Petrol.*, *78*(4), 413–422.

Rabinowicz, M. (1987), Melt segregation and flow in mantle diapirs below spreading centers: Evidence from the Oman ophiolite, *J. Geophys. Res.*, *92*(B5), 3475–3486.

Reuber, I. (1988), Complexity of the crustal sequence in the northern Oman ophiolite (Fizh and southern Aswad blocks): The effect of early slicing?, *Tectonophysics*, *151*, 137–165.

Reuber, I., P. Nehlig, and T. Juteau (1989), A fossil off-axis mantle diapir, deduced from crustal structures in the Haylayn Block (Semail Ophiolite, Oman), *Terra Cognita*, *1–1*, 162.

Reuber, I., P. Nehlig, and T. Juteau (1991), Axial segmentation at a fossil oceanic spreading center in the Haylayn block (Semail nappe, Oman): Off-axis mantle diapir and advancing ridge tip, *J. Geodyn.*, *13*, 253–278.

Reynolds, J. R., and C. H. Langmuir (1997), Petrological systematics of the Mid-Atlantic Ridge south of Kane: Implications for ocean crust formation, *J. Geophys. Res.*, *102*(B7), 14,915–14,946.

Reynolds, J. R., C. H. Langmuir, J. F. Bender, K. A. Kastens, and W. B. F. Ryan (1992), Spatial and temporal variability in the geochemistry of basalts from the East Pacific Rise, *Nature*, *359*(6395), 493–499.

Ringwood, A. E. (1975), *Composition and Petrology of the Earth's Mantle*, 618 pp., McGraw-Hill, New York.

Rochette, P., L. Jenatton, C. Dupuy, F. Boudier, and I. Reuber (1991), Diabase dikes emplacement in the Oman ophiolite: A magnetic fabric study with reference to geochemistry, in *Ophiolite Genesis and Evolution of the Oceanic Lithosphere*, edited by T. Peters, A. Nicolas, and R. G. Coleman, pp. 55–82, Springer, New York.

Roeder, P. L., I. H. Campbell, and H. E. Jamieson (1979), A re-evaluation of the olivine-spinel geothermometer, *Contrib. Mineral. Petrol.*, *68*, 325–334.

Rothery, D. A. (1982), The evolution of the Wuqbah block and the applications of remote sensing in the oman ophiolite, Ph D. thesis, 414 pp., Open Univ., Oman.

Sack, R. O., and M. S. Ghiorso (1991), Chromian spinel as a petrogenetic indicator: Thermodynamics and petrological implications, *Am. Mineral.*, *76*, 827–847.

Sauter, D., P. Patriat, C. Rommevaux-Jestin, M. Cannat, and A. Briais (2001), The Southwest Indian Ridge between 49°15′E and 57°E: focused accretion and magma redistribution, *Earth Planet. Sci. Lett.*, *192*(3), 303–317.

Schiano, P., R. Clocchiatti, J.-P. Lorand, D. Massare, E. Deloule, and M. Chaussidon (1997), Primitive basaltic melts included in podiform chromites from the Oman Ophiolite, *Earth Planet. Sci. Lett.*, *146*(3–4), 489–497.

Schilling, J. G., M. Zajac, R. Evans, T. Jonston, W. White, J. D. Devine, and R. Kingsley (1983), Petrologic and geochemical variations along the Mid-Atlantic Ridge from 29°N to 73°N, *Am. J. Sci.*, *283*, 510–586.

Schouten, H., K. D. Klitgord, and J. A. Whitehead (1985), Segmentation of mid-ocean ridges, *Nature*, *317*, 225–229.

Sempéré, J. C., and K. C. MacDonald (1987), Marine tectonics: Processes at mid-ocean ridges, *Rev. Geophys.*, *25*(6), 1313–1347.

Sempéré, J. C., J. Lin, and H. S. Brown (1993), Segmentation and morphotectonic variations along a slow-spreading center: The Mid-Atlantic Ridge (24°00′N–30°40′N), *Mar. Geophys. Res.*, *15*, 153–200.

Seyler, M., and E. Bonatti (1997), Regional-scale melt-rock interaction in lherzolitic mantle in the Romanche Fracture Zone (Atlantic Ocean), *Earth Planet. Sci. Lett.*, *146*(1–2), 273–287.

Seyler, M., M. Cannat, and C. Mével (2003), Evidence for major-element heterogeneity in the mantle source of abyssal peridotites from the Southwest Indian Ridge (52° to 68°E), *Geochem. Geophys. Geosyst.*, *4*(2), 9101, doi:10.1029/2002GC000305.

Shaw, D. M. (1970), Trace element fractionation during anatexis, *Geochim. Cosmochim. Acta*, *52*, 2177–2182.

Shaw, P. R. (1992), Ridge segmentation, faulting and crustal thickness in the Atlantic Ocean, *Nature*, *358*, 490–493.

Shervais, J. W. (2001), Birth, death, and resurrection: The life cycle of suprasubduction zone ophiolites, *Geochem. Geophys. Geosyst.*, *2*(1), doi:10.1029/2000GC000080.

Sinton, J. M., and R. S. Detrick (1992), Mid-ocean ridge magma chambers, *J. Geophys. Res.*, *97*, 197–216.

Sinton, J. M., S. M. Smaglik, J. J. Mahoney, and K. C. MacDonald (1991), Magmatic processes at superfast spreading mid-ocean ridges: Glass compositional variations along the East Pacific Rise, 13°–23°S, *J. Geophys. Res.*, *96*, 6133–6155.

Smewing, J. D. (1980), Regional setting and petrological characteristics of the Oman ophiolite in North Oman, *Ofioliti*, *2*, spec. issue, 334–378.

Snow, J. E., and H. J. B. Dick (1995), Pervasive magnesium loss by marine weathering of peridotite, *Geochim. Cosmochim. Acta*, *59*(20), 4219–4235.

Suhr, G. (1999), Melt migration under ocean ridges: inferences from reactive transport modelling of upper mantle hosted dunites, *J. Petrol.*, *40*, 575–600.

Sun, S. S., and W. F. McDonough (1989), Chemical and isotopic systematics of oceanic basalts: Implications for mantle composition and processes, in *Magmatism in the Ocean Basins*, edited by A. D. Saunders and J. M. Norry, *Geol. Soc. Spec. Publ.*, *42*, 313–345.

Takazawa, E., F. A. Frey, N. Shimizu, M. Obata, and J. L. Bodinier (1992), Geochemical evidence for melt migration and reaction in the upper mantle, *Nature*, *359*(6390), 55–58.

Takazawa, E., F. A. Frey, N. Shimizu, and M. Obata (2000), Whole rock composition variations in an upper mantle peridotites (Horoman, Hokkaido, Japan): Are they consistent with a partial melting process?, *Geochim. Cosmochim. Acta*, *64*, 695–716.

Takazawa, E., T. Okayasu, and K. Satoh (2003), Geochemistry and origin of the basal lherzolites from the northern Oman ophiolite (northern Fizh block), *Geochem. Geophys. Geosyst.*, *4*(2), 8605, doi:10.1029/2001GC000232.

Tartarotti, P., S. Susini, P. Nimis, and L. Ottolini (2002), Melt migration in the upper mantle along the Romanche Fracture Zone (equatorial Atlantic), *Lithos*, *63*(3–4), 125–149.

Taylor, B., and G. D. Karner (1983), On the evolution of marginal basins, *Rev. Geophys.*, *21*, 1727–1741.

Taylor, B., K. Zellmer, F. Martinez, and A. Goodliffe (1996), Sea-floor spreading in the Lau back-arc basin, *Earth Planet. Sci. Lett.*, *144*(1–2), 35–40.

Tilton, G. R., C. A. Hopson, and J. E. Wright (1981), Uranium-lead isotopic ages of the Semail Ophiolite, Oman, with applications to Tethyan ridge tectonics, *J. Geophys. Res.*, *86*, 2763–2775.

Umino, S., S. Yanai, A. R. Jaman, Y. Nakamura, and J. T. Iiyama (1990), The transition from spreading to subduction: Evidence from the Semail ophiolite, northern Oman mountains, in *Ophiolites, Oceanic Crustal Analogues*, edited by J. Malpas, pp. 375–384, Geol. Surv. Dep., Nicosia, Cyprus.

Vernières, J., M. Godard, and J.-L. Bodinier (1997), A plate model for the simulation of trace element fractionation during partial melting and magma transport in the Earth's upper mantle, *J. Geophys. Res.*, *102*, 24,771–24,784.

Wang, Z., S. S. Sun, Q. Hou, and J. P. Li (2001), Effect of melt-rock interaction on geochemistry in the Kudi ophiolite (western Kunlun Mountains, northwestern China): Implication for ophiolite origin, *Earth Planet. Sci. Lett.*, *191*(1–2), 33–48.

Weissel, J. K. (1977), Evolution of the Lau Basin by the growth of small plates, in *Island Arcs, Deep Sea Trenches, and Back Arc Basins*, *Maurice Ewing Ser.*, vol. 1, edited by M. Talwani and W. C. Pitman, pp. 429–436, AGU, Washington, D. C.

Weissel, J. K. (1981), Magnetic lineations in marginal basins of the western Pacific, *Philos. Trans. R. Soc. London, Ser. A*, *300*, 223–247.

Welland, M. P. J., and A. H. G. Mitchell (1977), Emplacement of the Oman ophiolite: A mechanism related to subduction and collision, *Geol. Soc. Am. Bull.*, *88*, 1081–1088.

White, S. M., K. C. MacDonald, and R. M. Haymon (2000), Basaltic lava domes, lava lakes, and volcanic segmentation on the southern East Pacific Rise, *J. Geophys. Res.*, *105*(B10), 23,519–23,536.

White, S. M., R. M. Haymon, D. J. Fornari, M. R. Perfit, and K. C. Macdonald (2002), Correlation between volcanic and tectonic segmentation of fast-spreading ridges: Evidence from volcanic structures and lava flow morphology on the East Pacific Rise at 9°–10°N, *J. Geophys. Res.*, *107*(B8), 2173, doi:10.1029/2001JB000571.

Whitehead, J. A., H. J. B. Dick, and H. Schouten (1984), A mechanism for magmatic accretion under spreading centres, *Nature*, *312*, 146–148.

Wilshire, H. G. (1984), Mantle metasomatism: The REE story, *Geology*, *12*, 395–398.

Witt-Eickschen, G., and H. A. Seck (1991), Solubility of Ca and Al in orthopyroxene from spinel-peridotite: An improved version of an empirical geothermometer, *Contrib. Mineral. Petrol.*, *106*, 431–439.